

# **Estimation and Optimization of Attenuation of High Frequency mmWave within 5G Spectrum**

by

**Md. Monzurul Hoque (170021081)**  
**Zubayer Kabir Eisham (170021094)**  
**Md. Samiur Rahman (170021120)**

A Thesis Submitted to the Academic Faculty in Partial Fulfillment of the  
Requirements for the Degree of

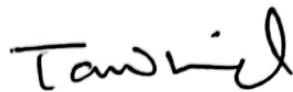
**BACHELOR OF SCIENCE IN ELECTRICAL AND ELECTRONIC  
ENGINEERING**



Department of Electrical and Electronic Engineering  
**Islamic University of Technology (IUT)**  
Gazipur, Bangladesh

# Estimation and Optimization of Attenuation of High Frequency mmWave within 5G Spectrum

Approved by:



**Dr. Mohammad Tawhid Kawser**

Supervisor and Professor,  
Department of Electrical and Electronic Engineering,  
Islamic University of Technology (IUT),  
Boardbazar, Gazipur-1704.

Date: 10-05-2022

Md. Monzowul Haque  
10.5.2022

Zubayer Kabir Eisham  
10.5.2022

Md. Samiur Rahman  
10.5.2022

# Table of Contents

|                                                         |              |
|---------------------------------------------------------|--------------|
| <b>List of Tables</b> .....                             | <b>ivv</b>   |
| <b>List of Figures</b> .....                            | <b>v</b>     |
| <b>Abstract</b> .....                                   | <b>vi</b>    |
| <b>Overview</b> .....                                   | <b>1</b>     |
| <b>1 Chapter 1</b> .....                                | <b>2</b>     |
| 1.1 INTRODUCTION .....                                  | 2            |
| 1.2 RELATED WORKS .....                                 | 3            |
| 1.3 BUILDING PENETRATION LOSS (BPL) .....               | 5            |
| 1.4 O2I MODELS .....                                    | 6            |
| 1.5 SIMULATION AND RESULTS .....                        | 3            |
| 1.6 CONCLUSION .....                                    | 3            |
| <b>2 Chapter 2</b> .....                                | <b>19</b>    |
| 2.1 INTRODUCTION .....                                  | 19           |
| 2.2 OPTIMIZATION ALGORITHMS .....                       | 21           |
| 2.2.1 PARTICLE SWARM OPTIMIZATION ALGORITHM (PSO) ..... | 21           |
| 2.2.2 MOTH FLAME OPTIMIZATION ALGORITHM (MFO) .....     | 21           |
| 2.2.3 WHALE OPTIMIZATION ALGORITHM (WHO) .....          | 21           |
| 2.2.4 GREY WOLF OPTIMIZATION ALGORITHM (GWO) .....      | 22           |
| 2.2.5 HARRIS HAWK OPTIMIZATION ALGORITHM (HHO) .....    | 23           |
| 2.2.6 SALP SWARM OPTIMIZATION ALGORITHM (SSA) .....     | 23           |
| 2.2.7 SINE COSINE OPTIMIZATION ALGORITHM (SCA) .....    | 23           |
| 2.2.8 DRAGONFLY ALGORITHM (DA) .....                    | 24           |
| 2.2.9 GRASSHOPPER OPTIMIZATION ALGORITHM (GOA) .....    | 24           |
| 2.3 PROBLEM STATEMENT .....                             | 25           |
| 2.4 RESULTS AND ANALYSIS .....                          | 27           |
| 2.4.1 ATTENUATION FACTOR OPTIMIZATION .....             | 27           |
| 2.4.2 FINDING THE BEST ALGORITHM .....                  | 30           |
| 2.4.3 Power Loss Optimization .....                     | 75           |
| 2.5 CONCLUSION .....                                    | 78           |
| <b>REFERENCES</b> .....                                 | <b>79-83</b> |

## List of Tables

|                                                                                  |    |
|----------------------------------------------------------------------------------|----|
| <b>Table 1.4.1</b> O2I Penetration Losses for Different Materials .....          | 6  |
| <b>Table 1.4.2</b> 3GPP TR 38.901 O2I Loss Models.....                           | 7  |
| <b>Table 1.4.3</b> NYUSIM O2I Loss Models .....                                  | 7  |
| <b>Table 1.5.1</b> Channel Parameters.....                                       | 8  |
| <b>Table 1.5.2</b> Antenna Properties .....                                      | 9  |
| <b>Table 1.5.3</b> NYUSIM O2I Loss Simulation Results.....                       | 9  |
| <b>Table 2.3.1</b> Omnidirectional PLE and shadow fading standard deviation..... | 26 |
| <b>Table 2.4.1</b> Measured values by different algorithms .....                 | 28 |
| <b>Table 2.4.2</b> Number of iterations for different algorithms .....           | 30 |
| <b>Table 2.4.3</b> Power Loss optimization values table.....                     | 76 |

## List of Figures

|                                                                                          |    |
|------------------------------------------------------------------------------------------|----|
| <b>Figure 1.5.1:</b> Omnidirectional PDPs for O2I High-Loss scenarios .....              | 12 |
| <b>Figure 1.5.2:</b> Omnidirectional PDPs for O2I Low-Loss scenarios.....                | 15 |
| <b>Figure 1.5.3:</b> NYUSIM O2I Loss Variation with Changing Frequency.....              | 15 |
| <b>Figure 1.5.4:</b> NYUSIM and 3GPP TR 38.901 O2I Low-Loss scenarios comparison.....    | 16 |
| <b>Figure 1.5.5:</b> NYUSIM and 3GPP TR 38.901 O2I High-Loss scenarios comparison .....  | 17 |
| <b>Figure 2.3.1:</b> Attenuation due to different scenarios in te environment .....      | 26 |
| <b>Figure 2.4.1:</b> Convergence Curve .....                                             | 27 |
| <b>Figure 2.4.2:</b> Attenuation Factor with respect to Humidity .....                   | 27 |
| <b>Figure 2.4.3:</b> PSO best case scenario .....                                        | 31 |
| <b>Figure 2.4.4:</b> PSO worst case scenario .....                                       | 31 |
| <b>Figure 2.4.5:</b> MFO best case scenario.....                                         | 32 |
| <b>Figure 2.4.4:</b> MFO worst case scenario .....                                       | 32 |
| <b>Figure 2.4.5:</b> Path loss for Urban Micro cell optimization convergence curve ..... | 76 |

## **Abstract**

Fifth-generation (5G) introduces the use of millimeter waves (mmWave) in cellular technology, and thus poses a great challenge in proper radio coverage. One of the difficulties in high-frequency coverage is the outdoor to indoor (O2I) penetration loss for indoor users. An estimation in O2I penetration losses can help operators decide to ensure proper usage of available radio resources in the range of 5G. The first part of the work presents an estimation of the variation pattern of penetration losses with varying frequencies, within 5G supported range, for different building exterior conditions. For the purposes of simulation two simulators have been used, mainly NYUSIM and a MATLAB based simulator developed using 3GPP TR 38.901. This paper also compares the simulation results from these two simulators.

The use of high frequency mmWave generates yet another issue of attenuation due to different environmental factors such as temperature, rain rate, humidity etc. This attenuation causes significant loss of transmission power, resulting in poor service and radio coverage quality. To mitigate this issue, it is of utmost necessity for the operators to be concerned about the optimum operating frequencies for certain environmental situation based on the loss due to environmental attenuation. The total problem becomes a multidimensional optimization problem which can be readily optimized using nature inspired metaheuristic algorithms. In the second part of this work, the multidimensional optimization problem of environmental attenuation is optimized by different well known optimization algorithms to investigate the optimum and worse operating points of operation for proper radio coverage.

# Overview:

Our whole work is basically divided into two major parts.

In the first part, we did an estimation of outdoor to indoor loss variation pattern within 5G spectrum and comparison of some famous O2I loss models.

## **Brief overview of part 1:**

- Introduction to 5G and importance of penetration loss in 5G
- Research Topic/Area
- Previous Studies/ Related Works
- Models & Simulation Software
- Results
- Conclusion

In the second part, we have performed the optimization of attenuation due to environmental factors for high frequency mmWave within 5G spectrum and figured out the optimum points of operation for cellular operators in certain conditions.

## **Brief overview of part 2:**

- Millimeter wave Model
- Attenuation Factor
- Multidimensional Function
- Applying stochastic Algorithm
- Finding Optimum operation point

# Chapter 1

## Part-1

### 1.1 Introduction

As the number of people and the number of user applications has been increasing, the demand in data rate has also been increasing rapidly. To meet the growing demand, cellular technologies have been evolving through different generations. Cellular technology heavily relies on the efficiency of wireless transmission of data, and operating frequency has the most impact on the efficiency. As a generation of cellular technology changes, it brings about significant changes in the wireless data transmission protocols, yet transmission of data heavily relies on electromagnetic (EM) wave frequency. Fifth-generation (5G) cellular technology uses relatively less congested high-frequency bandwidth, allowing a higher data rate. To ensure various demands, the cellular operators need to choose the frequencies that can incur less amount of power loss. One such factor that contributes to power loss is penetration loss, especially when the user is inside a building. Since 5G supports a vast frequency spectrum, unlike previous technologies, a detailed understanding regarding the variation pattern of outdoor to indoor (O2I) loss in this frequency range is crucial for operators to make various decisions for radio planning. This paper demonstrates the variation pattern of O2I penetration loss for two different forms, high-loss and lowloss, with frequency and compares the results of two different O2I models.

The remaining sections of this part of the work are arranged as follows: section 1.2 addresses the previous studies and experiments related to this work, and in section 1.3, a brief discussion regarding building penetration loss (BPL) has been mentioned. The mathematical representations of two different O2I models are stated in section 1.4. Simulation and results of section 1.5 are there to illustrate the channel parameters and antenna properties, analysis and simulation of O2I loss in various frequencies, and comparison between two different models. In the end, the conclusion of the holistic view of this portion of the work is represented in section 1.6.



## 1.2 Related Works

Since the advent of 5G cellular technology, a good number of studies and experiments have been performed to help radio network planning. In [1], a detailed survey has been conducted on 5G network architecture, performance requirements and ways or technologies to fulfill varieties of demands and versatile requirements. The paper [2] discusses the channel models that will be used to design 5G technologies. In the similar context, the authors in [3] have provided a good overview of the features implemented in 5G communication, operated in mmWave frequency bands. As more bandwidth capable mmWaves are supported in 5G technology, some research has already been performed to analyze the behavior of the penetration loss at these newly used frequencies. In the works of [4], the indoor coverage at high frequencies have been analyzed for a single building scenario: namely for 10, 30 and 60 GHz. Authors in [5] studied 4.5, 28, and 38 GHz frequency and propounded that the channel characterization and propagation models for bands of less than 6 GHz are not of much help for bands above 6 GHz. Authors in [6] explored urban outdoor and O2I characteristics for 38 GHz frequency band in details. Similar experiments on O2I penetration loss can be found in the works of [7]–[9]. In [7], authors used multi-band channel sounder to measure O2I loss at 3.5, 4.9 and 28 GHz concurrently. In [8], authors conducted experiments in different room configurations like classrooms, halls, etc., and measured different propagation parameters and channel parameters at 27-29 frequency bands, and analyzed the results. In [9], the writers discussed the O2I path-loss attributes and founded the modeling of it on the found results for 0.8 to 3.7 GHz frequency bands in urban micro-cell scenario. They demonstrated that their suggested model is more accurate than 3GPP 3D channel model. In very recent times, in [10], the authors developed an O2I penetration loss model that takes into account incident angles in both planes, vertical and horizontal. They measured the loss in the 0.9/2.3/5.1 GHz band, and in [11], the authors used separate incident angles for both the vertical and horizontal planes to demonstrate characteristics of O2I penetration loss at 5 GHz. There has been a good number of simulation-based works regarding O2I loss. In [12], channel modeling for communication through 5G mmWave has been simulated. The authors in [13] simulated three different scenarios using NYUSIM for 26 GHz frequency band: no penetration loss, low penetration loss (standard glass) and high penetration loss (infrared reflecting glass). They observed how the received power varied as they had increased the distance for three different cases. In the works of [14], the authors have performed simulations using NYUSIM simulator to analyze the

behavior of O2I loss for 28, 38, 60 and 73 GHz for both low loss and high loss scenarios with two different values of antenna elevations. In [15], the authors conducted detailed measurements at 28 and 140 GHz and proposed a 3-D spatial statistical channel model based on the results. NYUSIM simulator was used to validate the presented model. To the best of the authors knowledge, the simulation-based research works published so far have not presented a clear variation pattern of O2I losses and a comparison between different loss models for the available wide 5G frequency-spectrum. In this part of work, the scenarios of high O2I losses and low O2I losses have been compared, using two different models: NYUSIM hyperbolic model and 3GPP TR 38.901 model, and a variation pattern of O2I losses has been presented.

### **1.3 Building Penetration Loss (BPL)**

Higher frequencies of 5G technologies have been widely investigated. 5G services support EM wave frequencies ranging from 500 MHz and 100 GHz. In contrast to 5G frequency spectrum, previous generations of cellular technology have very limited and highly congested frequency spectrum. Significant number of investigations have been performed on those limited frequency range, mainly up to 6 GHz.

The use of mmWave in 5G gives rise to many challenges. One of these challenges is the high penetration losses. Various elements in the environment, vehicles, building walls, humans, flying birds etc., can cause significant penetration loss. For indoor users, wireless signals have to penetrate through building walls, infrared reflecting (IRR) glasses, concrete, windows and different things inside buildings, resulting in significant reduction in Carrier to Interference plus Noise Ratio (CINR), especially for high-frequency signals. Because of the growing use of high frequencies, recently, quite a bit of investigations have been performed for building penetration loss (BPL) for frequencies ranging up to 100 GHz. The authors of [16] present the penetration loss of different materials commonly used in buildings. It indicates a rapid rise in concrete and brick penetration losses as the frequency increases. The ordinary glass offers low losses and also, these losses increase slowly with frequency. However, modern buildings are using tinted glass for better thermal insulation and this kind of glass offers high penetration loss, especially at high frequency. At 28 GHz, transparent non-tinted glass and tinted glass had 3.9 dB and 40.1 dB penetration losses, respectively [17]. These results resemble a significant impact on proper radio coverage for mmWaves due to penetration loss. That is why, insight in the variation pattern of O2I penetration loss in this newly available frequency spectrum supported in 5G is crucial. As penetration loss is higher for the use of higher frequencies, 5G deployments have to be denser than previous generation of technologies. Dense deployment results in employing more base stations, antennas, cell towers, human employment, and monetary investment from the industry. Rigorous analysis regarding variation patterns of O2I penetration losses can be helpful for proper roll out of 5G technology.

## 1.4 O2I Models

### A. 3GPP TR 38.901

Several models have been proposed to measure O2I loss. In this paper, a MATLAB based code has been developed to simulate penetration loss using 3GPP TR 38.901 model. 3GPP TR 38.901 model measures O2I building penetration loss as follows [18]:

$$PL = PL_b + PL_{tw} + PL_{in} + N(0, \sigma_p^2) \dots\dots\dots (1)$$

where  $PL_b$  is the basic outdoor path loss;  $PL_{tw}$  denotes the penetration loss through the exterior wall of the building;  $PL_{in}$  stands for inside loss, which is proportional to the depth of the building, and  $\sigma_p$  is the standard deviation for the penetration loss.  $PL_{tw}$  is characterized as shown next:

$$PL_{tw} = PL_{npi} - 10 \log_{10} \sum_{i=1}^N (p_i \times 10^{-\frac{L_{material}}{10}}) \dots\dots\dots (2)$$

To account for non-perpendicular incidence, the extra loss  $PL_{npi}$  is applied to the exterior wall loss.  $p_i$  is the proportion of  $i$  th materials, and  $N$  is the number of materials where

$$\sum_{i=1}^N p_i = 1 \dots\dots\dots (3)$$

Penetration loss of material  $i$  is expressed as

$$L_{material} = a_{material} + b_{material} \times f \dots\dots\dots (4)$$

Example values of  $L_{material}$  can be found in Table 1.4.1. Table 1.4.2 gives  $PL_{tw}$ ,  $PL_{in}$  and  $\sigma_p$  for two O2I penetration loss models

**Table 1.4.1: O2I PENETRATION LOSSES FOR DIFFERENT MATERIALS**

| Material                   | Penetration Loss[dB]       |
|----------------------------|----------------------------|
| Standard multi-plane glass | $L_{glass} = 2 + 0.2f$     |
| IRR Glass                  | $L_{IRRglass} = 23 + 0.3f$ |
| Concrete                   | $L_{concrete} = 5 + 4f$    |
| Wood                       | $L_{wood} = 4.85 + 0.12f$  |

In Table 1.4.2, for urban macrocell (UMa) and urban microcell (UMi) street canyons,  $d_{2D-in}$  is a minimum of two independently generated uniformly distributed variables between 0 and 25 m, and for rural microcell (RMa) street canyons,  $d_{2D-in}$  is a minimum of two independently generated uniformly distributed variables between 0 and 10 m.  $d_{2D-in}$  shall be UT-specifically generated

**Table 1.4.2: 3GPP TR 38.901 O2I LOSS MODELS**

| <b>3GPP TR 38.901</b> | <b>Path loss through exterior wall <math>PL_{tw}</math> in [dB]</b>                                    | <b>Indoor Loss <math>PL_{in}</math> in [dB]</b> | <b>Standard Deviation <math>\sigma_p</math> in [dB]</b> |
|-----------------------|--------------------------------------------------------------------------------------------------------|-------------------------------------------------|---------------------------------------------------------|
| Low-Loss Model        | $5 - 10\log_{10}(0.3 \times 10^{-\frac{L_{glass}}{10}} + 0.7 \times 10^{-\frac{L_{concrete}}{10}})$    | $0.5d_{2D-in}$                                  | 4.4                                                     |
| High-Loss Model       | $5 - 10\log_{10}(0.3 \times 10^{-\frac{L_{IRRglass}}{10}} + 0.7 \times 10^{-\frac{L_{concrete}}{10}})$ | $0.5d_{2D-in}$                                  | 6.5                                                     |

**B. NYUSIM**

NYUSIM uses a parabolic model to determine O2I penetration loss. The model has two forms depending on the type of building material. They are low loss and high loss. The form of loss is determined by the type of building surface. The low-loss model can be used when the outer building materials consists of wood and standard glass, and when the outer building materials are IRR glass and concrete, the latter model of the two can be used. The parabolic model is given below [19]:

$$BPL[dB] = 10\log_{10}(A + B \times f_c^2) + N(0, \sigma_p^2) \dots \dots \dots (5)$$

In “(5)”,  $f_c$  is the carrier frequency; for the low loss model the values of A, B, and  $\sigma_p$  are 5.0, 0.03, 4.0 respectively; concurrently their values are 10.0, 5.0, 6.0 respectively for high-loss model

**Table 1.4.3: NYUSIM O2I LOSS MODELS**

| <b>NYUSIM model</b> | <b>Path loss through external wall <math>PL_{tw}</math> in [dB]</b> | <b>Standard Deviation <math>\sigma_p</math> in [dB]</b> |
|---------------------|---------------------------------------------------------------------|---------------------------------------------------------|
| Low-Loss Model      | $10\log_{10}(5 + 0.03 \times f_c^2)$                                | 4                                                       |
| High-Loss Model     | $10\log_{10}(5 + 5 \times f_c^2)$                                   | 6                                                       |

## 1.5 Simulation and Results

### A. Simulation and Results analysis of O2I Loss for varying frequencies

The simulations have been performed using fixed channel parameters and antenna settings. We observed how the O2I loss varies as we keep changing the frequency for two distinct scenarios: low loss and high loss, taking ten different readings for ten different frequencies for each case. The channel parameters are shown in Table 1.5.1, and the antenna properties are shown in Table 1.5.2. Figures were used to represent the results of each simulation.

**Table 1.5.1:** Channel Parameters

|                         |              |
|-------------------------|--------------|
| RF Bandwidth            | 800 MHz      |
| Scenario                | UMi          |
| T-R Separation Distance | 100m         |
| TX Power                | 30 dBm       |
| Base Station Height     | 35m          |
| User Terminal Height    | 1.5m         |
| Barometric Pressure     | 1013.25 mbar |
| Humidity                | 50%          |
| Temperature             | 20°C         |
| Rain Rate               | 0 mm/hour    |
| Foilage Loss            | No           |

For both low loss and high loss scenarios, simulations have been performed from 10 GHz to 100 GHz at 10 GHz spacing. The penetration losses for high loss and low loss cases have been shown in Table 1.5.3. The omnidirectional Power Delay Profiles (PDP) for high loss cases and low loss cases have been shown in “Fig. 1.5.1” and “Fig. 1.5.2” respectively. Simulations for both omnidirectional and directional settings have been performed, and O2I loss have been found same for both cases because O2I loss is independent of how the signal is arriving from the transmitting end. O2I penetration losses for high loss and low loss have been plotted in “Fig. 1.5.3” from the NYUSIM simulation result.

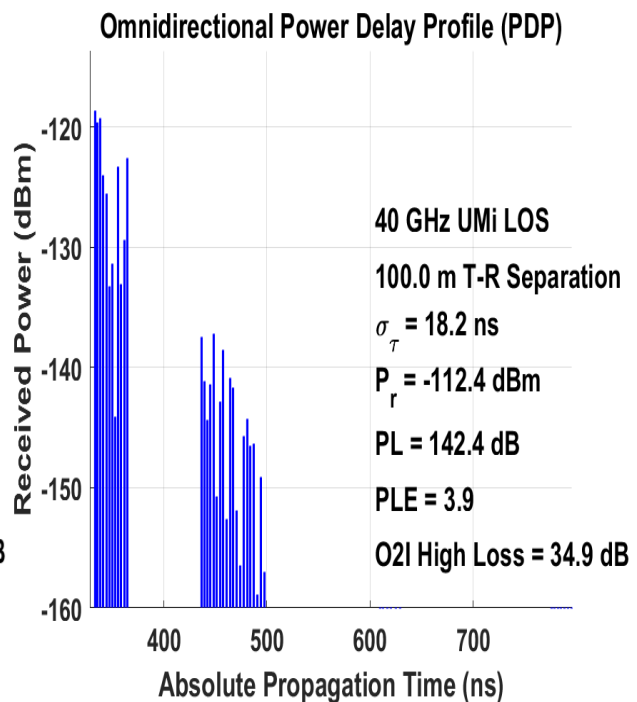
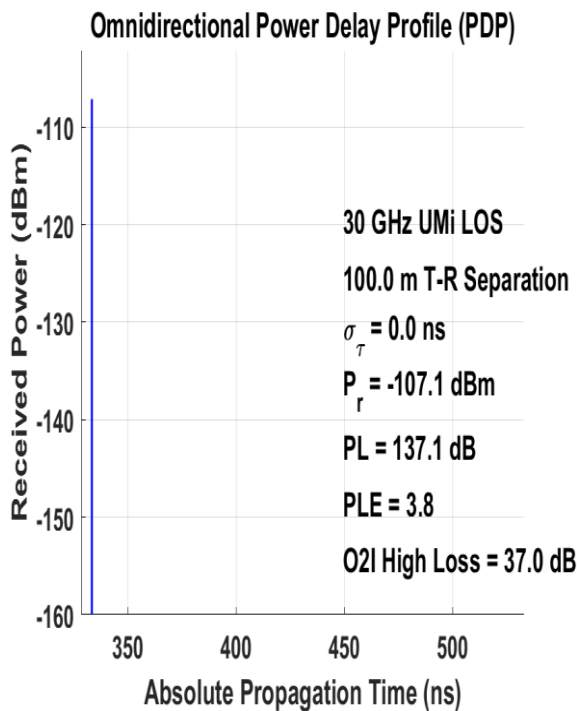
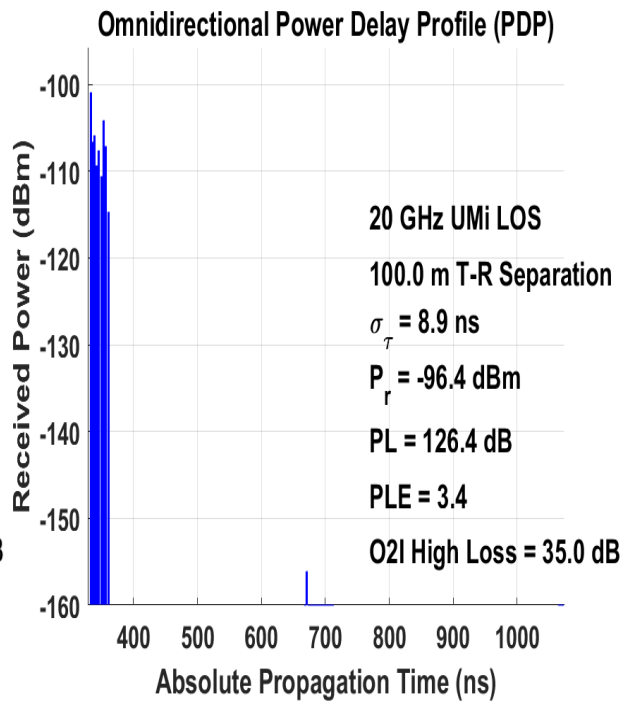
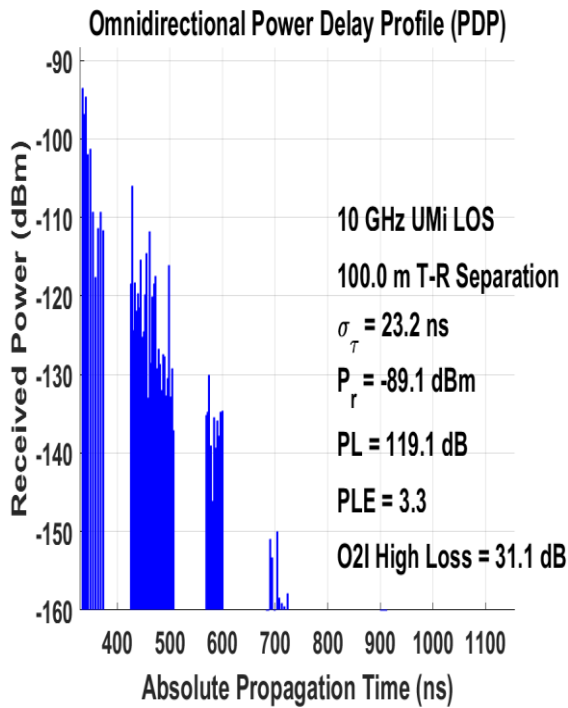
**Table 1.5.2: ANTENNA PROPERTIES**

|                                       |        |
|---------------------------------------|--------|
| Polarization                          | Co-Pol |
| TX Array Type                         | ULA    |
| RX Array Type                         | ULA    |
| Number of TX Antenna Elements         | 1      |
| Number of RX Antenna Elements         | 1      |
| TX Antenna spacing (in wavelength)    | 0.5    |
| RX Antenna spacing (in wavelength)    | 0.5    |
| Number of TX Antenna Elements per row | 1      |
| Number of RX Antenna Elements per row | 1      |
| TX Antenna Azimuth HPBW               | 10°    |
| RX Antenna Azimuth HPBW               | 10°    |
| TX Antenna Elevation HPBW             | 10°    |
| RX Antenna Elevation HPBW             | 10°    |

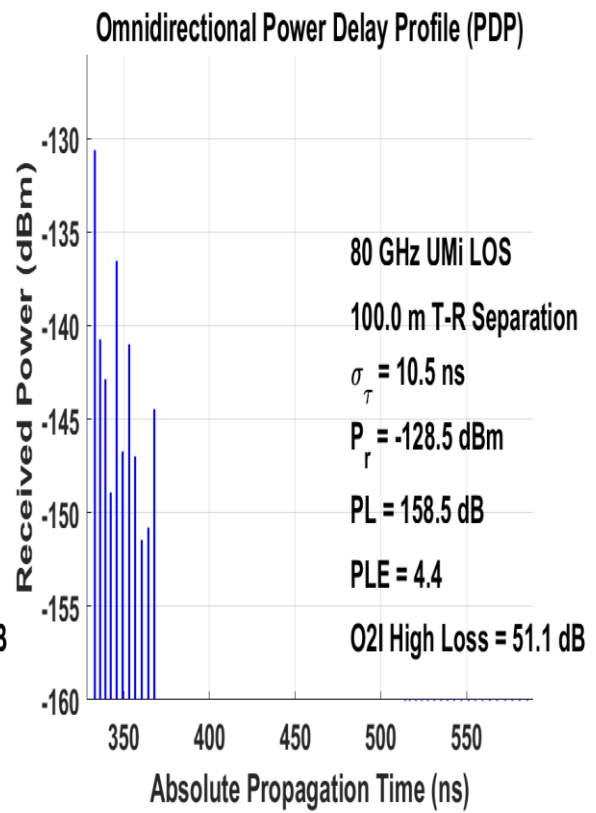
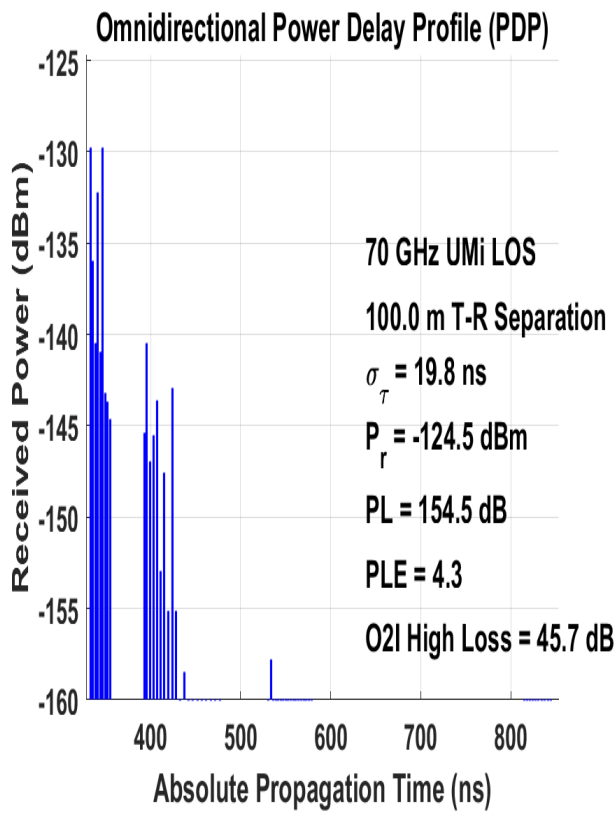
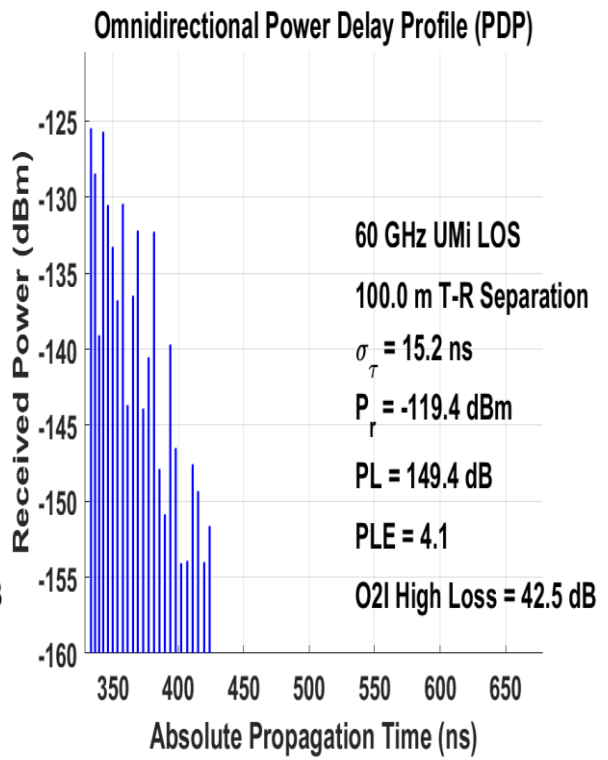
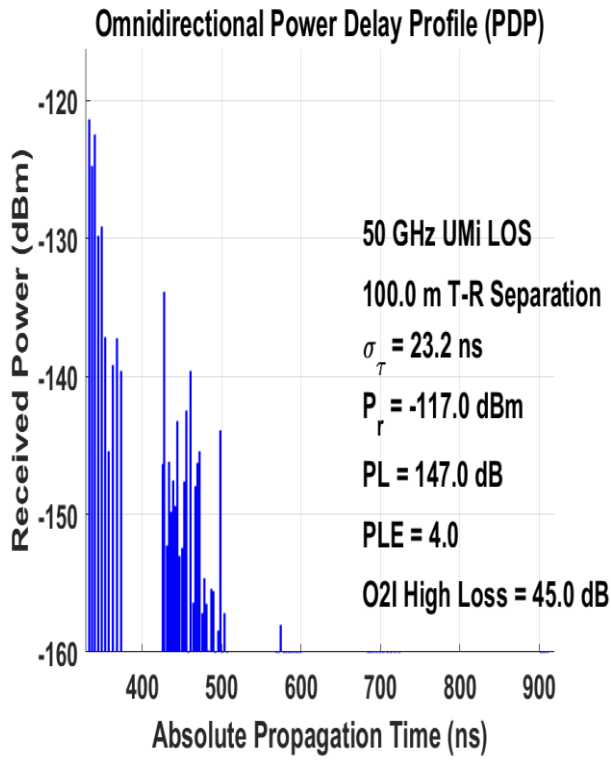
**Table 1.5.3: NYUSIM O2I LOSS SIMULATION RESULTS**

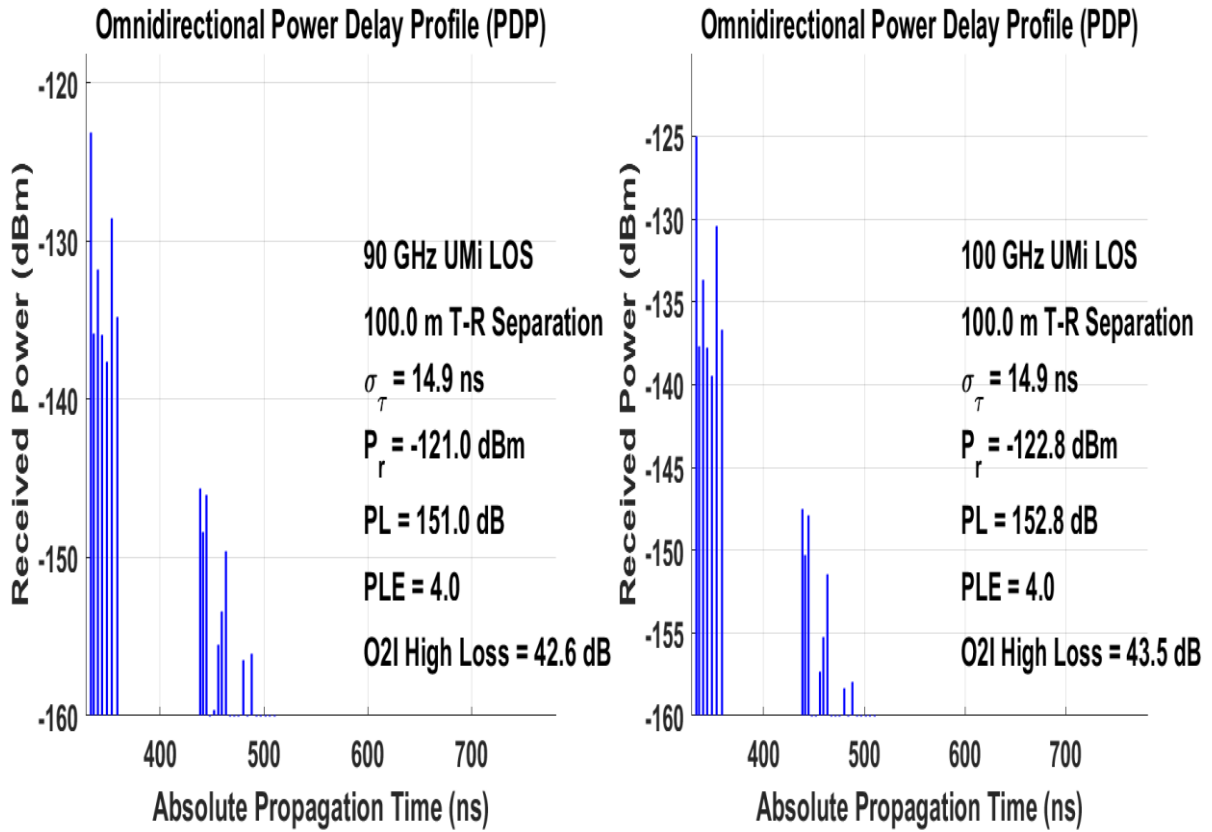
| <b>Frequency (GHz)</b> | <b>High Loss(dB)</b> | <b>Low Loss(dB)</b> |
|------------------------|----------------------|---------------------|
| 10                     | 31.1                 | 10.2                |
| 20                     | 35                   | 9.7                 |
| 30                     | 37                   | 13.1                |
| 40                     | 34.9                 | 19.4                |
| 50                     | 45                   | 19.3                |
| 60                     | 42.5                 | 17.8                |
| 70                     | 45.7                 | 18.3                |
| 80                     | 51.1                 | 24.3                |
| 90                     | 42.6                 | 23.4                |
| 100                    | 43.5                 | 22.7                |

An upward trend can be observed for both type of O2I penetration losses with the rise of frequencies, available in the wide spectrum. However, these upward trends don't follow any fixed pattern.



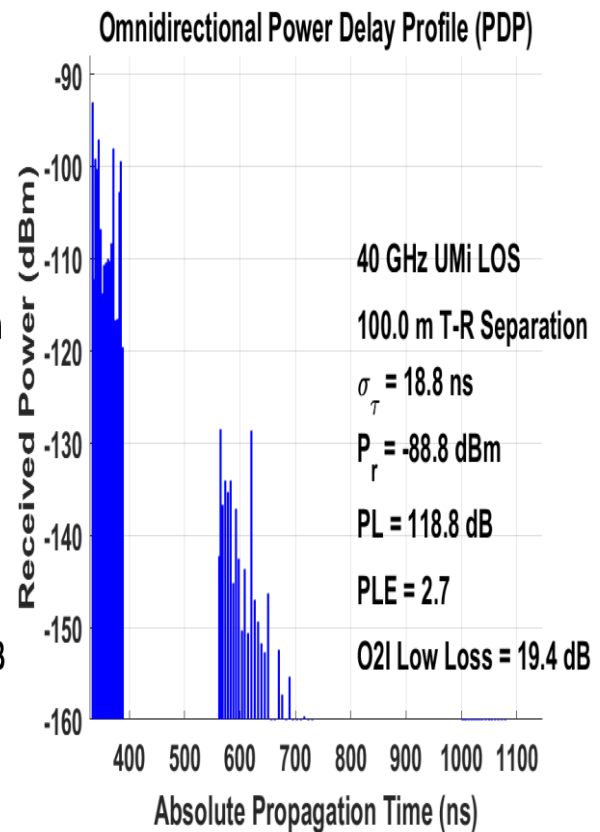
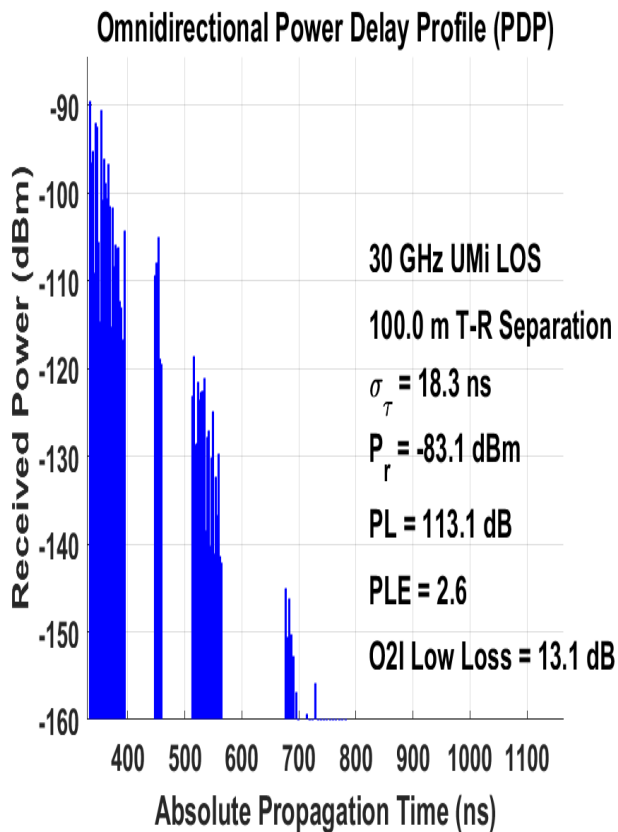
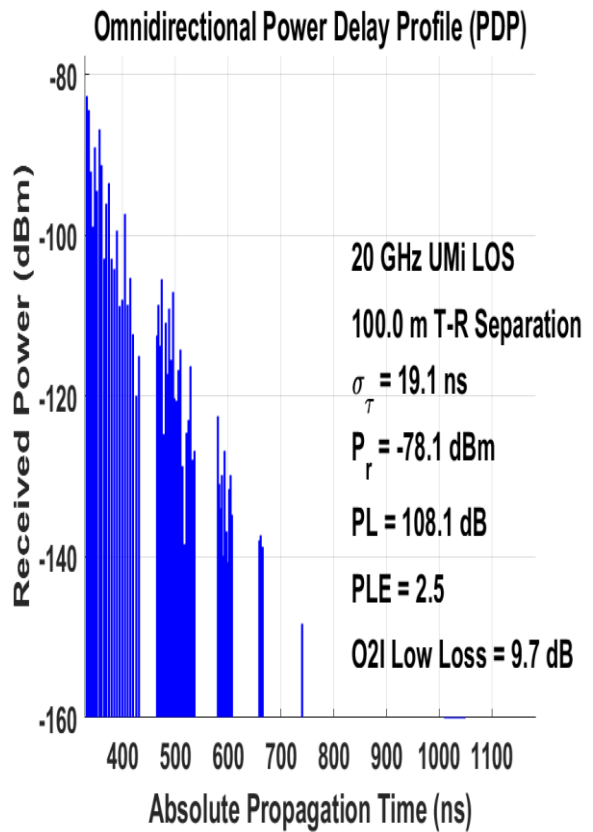
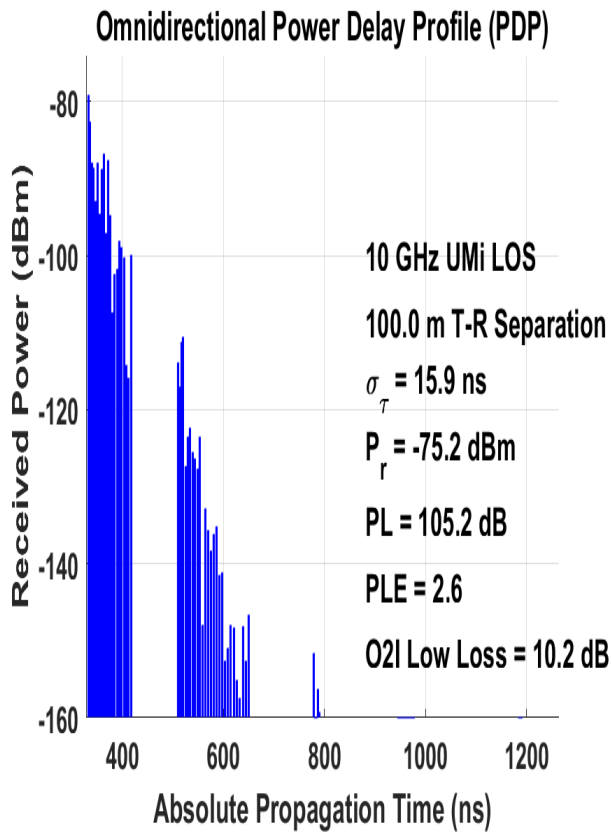


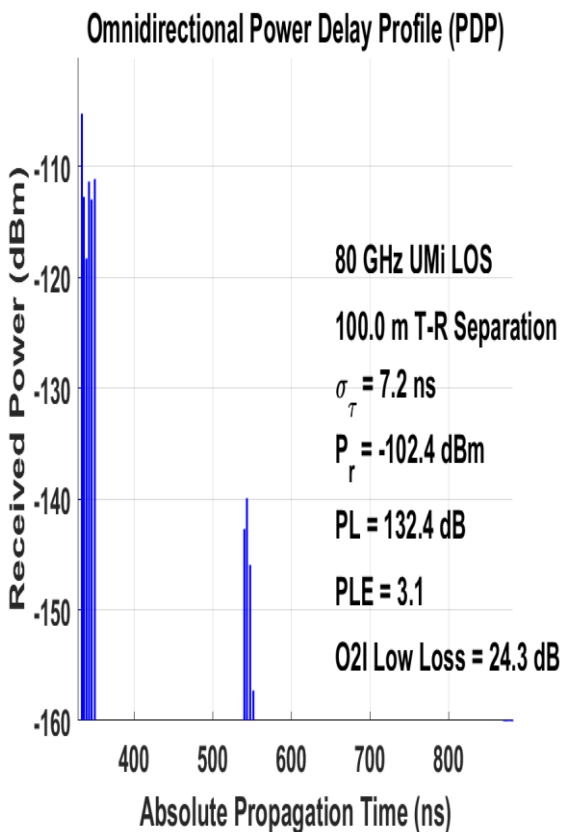
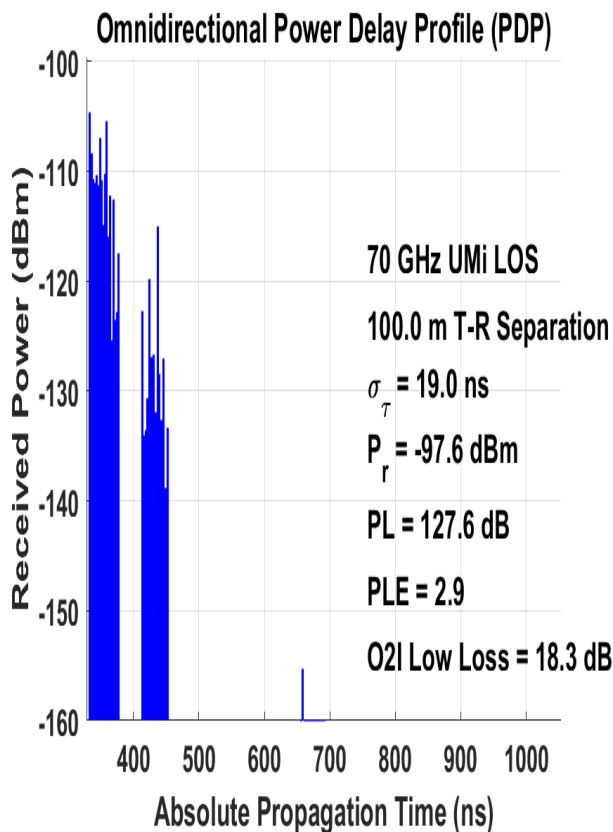
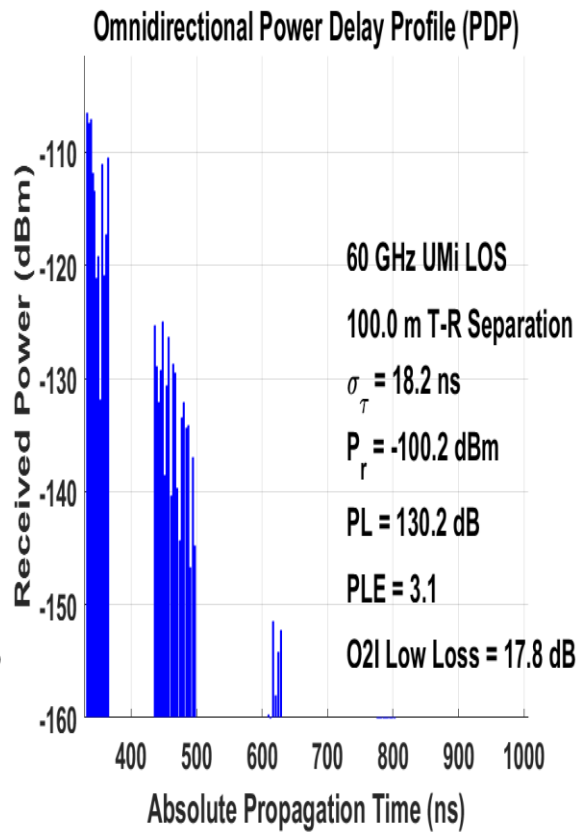
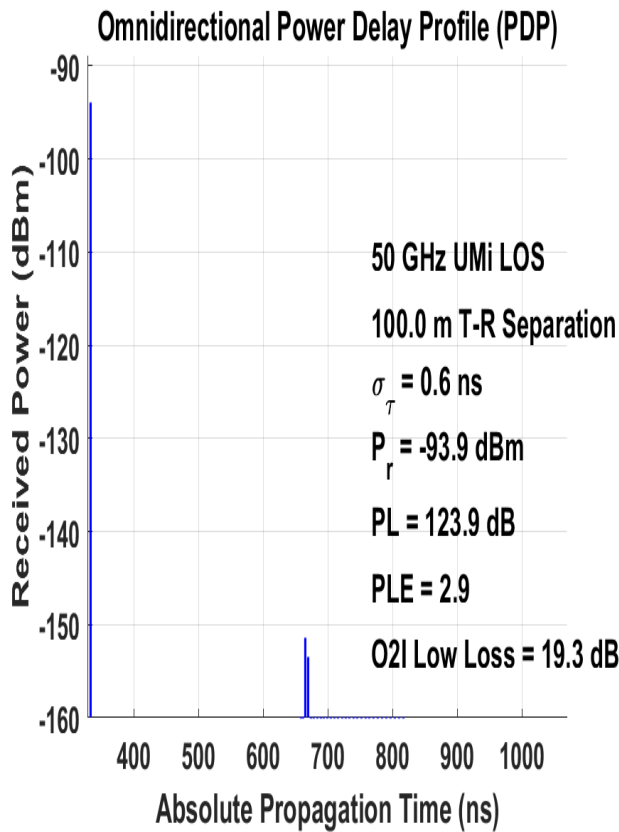




**Figure 1.5.1:** Omnidirectional PDPs for O2I High-Loss scenarios

These irregularities in “Fig. 1.5.3” are primarily due to random number used as standard deviation; one cause for this randomness is the incident angle of electromagnetic wave on the material surface. The difference between O2I high loss and low loss from NYUSIM simulation is approximately 25 dB over the whole frequency range. In “Fig. 1.5.3”, it is apparent that O2I low loss has a smoother rise than the rise of O2I high loss. From 10 GHz to 40 GHz frequency band, O2I low loss has a somewhat linear growth whereas O2I high loss has a sharp drop at 40 GHz, but for the rest of the frequency range, sharp fluctuations are apparent for the high loss cases. In contrast to high loss cases, low loss scenarios have nominal fluctuations from 40 GHz to 70 GHz frequency band. Around 5 dB rise is visible as frequency was changed to 80 GHz, and from 80 GHz to 100 GHz, the variation pattern was somewhat steady. In summary, NYUSIM O2I loss ranges from approximately 10 dB to 25 dB whereas high loss ranges from about 30 dB to 55 dB





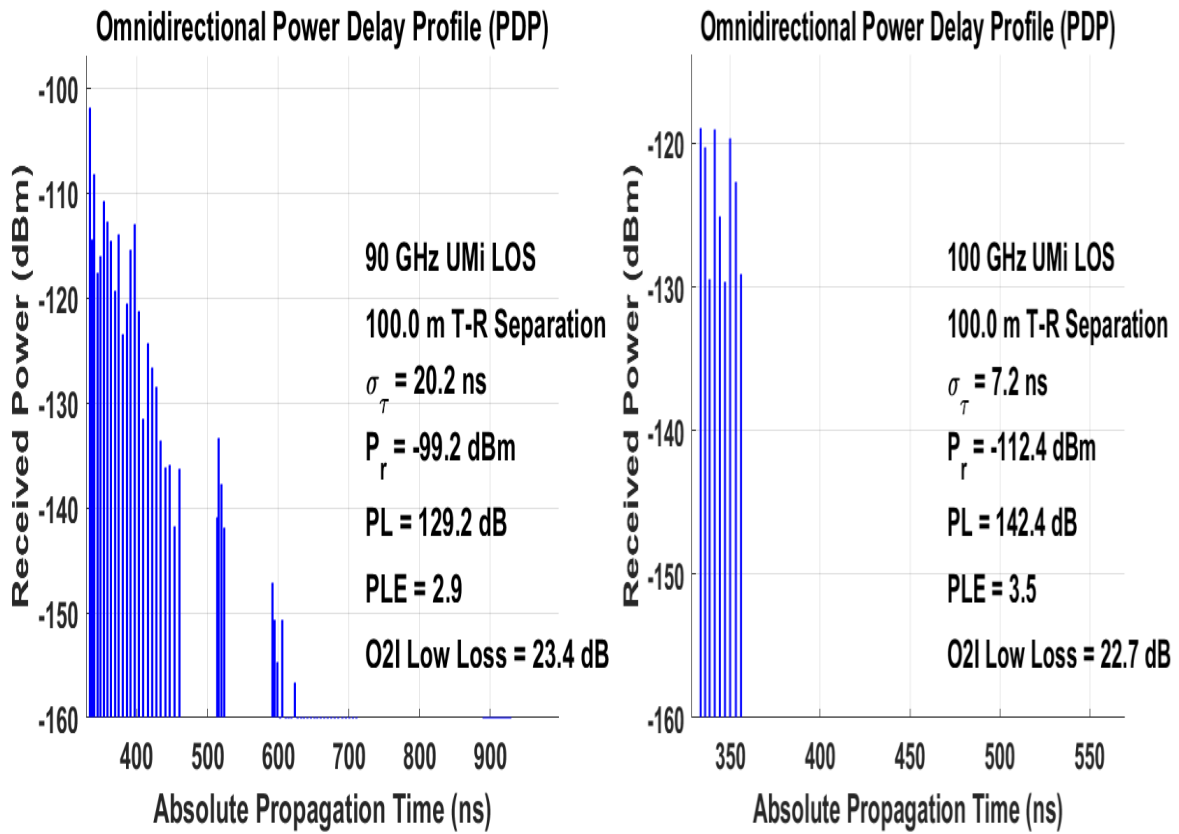


**Figure 2.5.2:** Omnidirectional PDPs for O2I Low-Loss scenarios

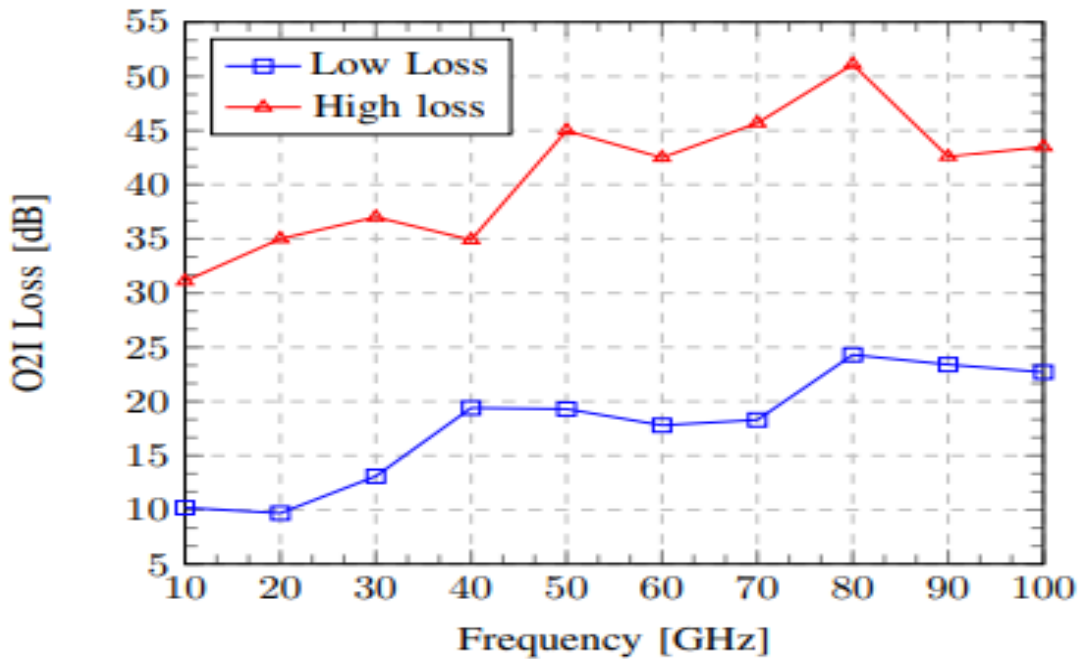


**Figure 3.5.3:** NYUSIM O2I Loss variation with changing frequency

*B. Comparison between simulation results from 3GPP TR 38.901 Model and NYUSIM hyperbolic model*

In this section, a comparison between O2I penetration loss of 3GPP TR 38.901 Model and NYUSIM simulation has been shown. To illustrate the comparison, we have simultaneously plotted the penetration loss through outer or external wall ( $PL_{tw}$  of“(2)”) of 3GPP TR 38.901 model and the simulated results we found for O2I penetration loss model of NYUSIM. For depicting the variation pattern of penetration loss of 3GPP 38.901 model, a MATLAB based simulator had been used.

For low-loss (“Fig. 1.5.4”) scenarios and high-loss (“Fig. 1.5.5”) scenarios, we have plotted separate graphs to have a better comparison of view.

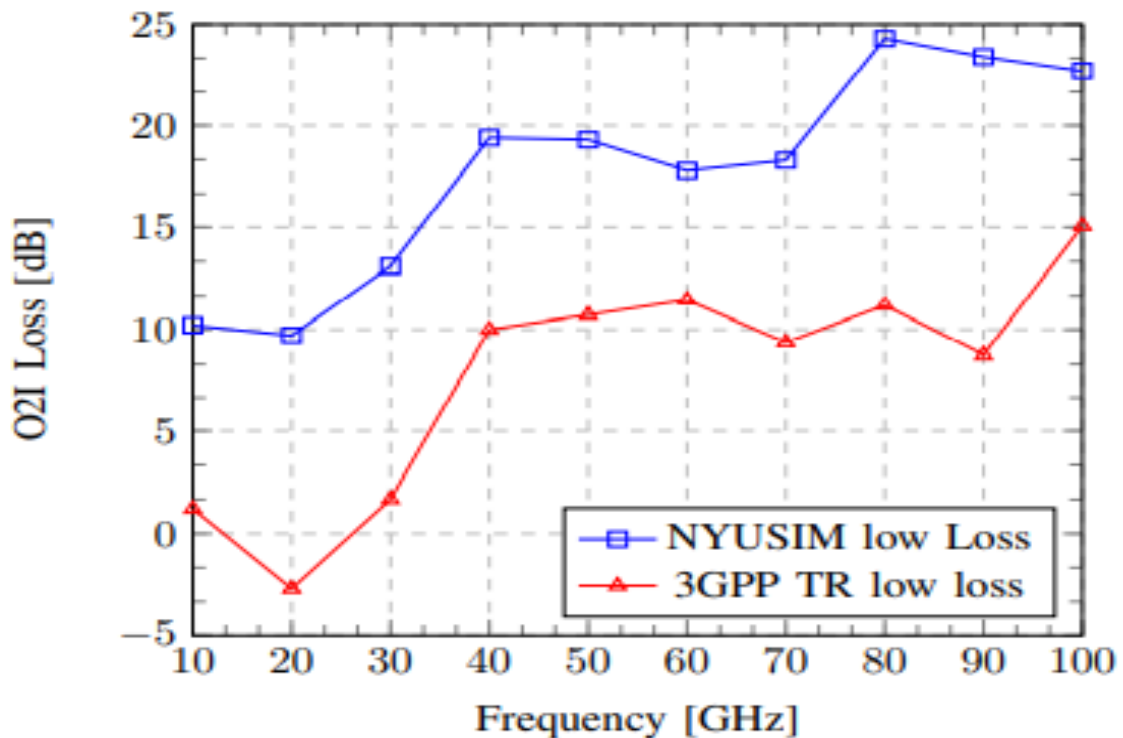


**Figure 4.5.4:** NYUSIM and 3GPP TR 38.901 O2I Low-loss scenarios’ comparison

A similar upward trend along with some irregular and random patterns can be perceived for the penetration loss of 3GPP TR 38.901 Model as we keep changing the frequency from 10 GHz up to 100 GHz with an interval of 10 GHz similar to what we had done in the case of NYUSIM simulation. In both low-loss and high-loss cases, an inconsistent difference has been observed at different frequencies between simulation results from NYUSIM hyperbolic model and 3GPP TR 38.901 model. Comparison between “Fig. 1.5.4” and “Fig. 1.5.5” shows that the difference of O2I losses between two loss models is higher for high-loss cases compared to low-loss cases. The difference between O2I losses of two models is around 30 dB for high-loss cases and around 10 dB for low-loss cases. It can be inferred from the simulation results that the assumed materials in NYUSIM are more opaque to the transmission of electromagnetic waves than the assumed materials of 3GPP TR 38.901.

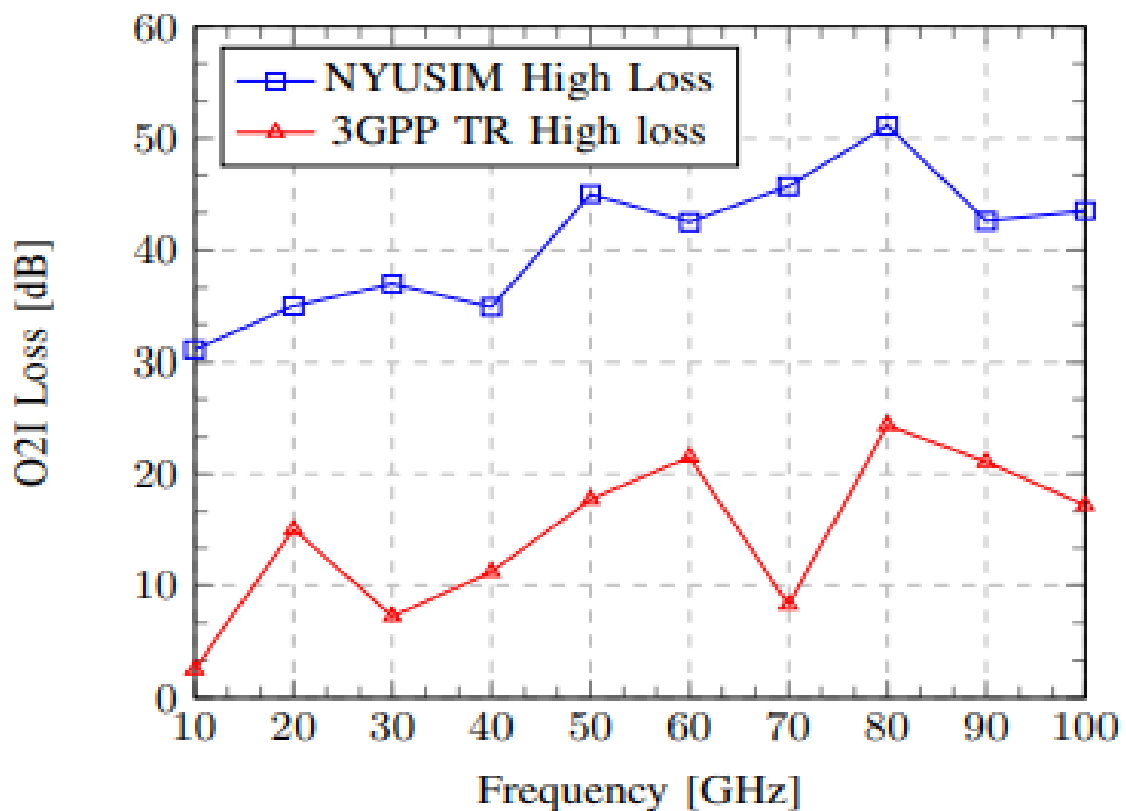


**Figure 5.5.5:** NYUSIM and 3GPP TR 38.901 O2I High-loss scenarios’ comparison

## **1.6 Conclusion**

The variation pattern of O2I penetration losses for different materials within 5G frequency spectrum have been demonstrated. From the analysis of the simulations done by NYUSIM, it can be concluded that the O2I Penetration loss follows an upward trend with an irregular and random fashion with the increment of the frequency for low-loss and high-loss materials. This paper also presented a comparison between the losses encountered due to the penetration through the external wall, measured by 3GPP TR 38.901 model, with the simulated results of O2I loss found from NYUSIM simulations. Both models followed an irregular upward trend as the frequencies were increased, while the O2I losses found from NYUSIM simulated results appeared to be higher than the losses measured by 3GPP TR 38.901 model. In the case of high-loss materials, the difference between 3GPP TR 38.901 model and NYUSIM simulated results were comparatively higher than that of the low-loss materials. These studies and analysis of O2I penetration loss can be quite vital for newer deployments where 5G mmWaves play significant impact



# Chapter 2

## Part-2

### 2.1 Introduction

The high frequency mmWave in 5G, as discussed in part 1, comes with major advantages like higher data rate, low latency, high mobility, higher spectrum density, higher area traffic capacity, broader connection density (higher number of devices in unit area), extended network energy efficiency, extensive peak data rate and so on. These advantages with high frequency mmWave allow newer applications like Enhanced Mobile BroadBand (eMBB) that allows higher data rate and extended traffic volume, massive Machine-Type Communication (mMTC), introducing massive number of low-priced devices with low power consumption and ultra-Reliable Low Latency Communication (uRLLC).

However, as discussed in the previous part, all these superior performances come with the expense of higher amount of attenuation due to the use of high frequencies. Up to the earlier generations of cellular technologies, the attenuation of signals in the environment was not that much of a significant issue, since the carrier frequency was limited below 6 GHz up to LTE. But as the frequency spectrum highly increased for 5G (up to 100 GHz), the attenuation of these high frequency mmWaves due to different environmental factors become unavoidable, and a significant ratio of the transmitted signal gets attenuated in the multipath environment. As a result, the received signal strength, as well as the user data rate drops significantly and the QoS (Quality of Service) gets highly interrupted. So, optimization of these attenuation of signal due to certain environmental factors becomes quite vital to maintain proper radio coverage by choosing optimum frequency points for certain environmental condition and avoiding the disadvantageous points.

So, in a nutshell, in this part of work, the authors focus on one of the key aspects of communication- transmission power loss. Power of the transmitted signal determines the SNR and Bandwidth of a signal. The authors focus on the overall transmission power in

the environment. There are many factors that impact the transmitted signal-humidity, rain drop, temperature, frequency of the signal, atmospheric pressure. The authors focus on the efficient calculation of the mathematical model for determining power loss that incorporates all the environmental factors. The mathematical model is a multidimensional problem with many local solutions, and the objective is to find the global solution in an efficient manner. The authors deploy algorithms for adjusting weights in the Neural Network to solve this mathematical model for power loss, and compare different algorithms of the same genre. The authors, in essence, optimize the mathematical model for power loss and the mathematical model for determining the attenuation caused by the environment. The authors also find the best algorithm for this particular problem among some selected and famous algorithms, and the authors also propose a way to determine other local optimum points.

Mathematical model of this environmental attenuation was first developed in 1993 [20]. The authors in that work investigated the propagation characteristics of atmosphere for the frequency range from 1GHz-100GHz. The model was developed considering dry air, water vapor, haze and rain. NYUSIM software was developed based on this model to calculate the environmental attenuation factor. But the scope is limited here, because this software operates based on constant values of variable, and it may need millions of simulations to find the optimum points of operation which is totally impractical. So, a method of optimization of this multidimensional attenuation factor appears to be highly desirable to minimize the transmission power loss.

Stochastic algorithms have become popular in the advent of ANN. Nature based stochastic algorithms gained popularity due to fast convergence to optimum solution and have famously solved complex optimization problems including cache optimization [21], resource allocation [22], power management in the network [23], secrecy rate optimization problem [24] and etc in the field of wireless and cellular communication.

## 2.2 Optimization Algorithms

A brief discussion on the optimization algorithms used to optimize the proposed problem is given below. These algorithms are mainly swarm based nature inspired optimization algorithms which are extensively used to solve complex engineering problems with faster convergence.

### 2.2.1 Particle Swarm Optimization Algorithm (PSO):

This algorithm first proposed in 1995 [25] as a global optimization technique for nonlinear functions. It imitates a flock's social and individual intelligence. An optimization issue is treated as an n-dimensional space in this approach, where n is the number of parameters. Each bird symbolizes one of the possible answers. PSO duplicates each population member's bodily changes. A search space is a solution space in this algorithm, and possible solutions are the positions of individuals in the search space. If an optimization problem has R variables, the solution space in the PSO algorithm is an R-dimensional search space, with positions in the kth dimension corresponding to the values of the kth variable.

Changes in individual locations are prompted by three elements in this algorithm: (i) inertia, (ii) the best position of individual (p), and (iii) the best location worldwide (g). Inertia is the individual's velocity in the previous iteration, which can be controlled by inertia weight. Inertia stops particles from retracing their steps. The best place discovered by an individual till now is the p location, and the best site discovered by the entire population until now is the g location. Each member has their own velocity, which is created at random in the p and g directions.

### 2.2.2 Moth Flame Optimization Algorithm (MFO):

The MFO is a metaheuristic algorithm designed to solve complicated optimization issues [26]. The MFO was inspired by moths' natural navigation method. The movement of moths towards lights at night while maintaining a fixed angle is offered as an effective strategy for achieving the goal. Members of the moth population represent actual search agents that move about the space according to a predetermined plan, whilst members of the flame population represent the moths' current ideal positions. In other words, flames can be thought of as pins or flags left by moths searching for the optimal environment.

The flame population in the first iteration consists of moths sorted by fitness ratings. The moth with the highest fitness value will be assigned first place in the flame population, followed by the rest. The position of each moth in relation to its matching flame is then updated. The best flame is always used to update the position of the first moth, and the worst flame is always used to update the position of the last moth.

### 2.2.3 Whale optimization algorithm (WOA):

Whale optimization algorithm (WOA) is a swarm-based meta-heuristic method for addressing difficult optimization problems that is based on the bubble-net hunting maneuver tactic used by humpback whales [27]. Because of its simple structure, low operator requirement, high convergence speed, and better balancing capabilities between exploration and exploitation stages, swarm intelligence has become extensively recognized in numerous technical domains.

The algorithm's applications have been widely used in various domains in recent years due to its superior performance and efficiency.

The humpback whale population in WOA searches for food in a multi-dimensional search space. Individual humpback whale positions are represented as choice variables, while the distance between the humpback whales and the food correlates to the value of objective cost. Three operational processes determine a whale's time-dependent location: (1) shrinking encircling prey, (2) bubble-net attacking strategy (exploitation phase), and (3) hunt for prey (exploration phase).

#### **2.2.4 Grey Wolf Optimization Algorithm (GWO) [28]:**

Grey wolves live in packs and hunt in packs. The following is a description of the searching and hunting process: (1) If a prey is discovered, they track, chase, and approach it first. (2) If the prey flees, the grey wolves will follow, encircle, and harass it until it comes to a halt. (3) Finally, the assault starts.

Grey wolves have long been considered apex predators at the top of the food chain. Grey wolves are more prone to living in packs. The typical group size is also 5–12. It's worth noting that they have a particularly complex social governance hierarchy.

Grey wolves' searching and hunting processes were used to develop the optimization algorithm. The best solution in the mathematical model is called alpha, the second best is beta, and the third best is delta. All of the remaining possible solutions are believed to be omegas.

Alpha's key responsibilities include hunting, sleeping, and waking times, among other things. As a result, the group would inherit alpha's decisions. Nonetheless, they achieved one type of democratic behavior, in which the alpha wolf follows the other wolves in the pack. The entire group would recognise alpha by raising its tail at meetings. Because the group must obey his commands, the alpha wolf is known as the dominating wolf.

Subwolves who help alpha with decision-making and other group activities are known as beta. This wolf beta could be female or male, and it will most likely be the best alpha contender if one of the alpha wolves dies or gets old. The wolf beta must obey alpha, although it can also command lower-level wolves. The alpha advisor and group regulator are these wolves. Beta distributes alpha commands to the rest of the group and gives alpha feedback.

Omega is the victim in this story. Omega wolves must submit to each dominant wolf on a regular basis. They are, in fact, the last wolves who are allowed to feed.

The alpha is always in charge of the searching and hunting process, whereas the beta has a little part and the delta has none. If he/she obtains the best, all of the other grey wolves transfer his/her status to the leader. It should be emphasized that the best location in real-world searching and hunting operations is closest to the prey, whereas the best position in optimization for a global optimum of a given problem is the greatest or lowest of the fitness value under specified constraints.

A postulated prey is always surrounded by dominants during the searching process, whereas a real prey is encompassed during the hunting process. In order of social hierarchy, the dominant grey wolves are positioned around the prey. This means that among the grey wolves, the alpha is the closest; the beta is the closest in the pack save for the alpha; and the

delta is third. Omega wolves take part in the processes and pass on their superior positions to the dominants.

### **2.2.5 Harris Hawks Optimizer (HHO):**

Heidari et al. developed HHO [29], which is a hunting mechanism that Harris hawks use naturally. This program updates the positions of hawks in a search space using a series of equations to imitate distinct hunting tactics that these birds execute to catch prey.

In this algorithm, a group of hawks attacks a hunt to surprise it (exploration phase). When it comes to the possibility of evasion and fleeing the hunt, the Hawks can do multiple fast dives close to the prey to startle it and tire it out (exploitation phase).

The HHO algorithm can change its phase from exploration to exploitation based on the prey's escaping energy, and then move between different exploitative modes. The running process can greatly reduce the energy of the hunt.

### **2.2.6 Salp Swarm Algorithm (SSA):**

The Salp Swarm Algorithm (SSA) is a new optimization technique that has been developed to handle a variety of optimization issues [30]. It replicates the natural activity of Salps, which are barrel-shaped planktonic tunicates belonging to the Salpidae family. Furthermore, their tissues are comparable to jellyfishes, and their movement behavior and weights have a high water percentage. They move by contracting and changing postures by pushing water through their jellied bodies.

SSA begins by segmenting the population into two groups: leaders and followers. The chain's front salp is known as the leader, while the others are known as the followers.

The salps' position is calculated in n-dimensions, where n represents the problem's variables and n represents the search space. These salps are looking for a food supply, which signals the swarm's target.

### **2.2.7 Sine Cosine algorithm (SCA):**

Mirjalili proposed the sine cosine algorithm (SCA), which is a powerful population-based optimization tool [31]. It has been applied to a wide range of settings since its inception.

By using mathematical models based on the sine and cosine functions, SCA creates a large number of origin random candidate solutions and causes them to oscillate outwards or towards the ideal agent. It not only improves convergence speed but also prevents local optimization, according to a significant number of test experiments.

### **2.2.8 Dragonfly Algorithm (DA):**

DA is created by imitating a dragonfly's swarming behavior [32]. Their swarming is caused by either migration or hunting (dynamic swarm or static swarm, respectively). Small groups of

dragonflies migrate over a small area to hunt other insects in a static swarm. Local movements and sudden alterations are typical of this sort of swarming.

However, in dynamic swarming, a large group of dragonflies forms and moves in one direction over a long distance. The major idea for DA is this swarming behavior.

Static and dynamic swarming behaviors correspond to the metaheuristic optimization algorithm's exploration and exploitation phases, respectively. Five weights were employed to lead artificial dragonflies down various paths: separation weight, alignment weight, cohesion weight, food factor, enemy factor, and inertia weight. High alignment and low cohesion weights are used to explore the search space; nevertheless, low alignment and high cohesion weights can be utilized to exploit the search space. In addition, to switch between exploration and exploitation, the radius of the neighborhood was increased proportionally to the number of repetitions. Another technique to balance exploration and exploitation is to adjust the swarming weights adaptively during the optimization process.

A random move must be introduced to the searching approach to increase the possibility of an optimization algorithm traversing the whole decision space. To promote randomness, stochastic behavior, and exploration of artificial dragonfly individuals when there are no neighboring solutions, dragonflies are required to fly around the search space using a random walk (Lévy flying).

### **2.2.9 Grasshopper Optimization Algorithm (GOA):**

The Grasshopper Optimization (GOA) is a new swarm intelligence algorithm that was inspired by grasshoppers' natural foraging and swarming activity [33]. The GOA algorithm has been successfully used to handle a variety of optimization problems in a variety of disciplines, and its benefits have been proved in the literature.

Grasshoppers are pest insects that have a negative impact on agricultural productivity and agriculture. Nymph and maturity are the two stages of their life cycle. Small steps and gradual movements describe the nymph phase, while long-range and rapid movements represent the maturity phase. The intensification and diversification phases of GOA are represented by nymphal and adult motions. A grasshopper's position is updated based on its current location, global best location, and the locations of other grasshoppers in the swarm. This prevents GOA from becoming stuck in local optima.

## 2.3 Problem Statement

There are two objective functions to be optimized: attenuation factor and close-in free space reference distance (CI) path loss model. The whole path loss can be expressed as follows [34][35][36].

$$PL^{CI}(f, d)[dB] = FSPL(f, 1m)[dB] + 10n \log_{10}\left(\frac{d}{d_0}\right) + AT[dB] + X_{\sigma}^{CI}, \quad d \geq d_0 \text{ m}$$

$f$  is the frequency in GHz,  $d$  is the separation between transmitter and receiver,  $n$  is the path loss exponent,  $d_0$  the free space reference distance.  $X_{\sigma}^{CI}$  is a zero-mean random variable with Gaussian distribution.  $FSPL$  is defined as follows.

$$FSPL(f, 1m)[dB] = 20 \log_{10}\left(\frac{4\pi \times 10^9}{c}\right)$$

$c$  is the light speed.  $AT$  is defined as follows.

$$AT[dB] = \alpha[dB/m] \times d[m]$$

$\alpha$ - the attenuation factor [20]- and  $PL^{CI}(f, d)[dB]$  are to be optimized. As can be seen from the Figure 2.3.4 that  $\alpha$  has peaks and troughs, and with all the environmental factors finding the global point gets critical. More complexity rises in the calculation of.  $PL^{CI}(f, d)[dB]$ .

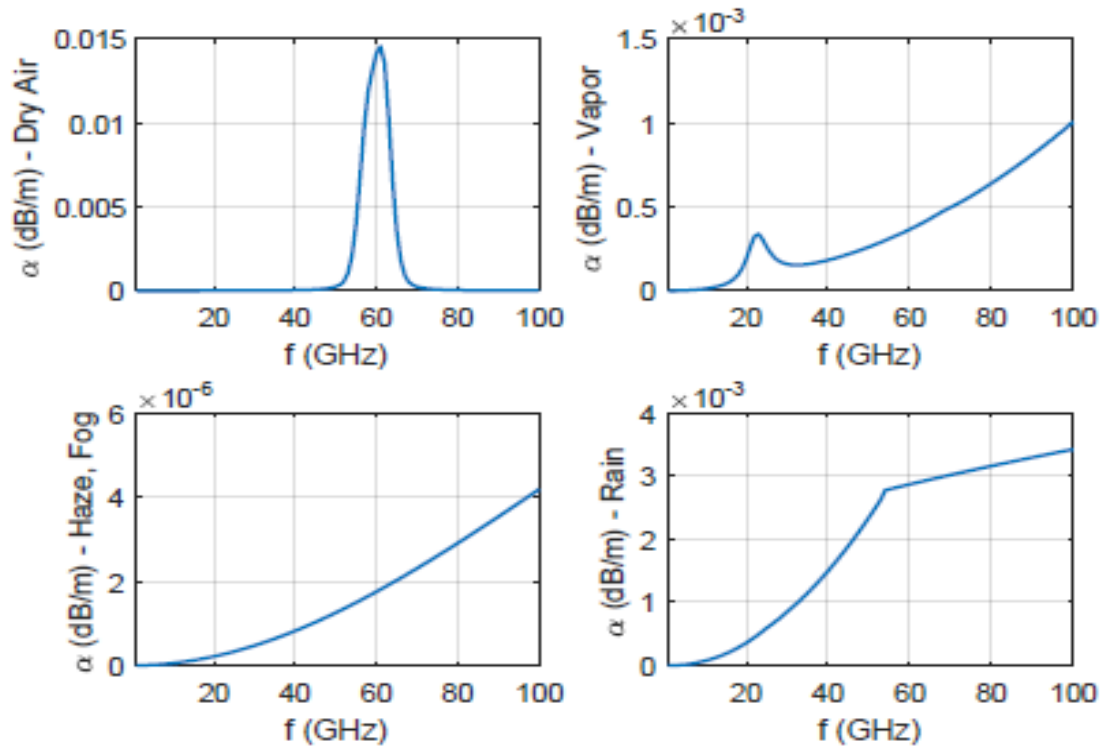


**Figure 2.3.1:** Attenuation due to different scenarios in the environment.

The value of  $n$  varies depending on the cell description so does the  $X_{\sigma}^{CI}$  as given in the table 2.3.1.

**Table 2.3.1** Omnidirectional PLE and shadow fading standard deviation

| Scenario |      | PLE  | Shadow fading standard Deviation [dB] |
|----------|------|------|---------------------------------------|
| UMi      | LOS  | 2    | 4.0                                   |
|          | NLOS | 3.2  | 7.0                                   |
| UMa      | LOS  | 2    | 4.0                                   |
|          | NLOS | 2.9  | 7.0                                   |
| RMa      | LOS  | 2.31 | 1.7                                   |
|          | NLOS | 3.07 | 6.7                                   |



## 2.4 Results and Analysis

The optimization of the functions was done in a laptop of processor intel i5, 7th generation with 12 GB RAM.

### 2.4.1 Attenuation Factor Optimization

Ten different stochastic optimization algorithms were applied to solve the attenuation factor in 100 iterations, and the whole process was repeated 100 times. At the end, the average of the hundred different runs were taken. As a result, a holistic convergence curve was obtained with hundred iterations where each iteration is the average of hundred different runs. Attenuation factor has 5 independent variables. Respective Ranges are given below.

| Frequency (GHz) | Pressure (mbar) | Humidity (%) | Temperature (°C) | Rain Rate (mm/hr) |
|-----------------|-----------------|--------------|------------------|-------------------|
| 1-100           | 300-1013        | 0-100        | (-100) - 50      | 0-150             |

Pressure lowest range was set to 300 mbar because of practical reasons. The lowest practical pressure can be conceived at the peak of Everest so the range was set accordingly.

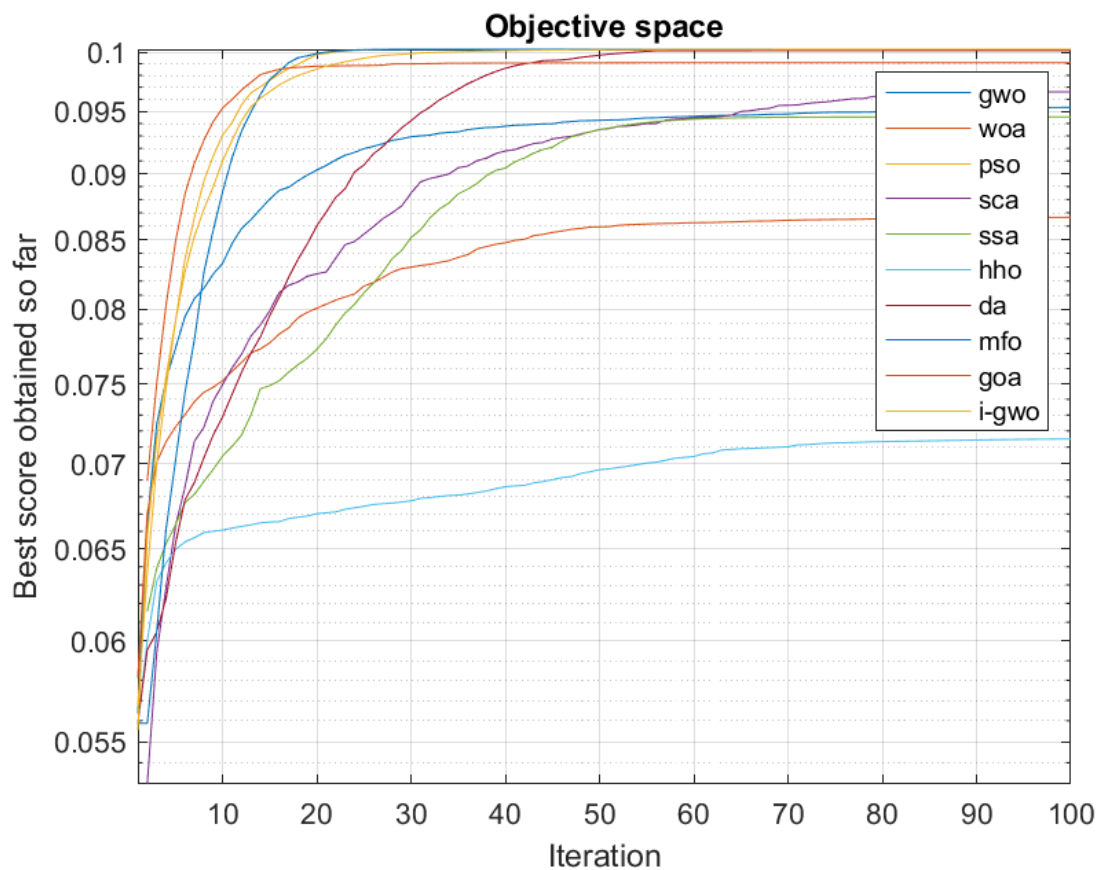


Figure 2.4.1: Convergence Curve

**Table 2.4.1: Measured values by different algorithms**

| Algorithm | Frequency              | Pressure                       | Humidity               | Temperature                 | Rain Rate                             | Attenuation[dB/m] |
|-----------|------------------------|--------------------------------|------------------------|-----------------------------|---------------------------------------|-------------------|
| GWO       | 60.192353<br>843116930 | 1.0132500<br>00000000e<br>+03  | 44.6823657<br>04820970 | -<br>82.546563058<br>116600 | 1.499<br>99897<br>45206<br>25e+0<br>2 | 0.0953            |
| WOA       | 60.331650<br>117882624 | 9.3666064<br>83796969e<br>+02  | 63.7158987<br>22730500 | -<br>53.699469184<br>544590 | 1.488<br>21638<br>41406<br>27e+0<br>2 | 0.0867            |
| PSO       | 60.124568<br>771873854 | 1.0132500<br>00000000e<br>+03  | 88.5866966<br>78674060 | -100                        | 150                                   | 0.1002            |
| SCA       | 59.965610<br>732878890 | 9.8576539<br>75893566e<br>+02  | 15.0370867<br>76311675 | -<br>96.605785075<br>555640 | 1.490<br>26122<br>62035<br>88e+0<br>2 | 0.0966            |
| SSA       | 60.190846<br>138930596 | 1.0117105<br>02593708e<br>+03, | 50.7806108<br>75478910 | -<br>81.051898065<br>449410 | 1.498<br>48577<br>25477<br>94e+0<br>2 | 0.0945            |
| HHO       | 63.921180<br>520629190 | 7.2023922<br>10850908e<br>+02  | 55.2029406<br>76603596 | -<br>39.128755976<br>970530 | 1.371<br>99936<br>76064<br>10e+0<br>2 | 0.0715            |
| DA        | 60.124444<br>749663380 | 1.0102000<br>29006350e<br>+03  | 59.5765476<br>98760060 | -100                        | 150                                   | 0.1001            |
| MFO       | 60.124570<br>334567870 | 1.0132500<br>00000000e<br>+03  | 99.9999999<br>99931750 | -100                        | 150                                   | 0.1002            |
| GOA       | 60.144556<br>788252790 | 1.0132499<br>99999889e<br>+03  | 58.0452457<br>70665770 | -<br>94.999996949<br>358250 | 1.499<br>99999<br>05543<br>26e+0<br>2 | 0.0991            |

|      |                        |                               |                        |                             |                                       |        |
|------|------------------------|-------------------------------|------------------------|-----------------------------|---------------------------------------|--------|
| IGWO | 60.125307<br>810643270 | 1.0132423<br>93294994e<br>+03 | 58.8683990<br>80388100 | -<br>99.999473537<br>860800 | 1.499<br>99372<br>48800<br>19e+0<br>2 | 0.1002 |
|------|------------------------|-------------------------------|------------------------|-----------------------------|---------------------------------------|--------|

It is apparent that the highest attenuation is 0.1002 dB/m, and the most accurate result should be the one given by MFO. The probable worst operating condition can be the one given by 60.124570334567870 GHz, .013250000000000e+03 mbar, 99.99999999931750 % humidity, -100°C, 150 mm/hr.

The reason for such a conclusion is that the humidity is a very sensitive variable to attenuation. Only humidity above 99%, the attenuation factor gives a peak.

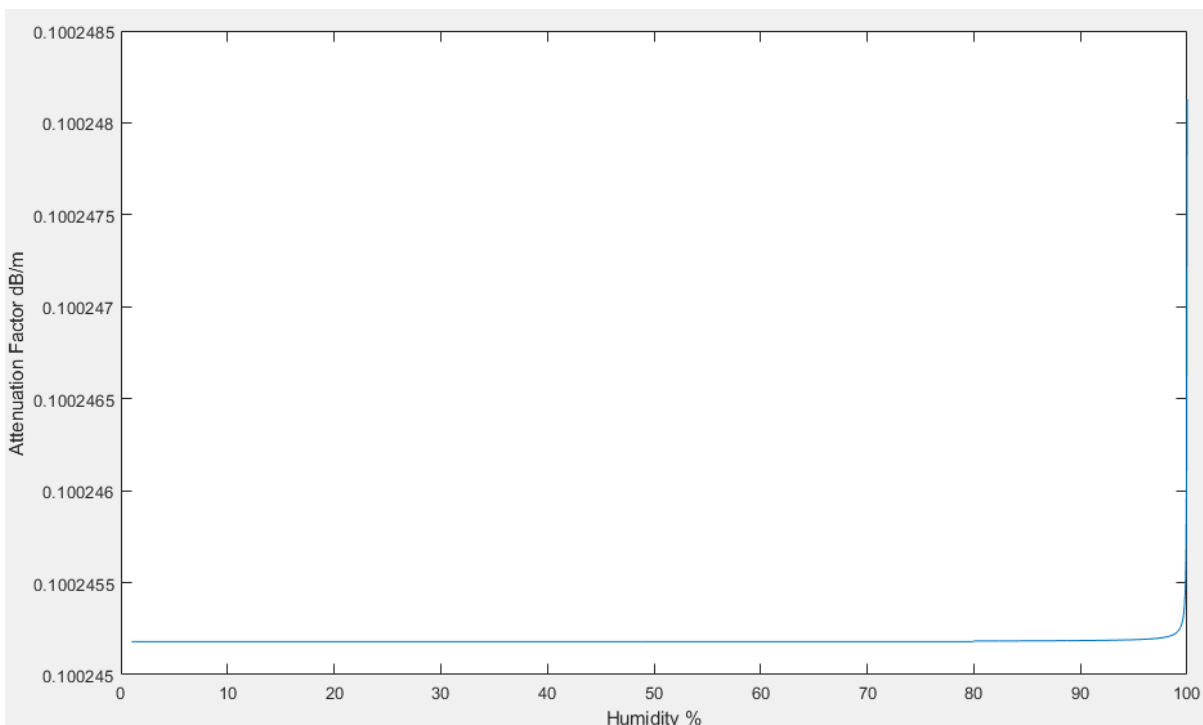


**Figure 2.4.2:** Attenuation Factor with respect to Humidity

This is a plot of attenuation factor with respect to humidity where frequency is 60.132GHz, temperature -100°C, pressure is 1013.25 mbar, and rain rate is 150 mm/hr. This is a very interesting result because maximum attenuation occurs near 60GHz where normal Free space loss occurs at the maximum possible frequency which in this case should be 100GHz.

## 2.4.2 Finding the best algorithm

For this part, the authors intend to find the algorithm that gives the near accurate result in the shortest iteration. 100 different runs were taken to determine the fastest algorithm. The determining condition was that if the algorithm hits the maximum attenuation point more than 3 times, the algorithm terminates the iteration. After the 100 runs, the number of iterations for an algorithm was averaged to determine the best algorithm. Rounded up values are listed in the table.

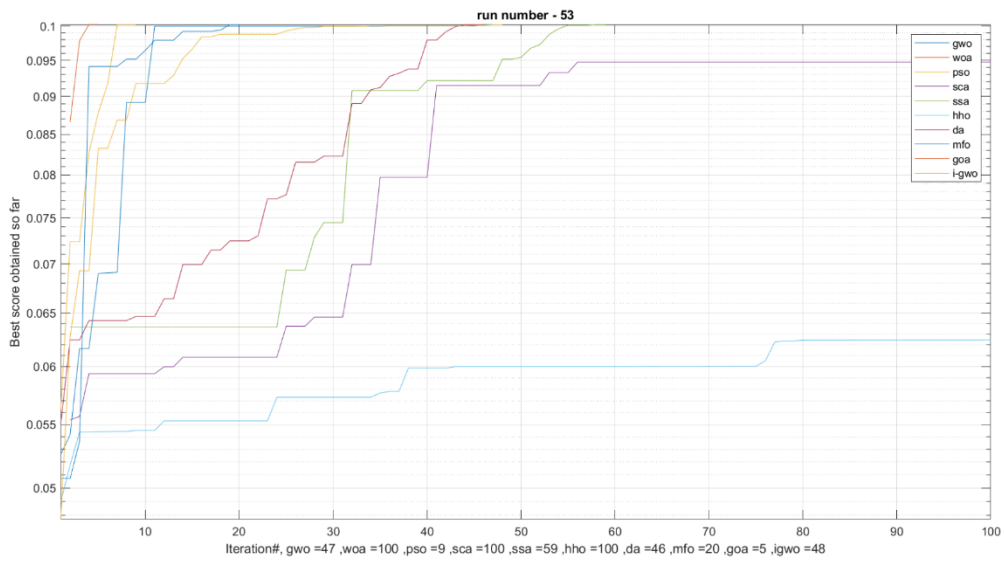
**Table 2.4.2: Number of iterations for different algorithms**

| GWO | WOA | PSO | SCA | SSA | HHO | DA | MFO | GOA | IGWO |
|-----|-----|-----|-----|-----|-----|----|-----|-----|------|
| 57  | 96  | 19  | 98  | 68  | 100 | 39 | 22  | 21  | 48   |

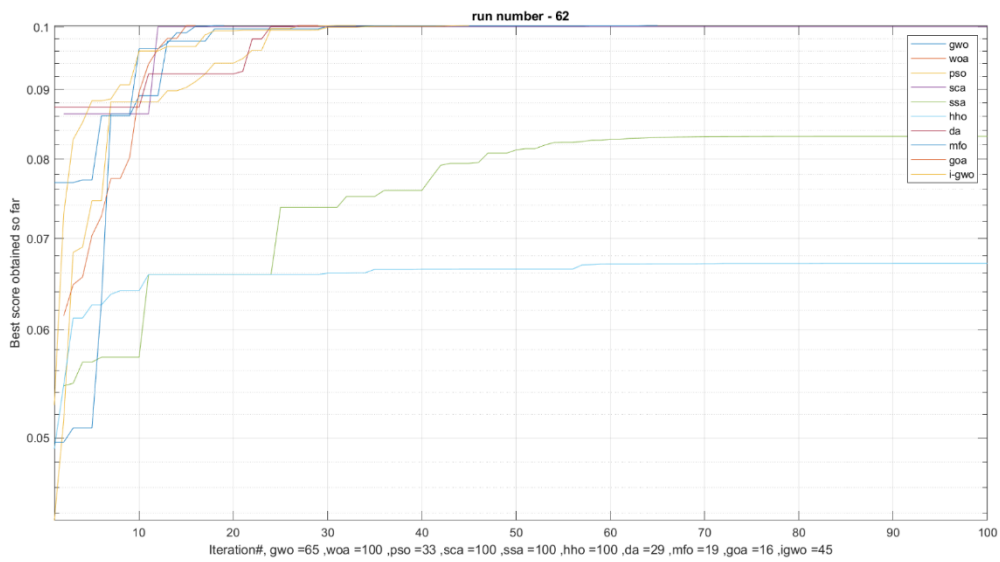
On average PSO can reach the maximum point within 19 iterations. In the best-case scenario among 100 different runs, PSO was able to reach the point within 9 iterations. In the worst - case scenario, PSO took 33 iterations. In the best case scenario, PSO gave the probable accurate result that is 60.0295581622350GHz frequency, 1013.25 mbar, 100% humidity, -100°C and 150 mm/hr rain rate. In the worst-case scenario, PSO gave the operating condition as 60.1144905688075 GHz, 1013.25mbar, 41.8539737488666 %, -100°C, 150 mm/hr

In the case of MFO, it takes 22 iterations on average. Best case scenario is when MFO finds the point within 13 iterations; on the contrary, worst case is when iteration is 30. In the best case, MFO gave the condition as 60.103063896557GHz, 1013.25mbar, 44.9466370543853 % , -100°C, 150 mm/hr, and for the worst case, the result is 60.1584836398928 GHz, 1013.25mbar, 5.90070148429986%, -100 °C, 150mm/hr.

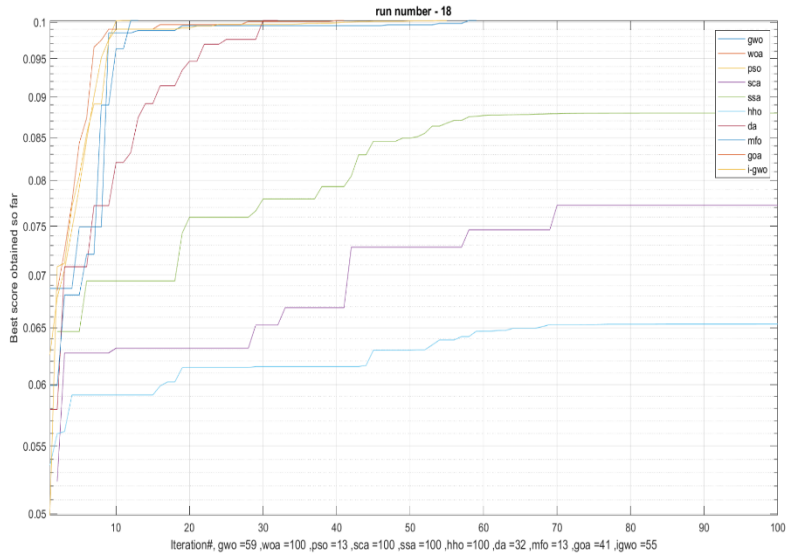
However, On average PSO is the fastest with the near accurate result among ten algorithms, and MFO is the second fastest with the most accurate result.



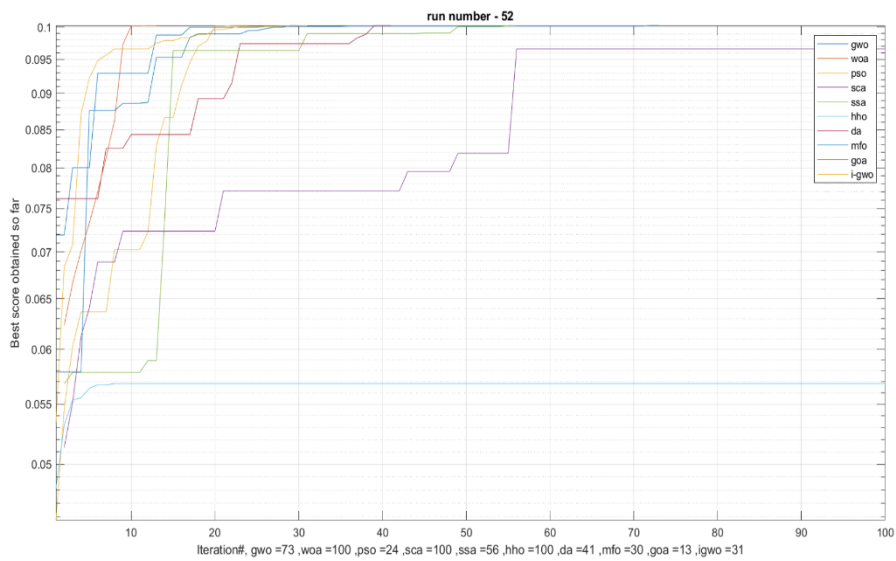
**Figure 2.4.3:** PSO best case scenario



**Figure 2.4.4:** PSO worst case scenario

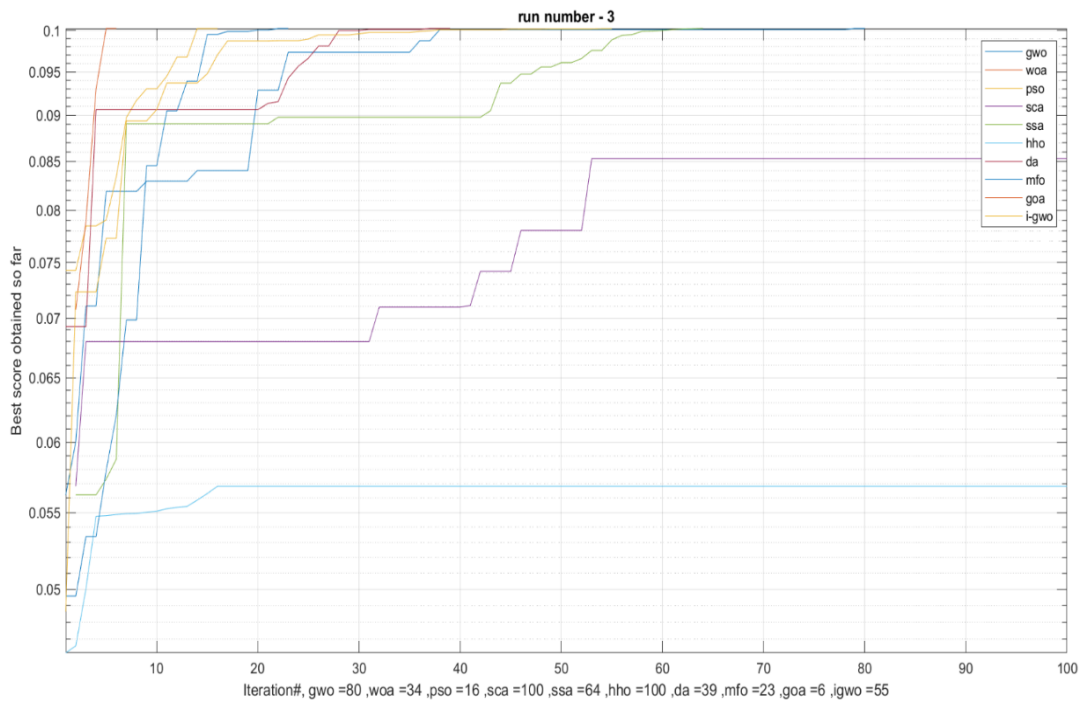
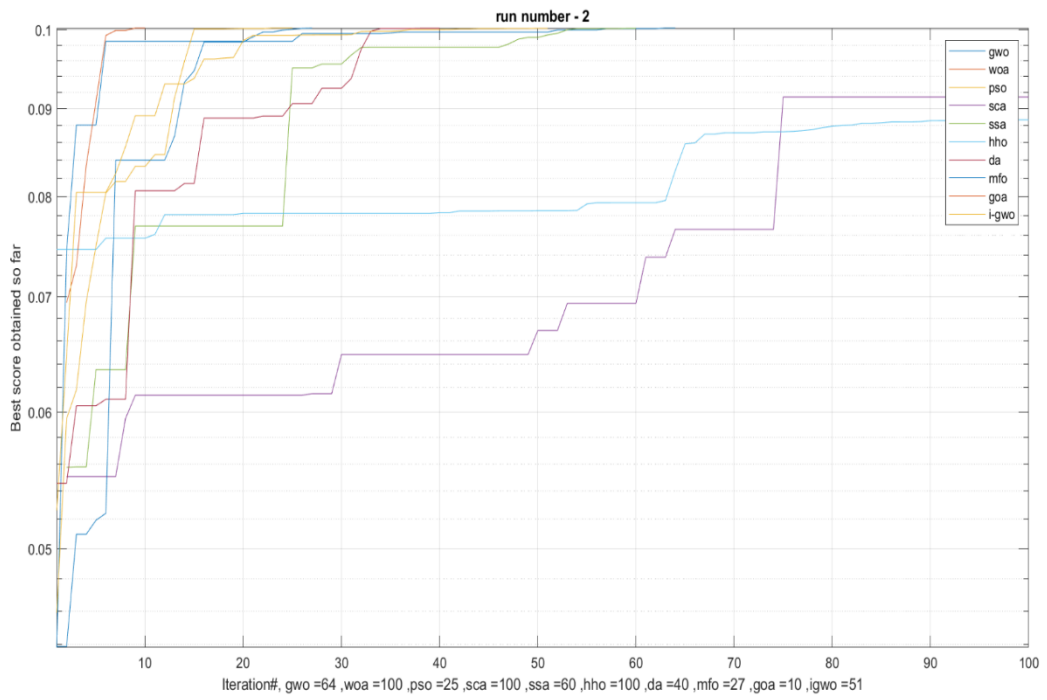


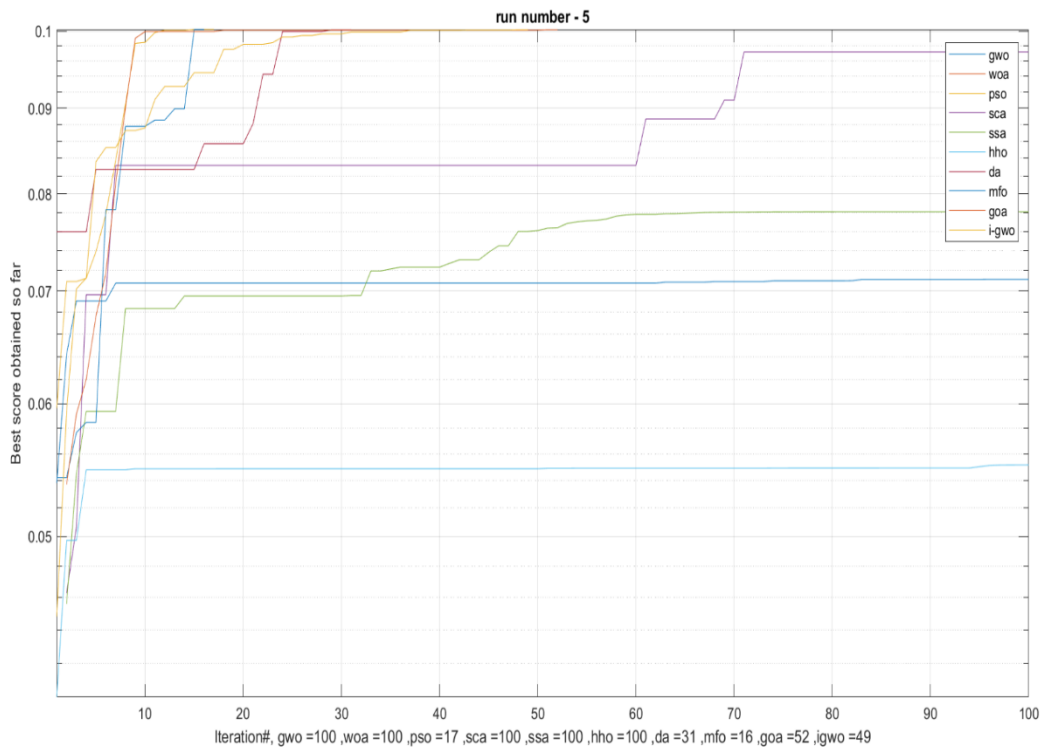
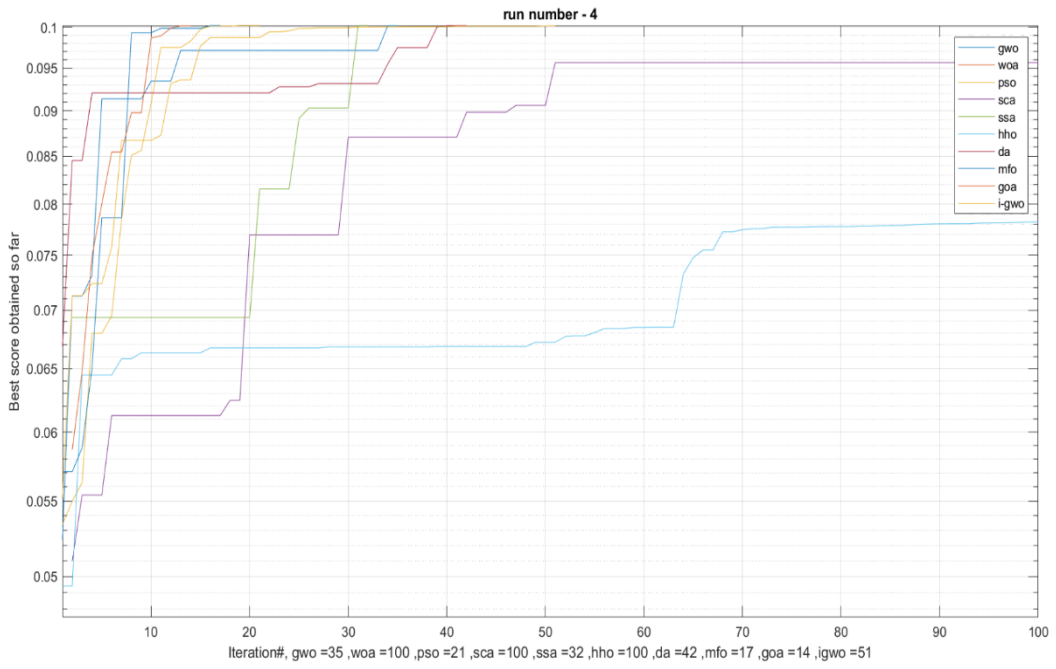
**Figure 2.4.5: MFO best case scenario**



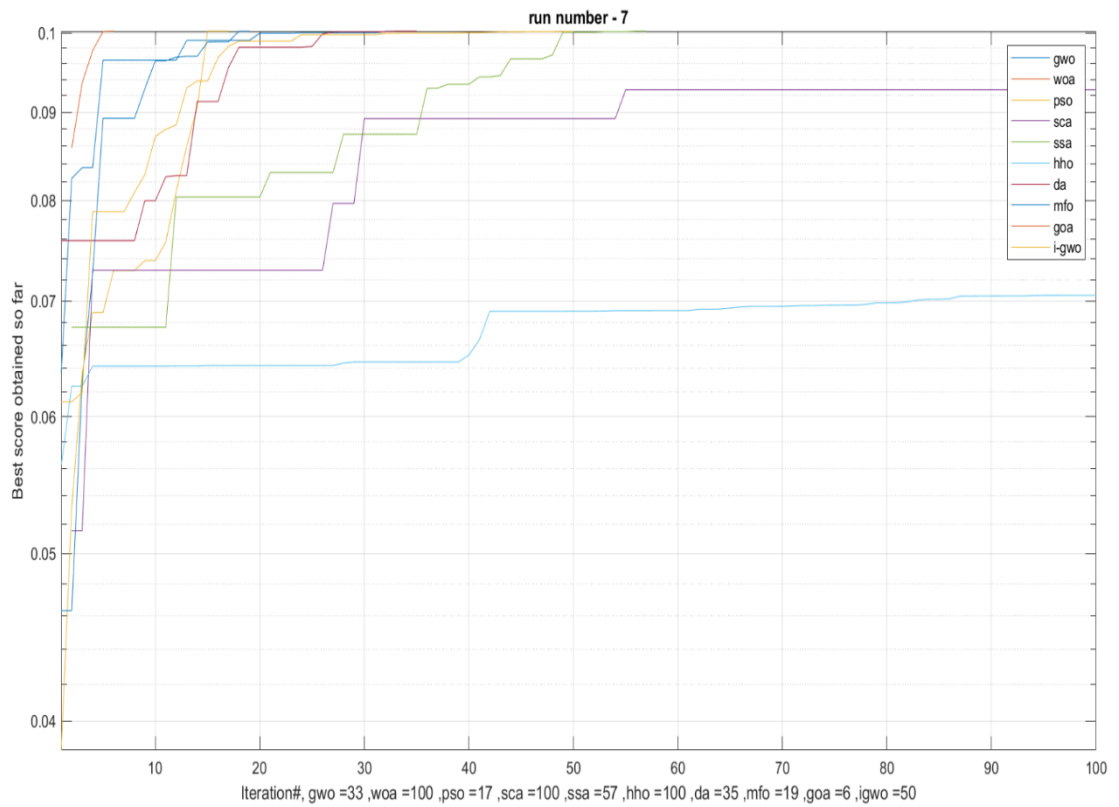
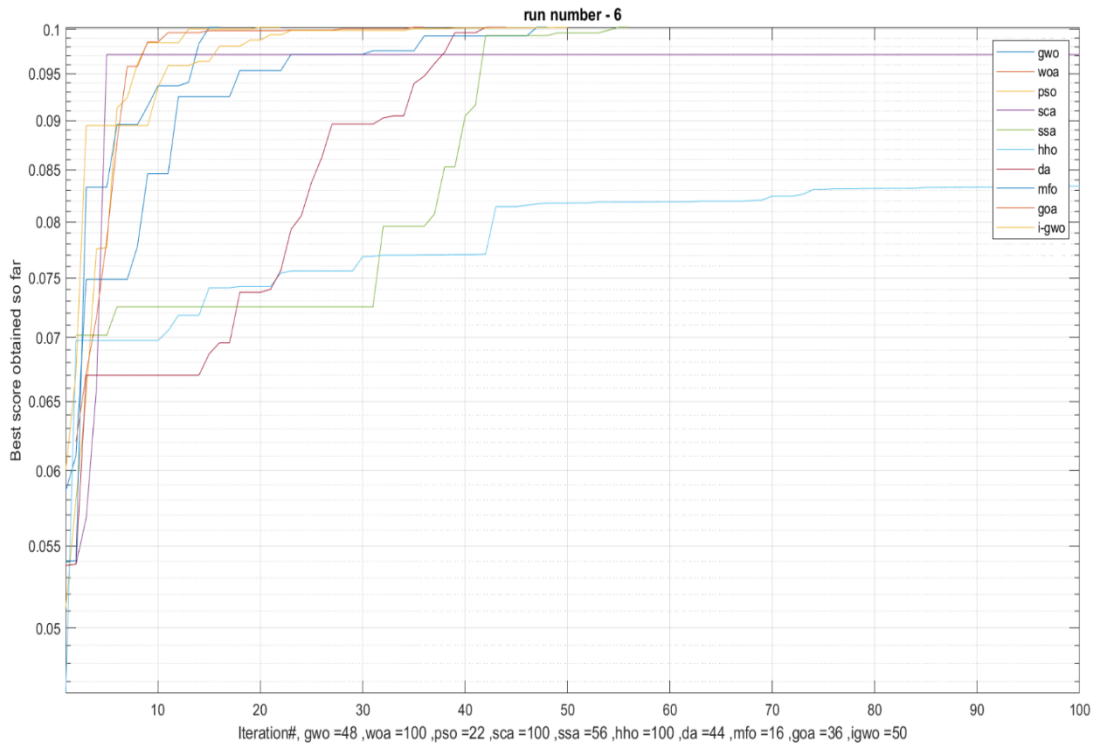
**Figure 2.4.6: MFO worst case scenario**

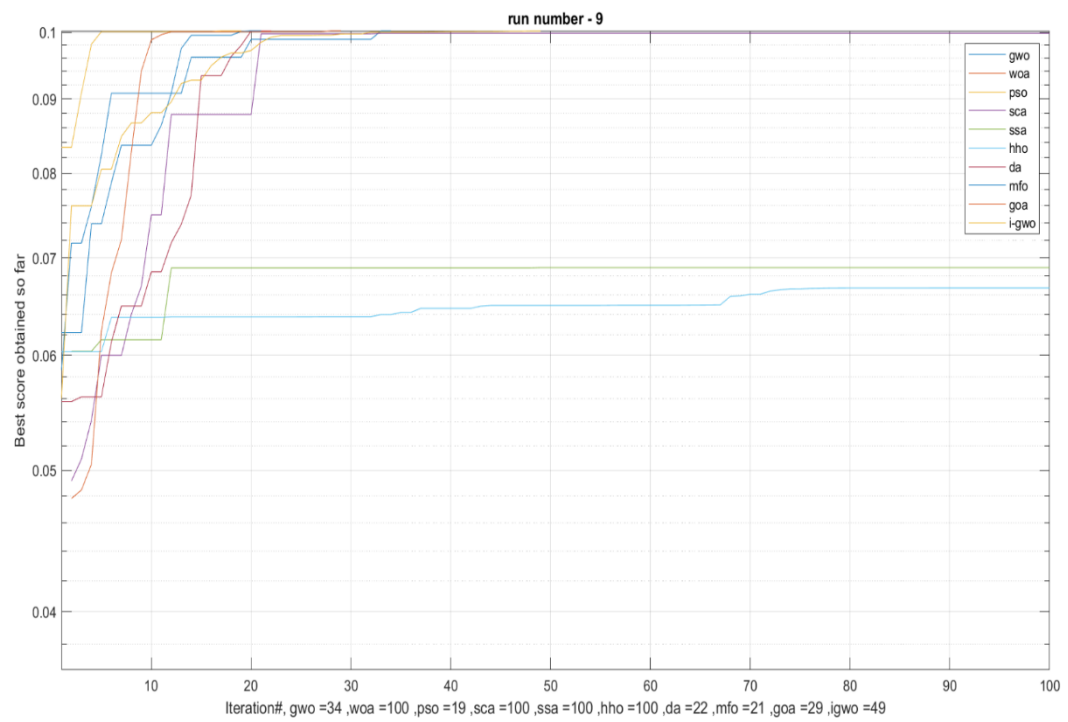
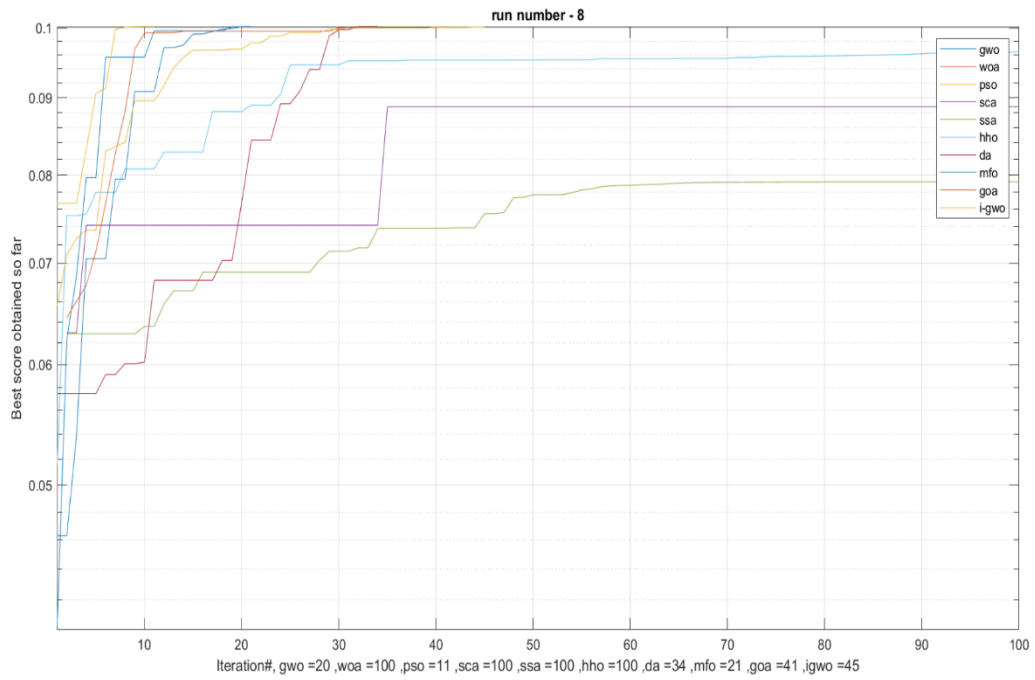
Figures (convergence curves) of other different run results are given below

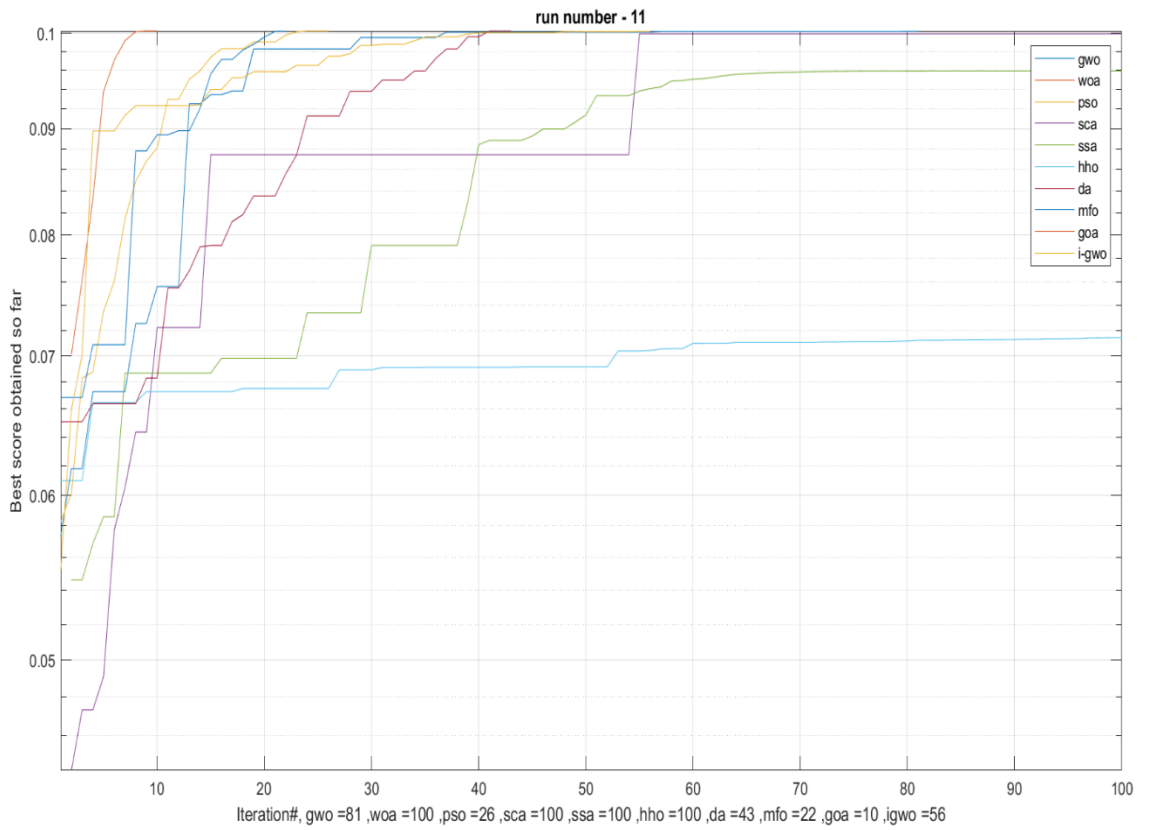
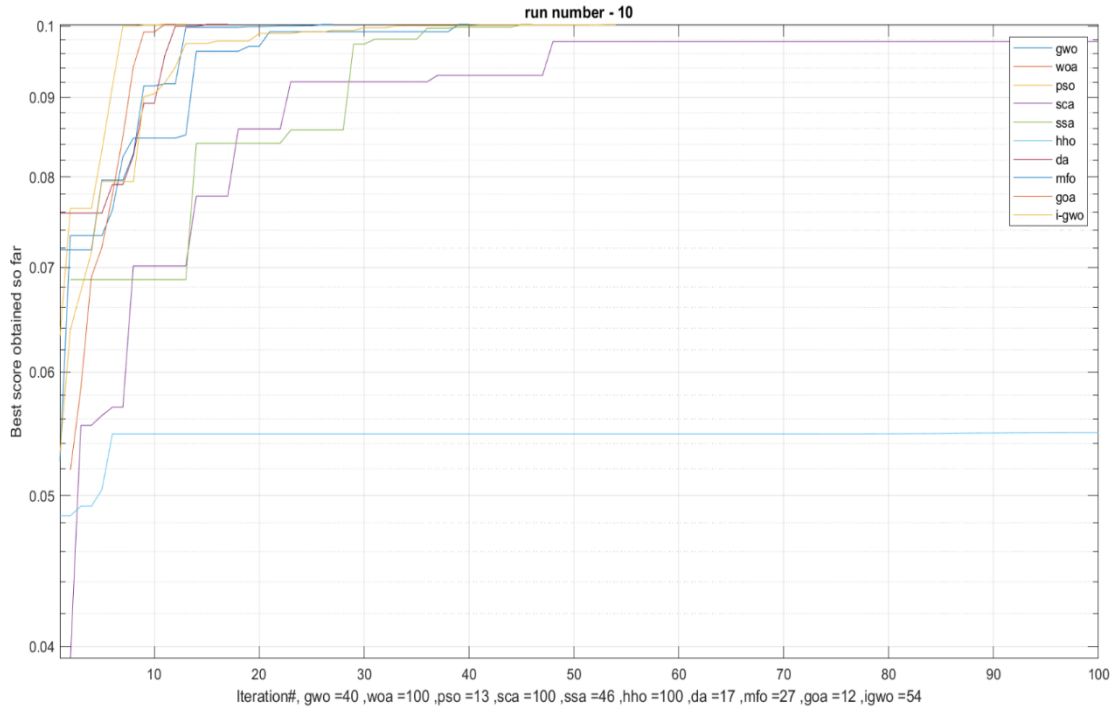


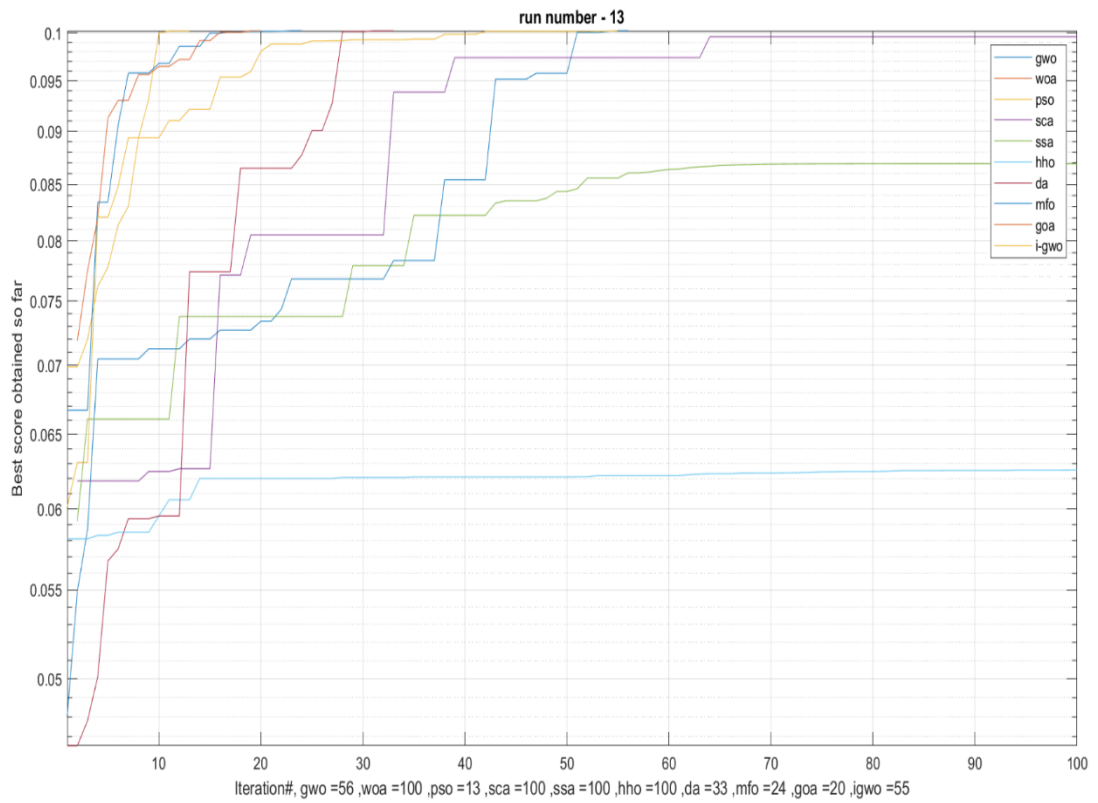
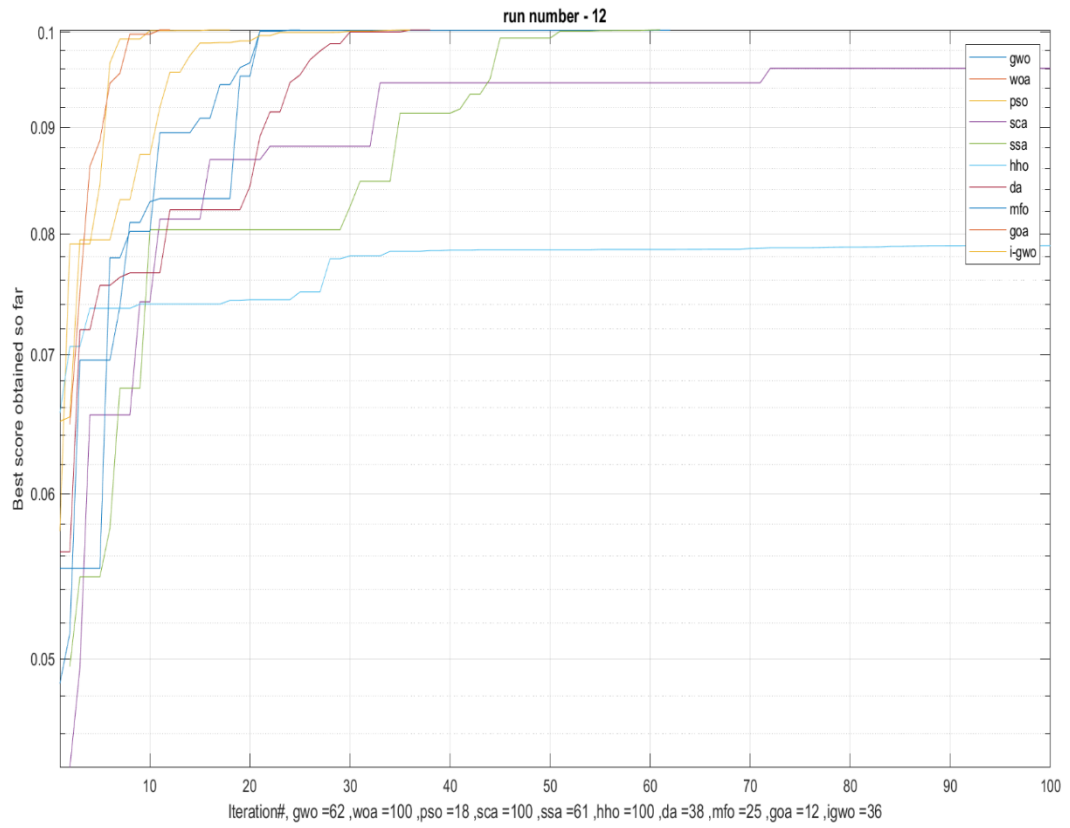


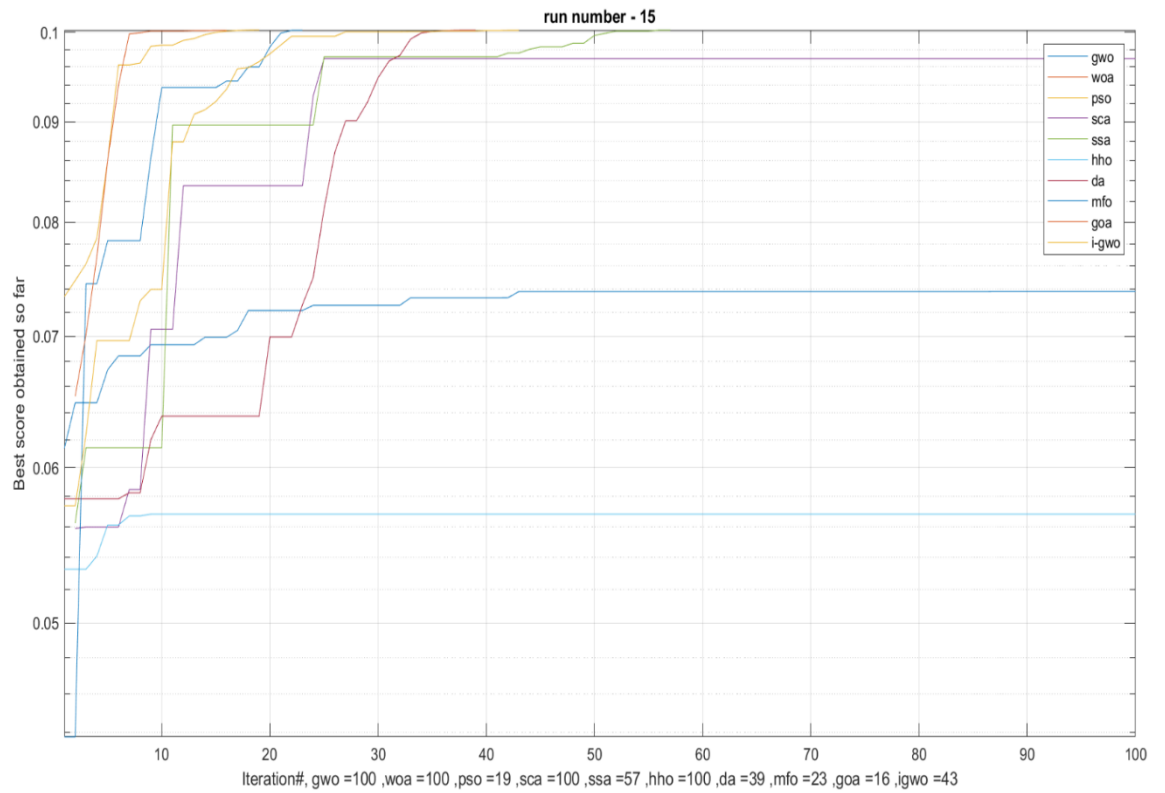
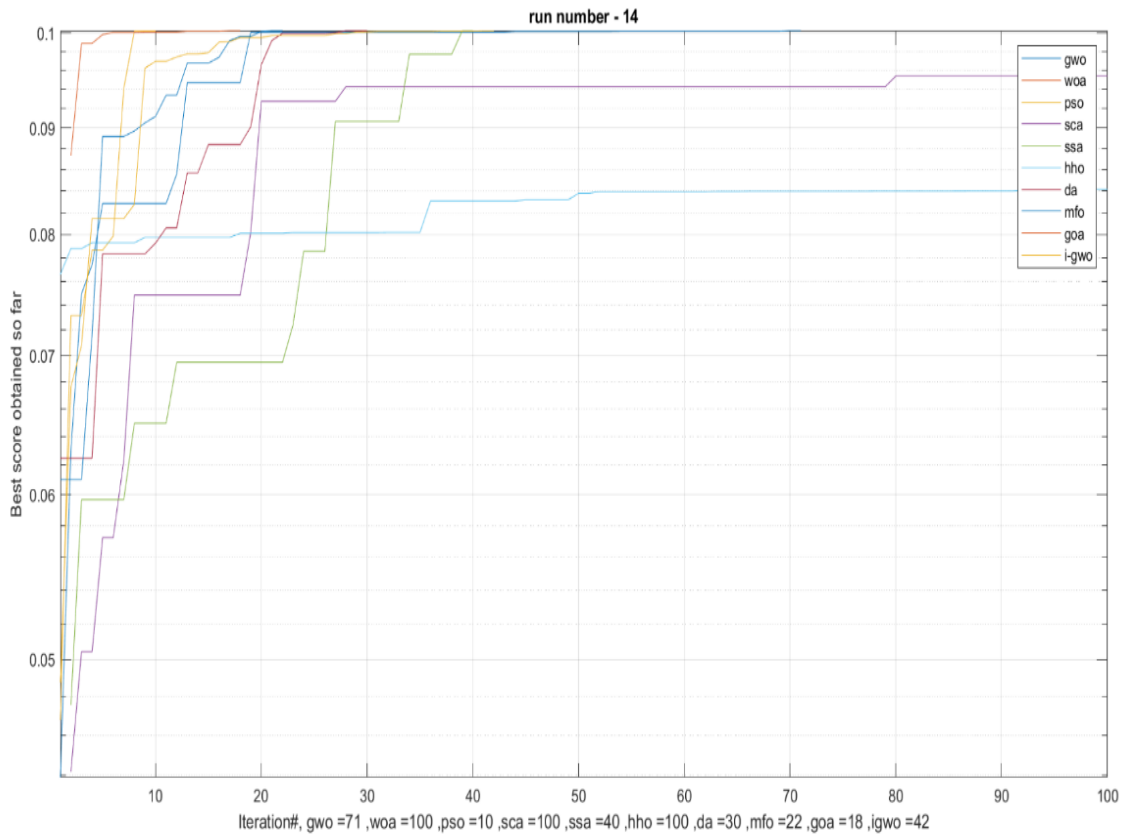


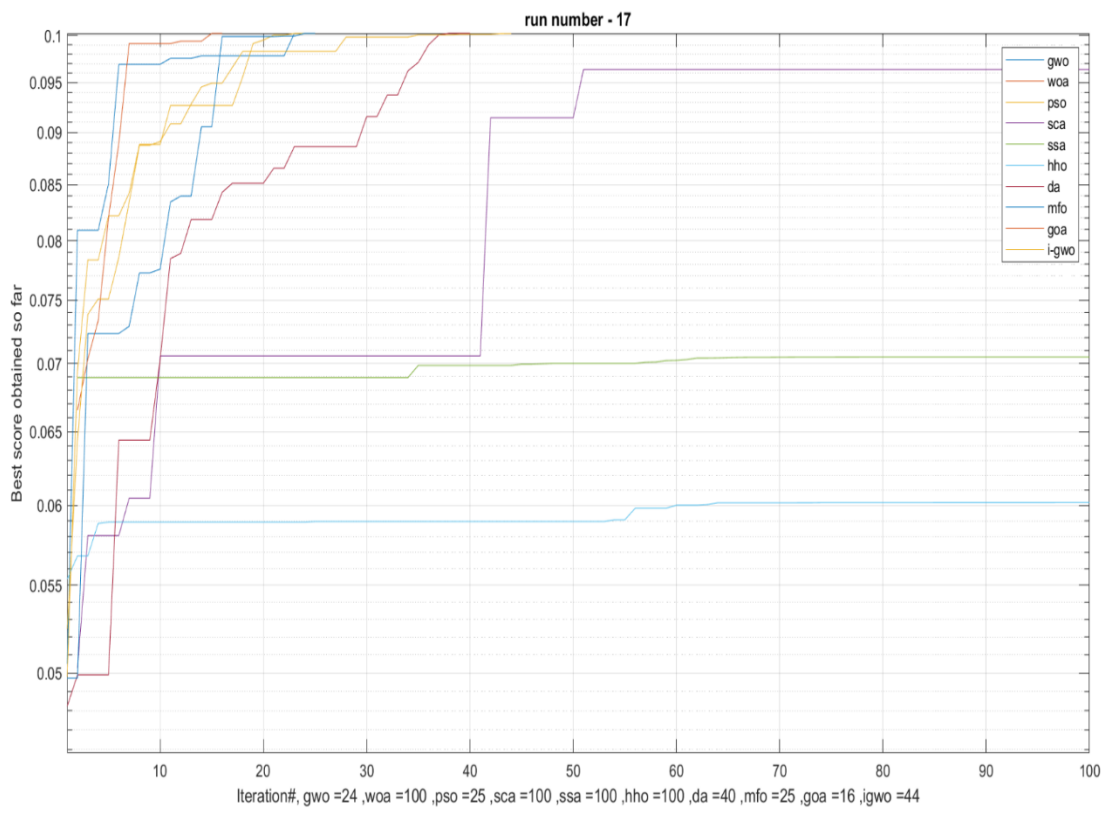
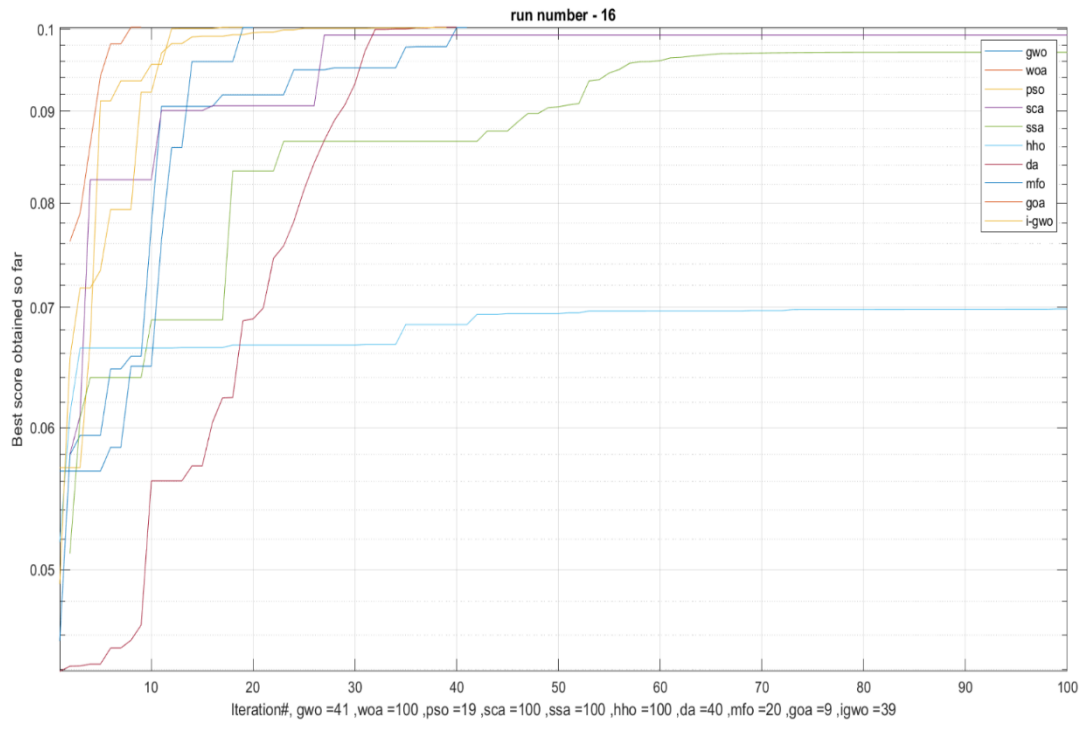


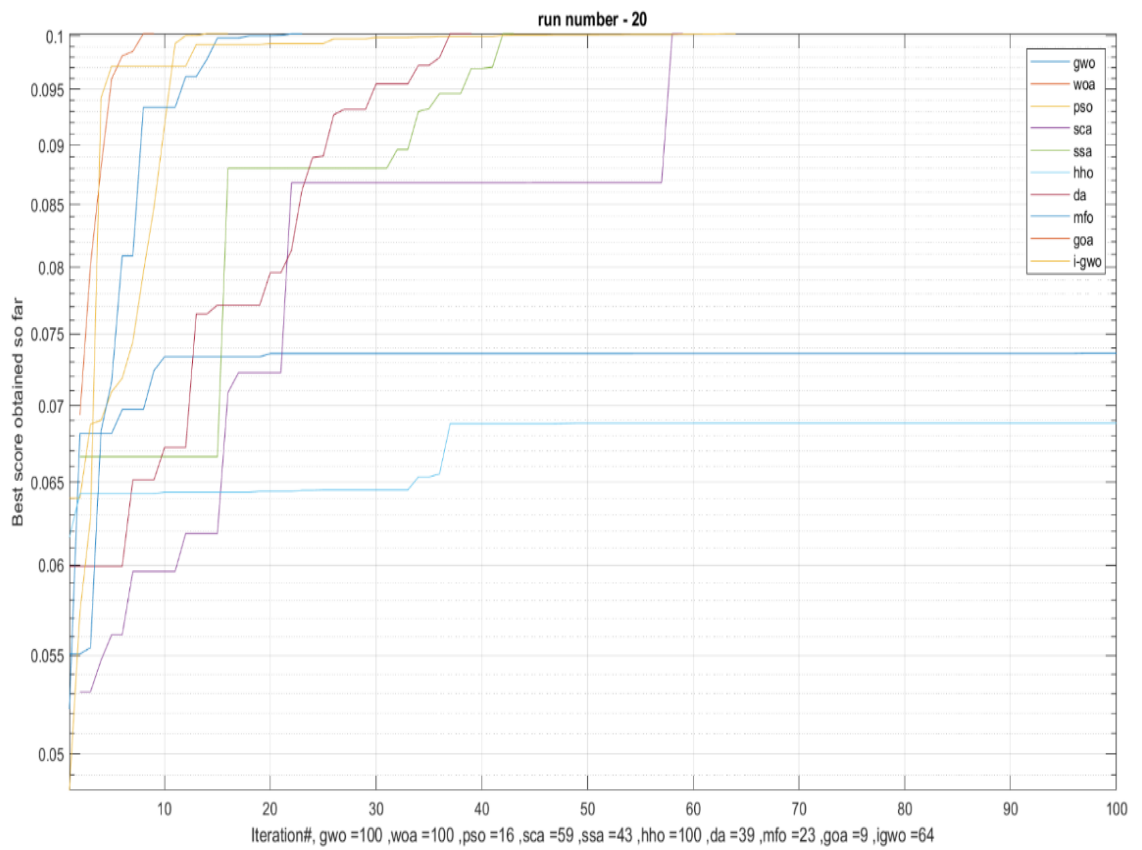
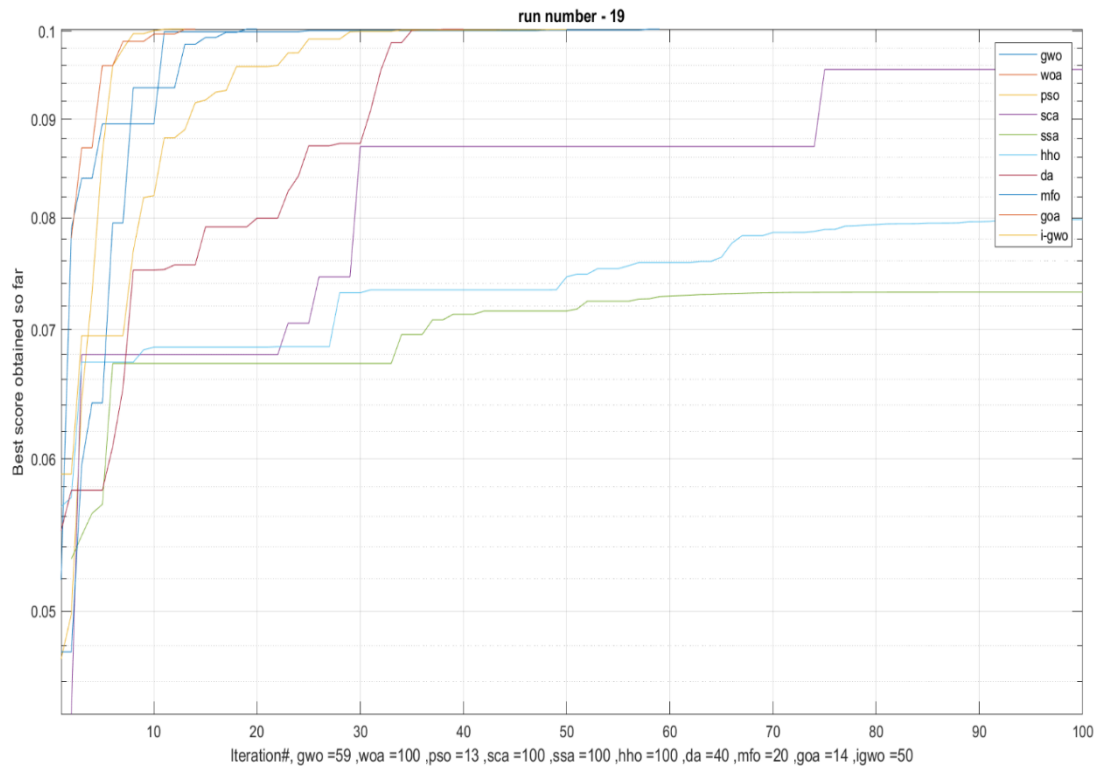


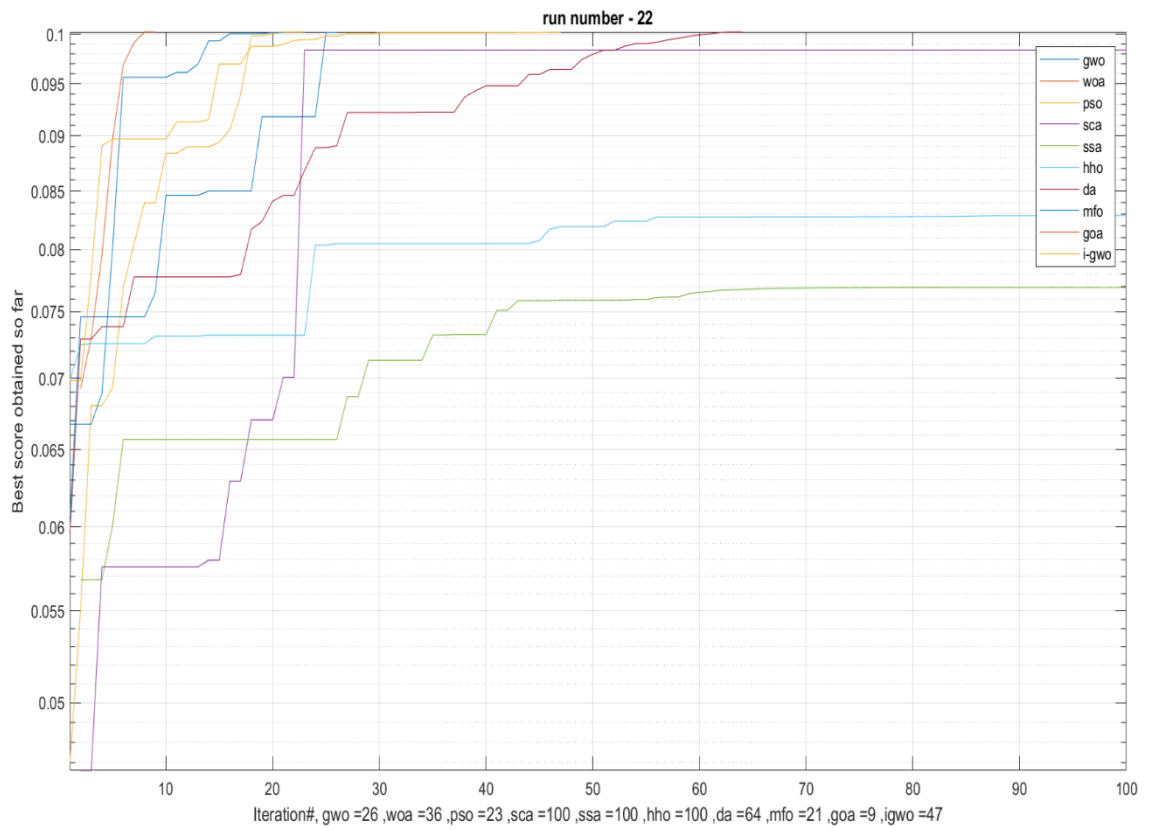
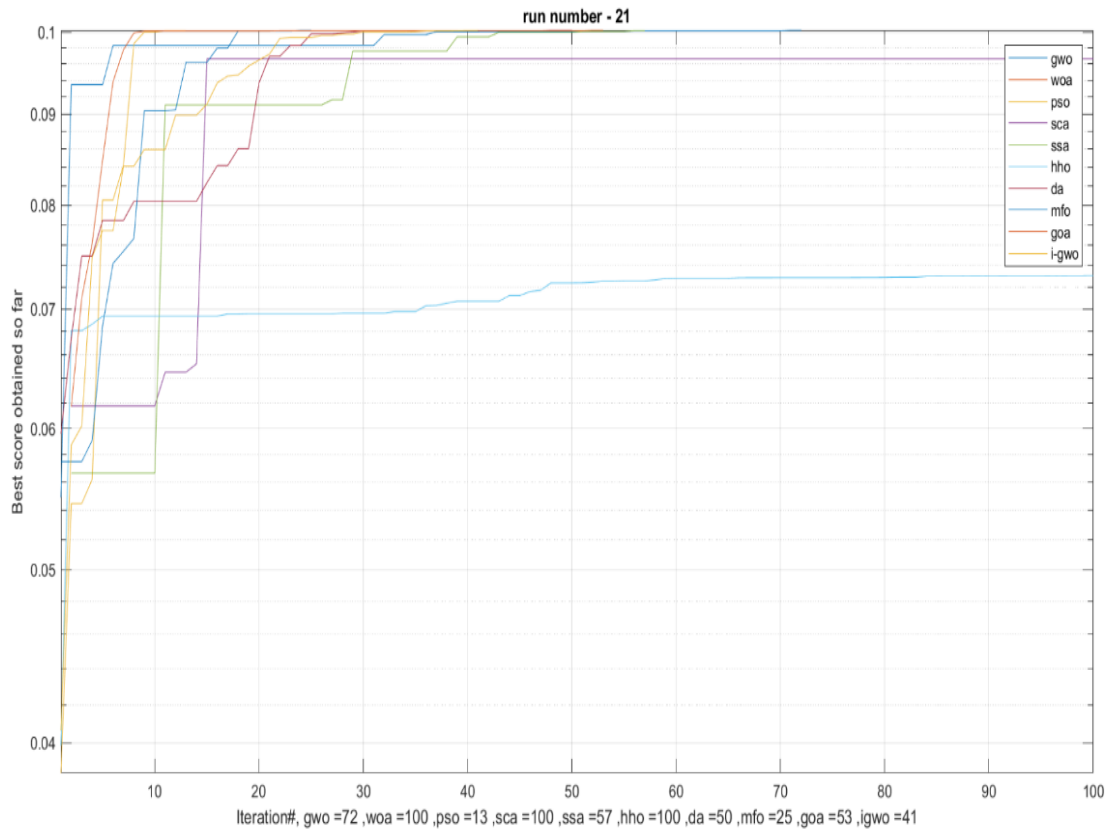




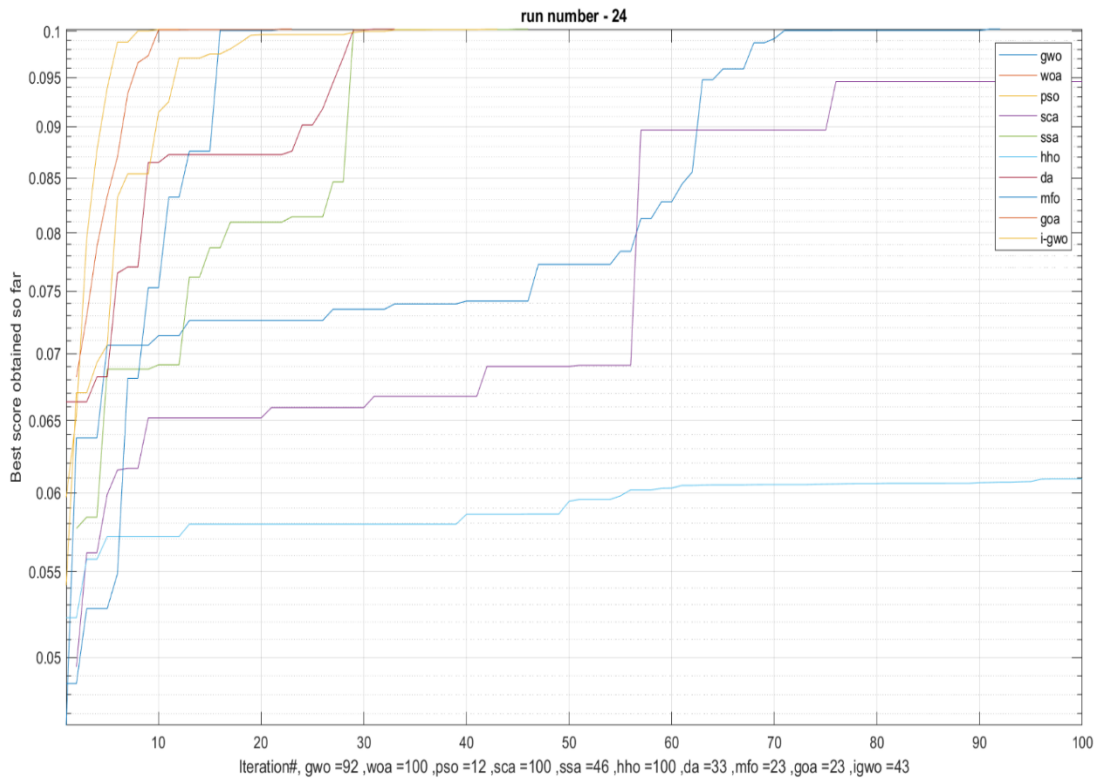
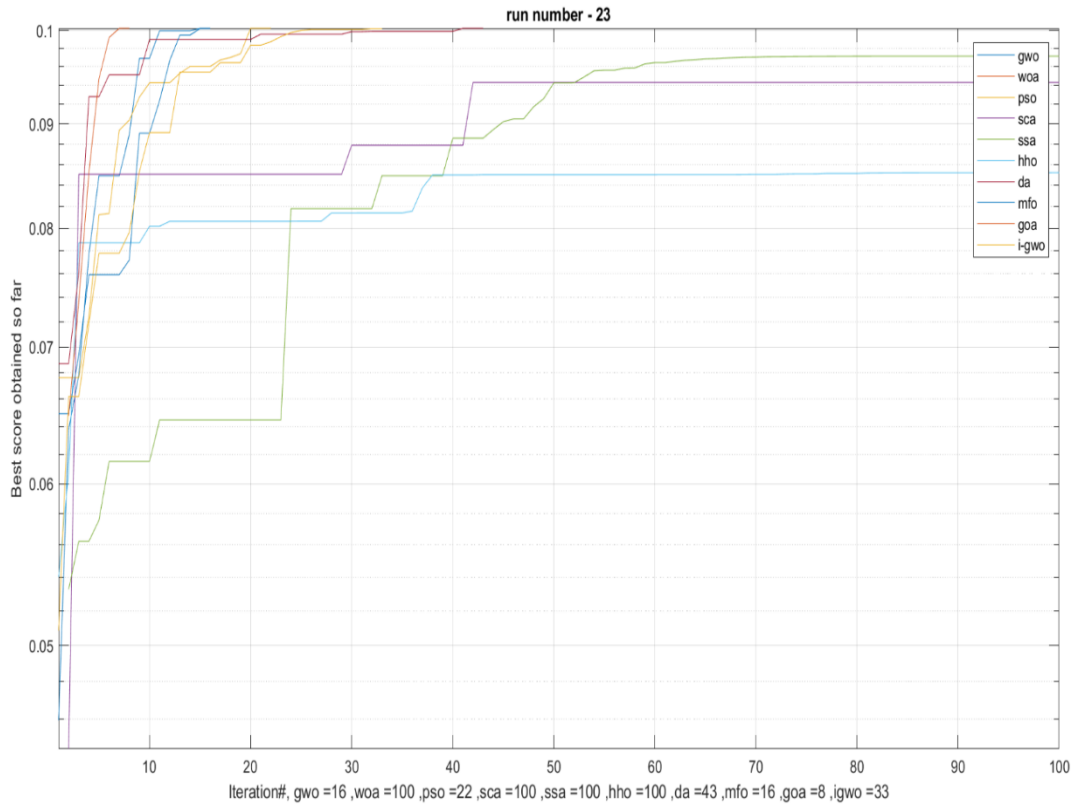


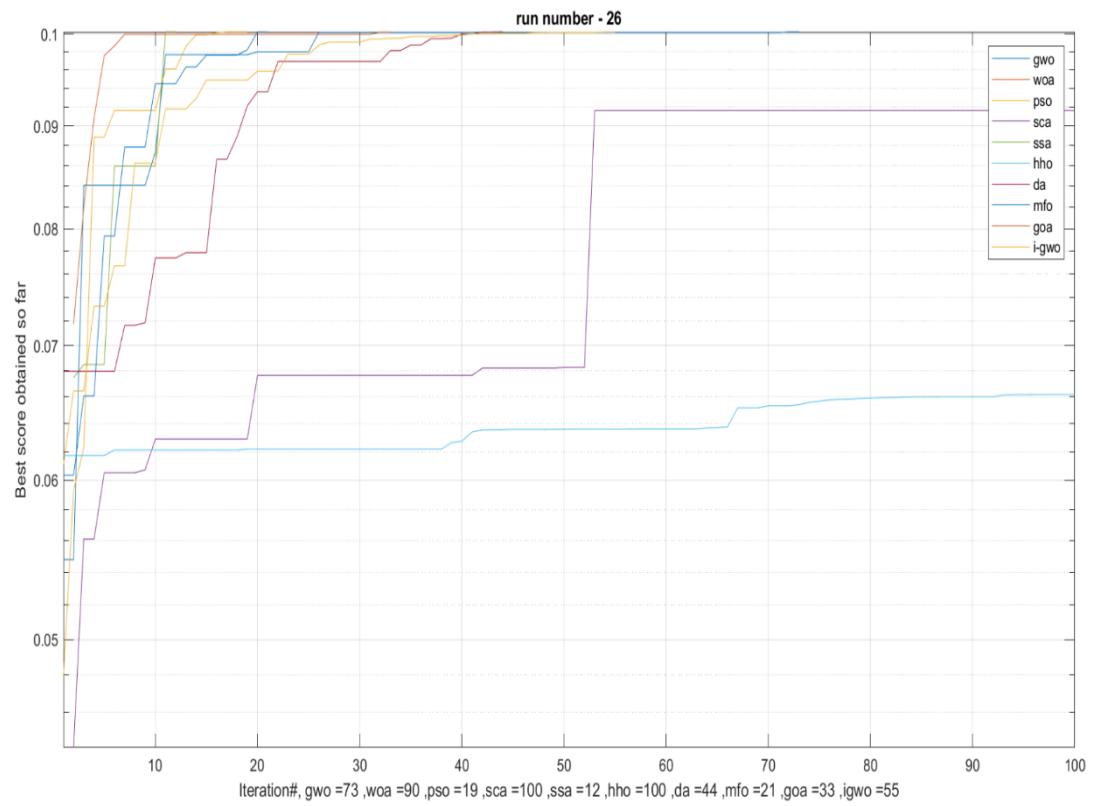
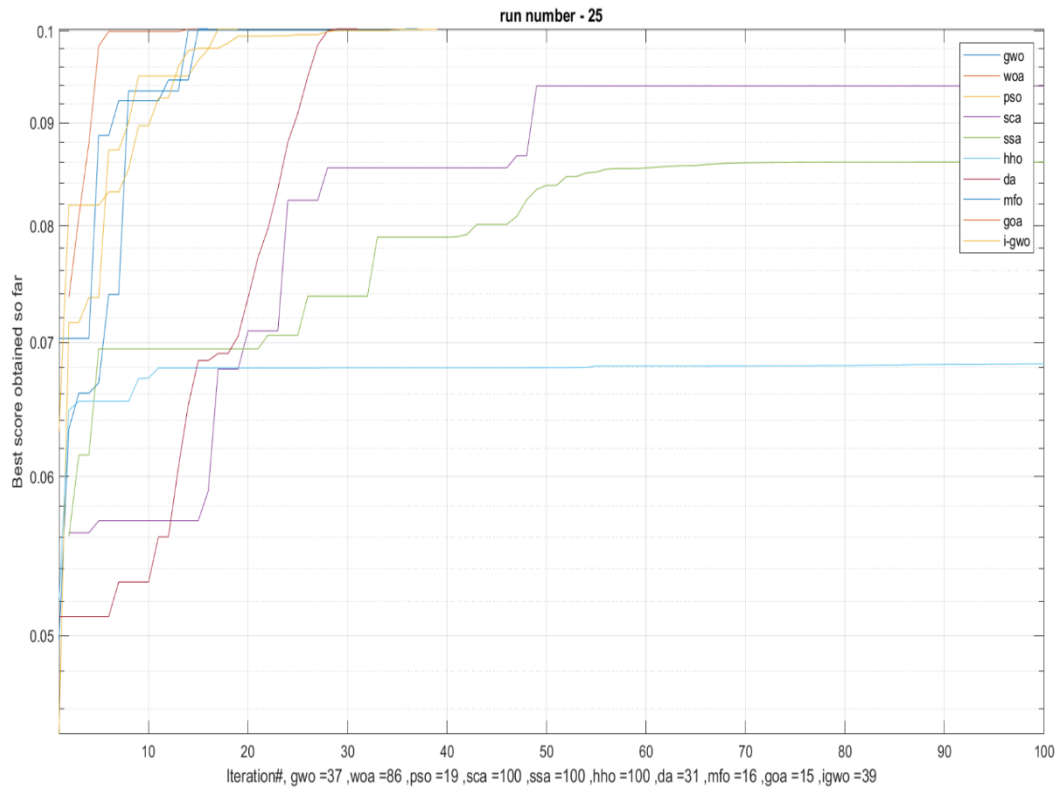


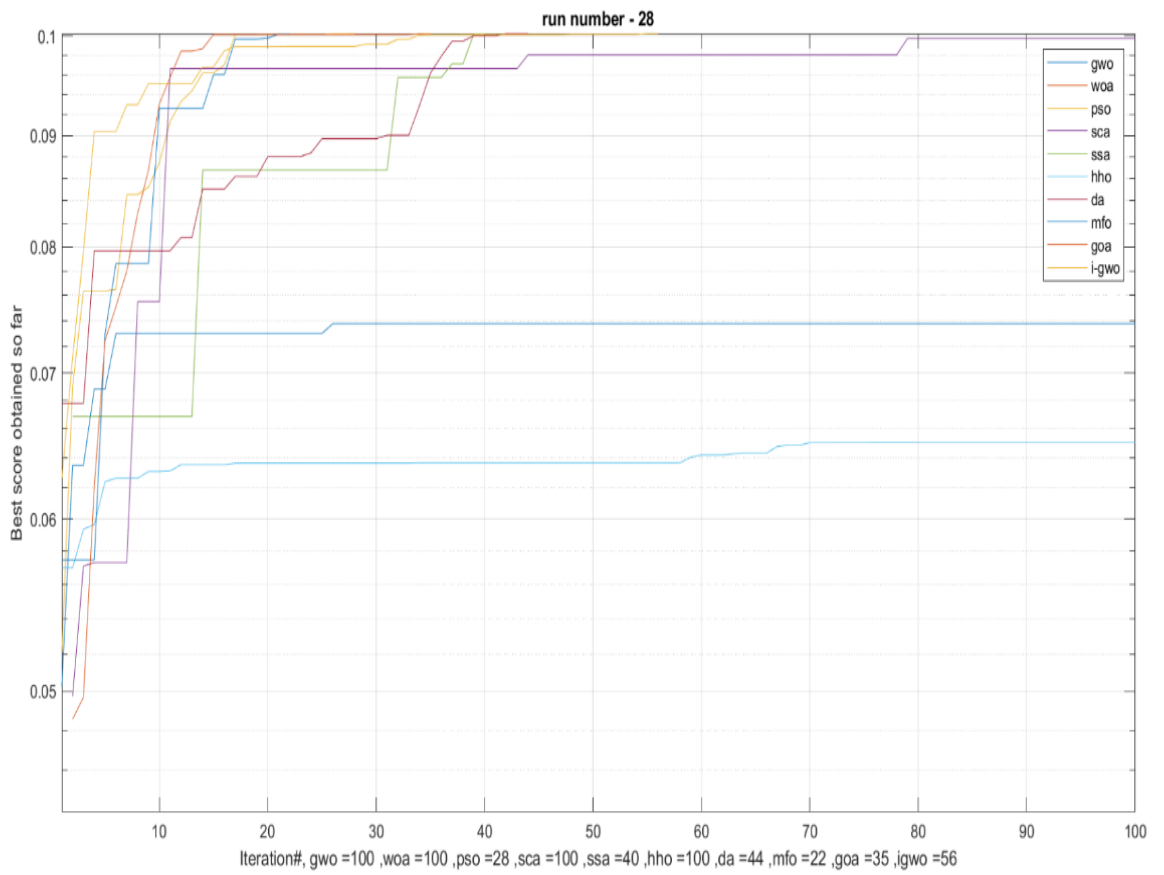
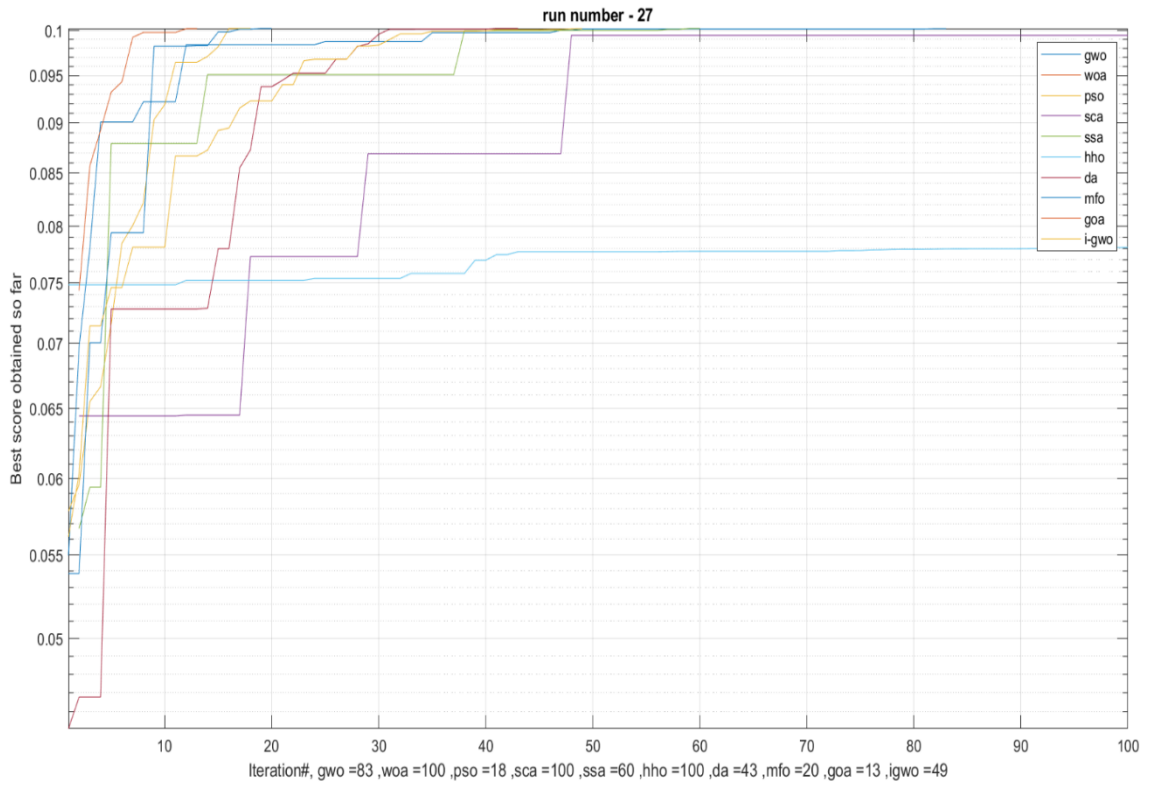


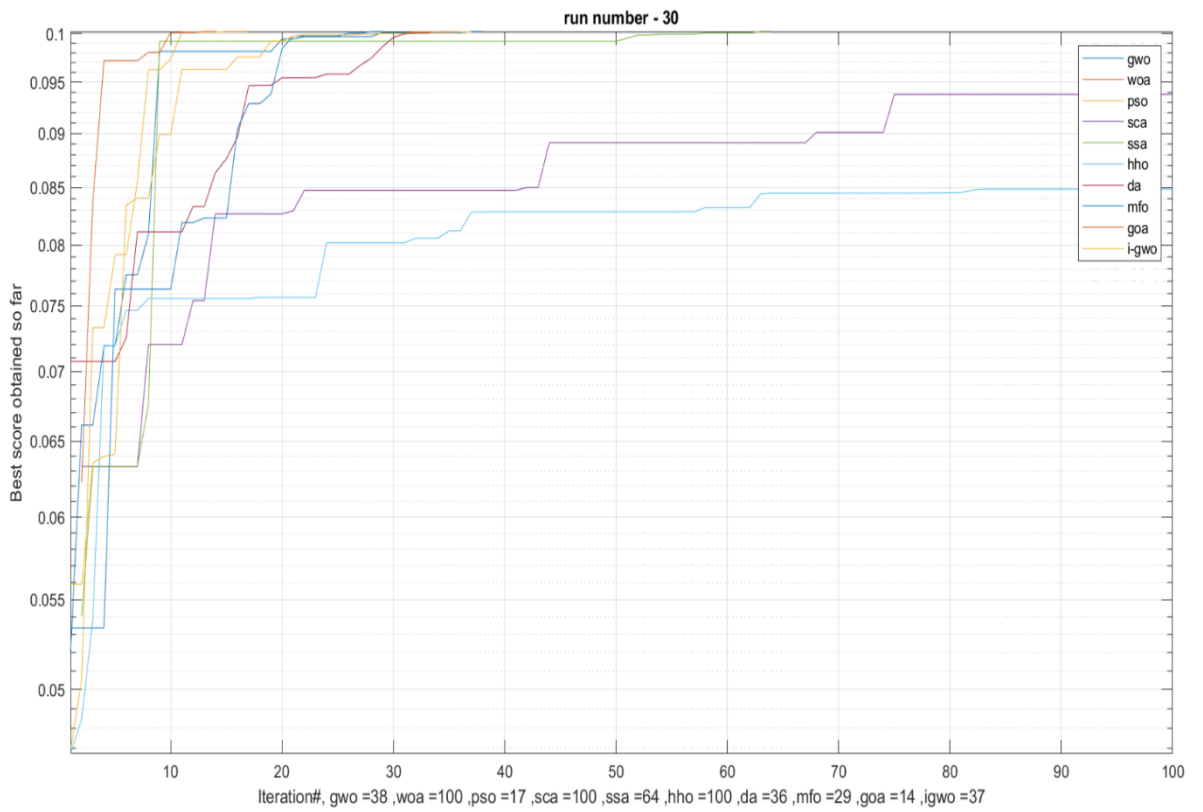
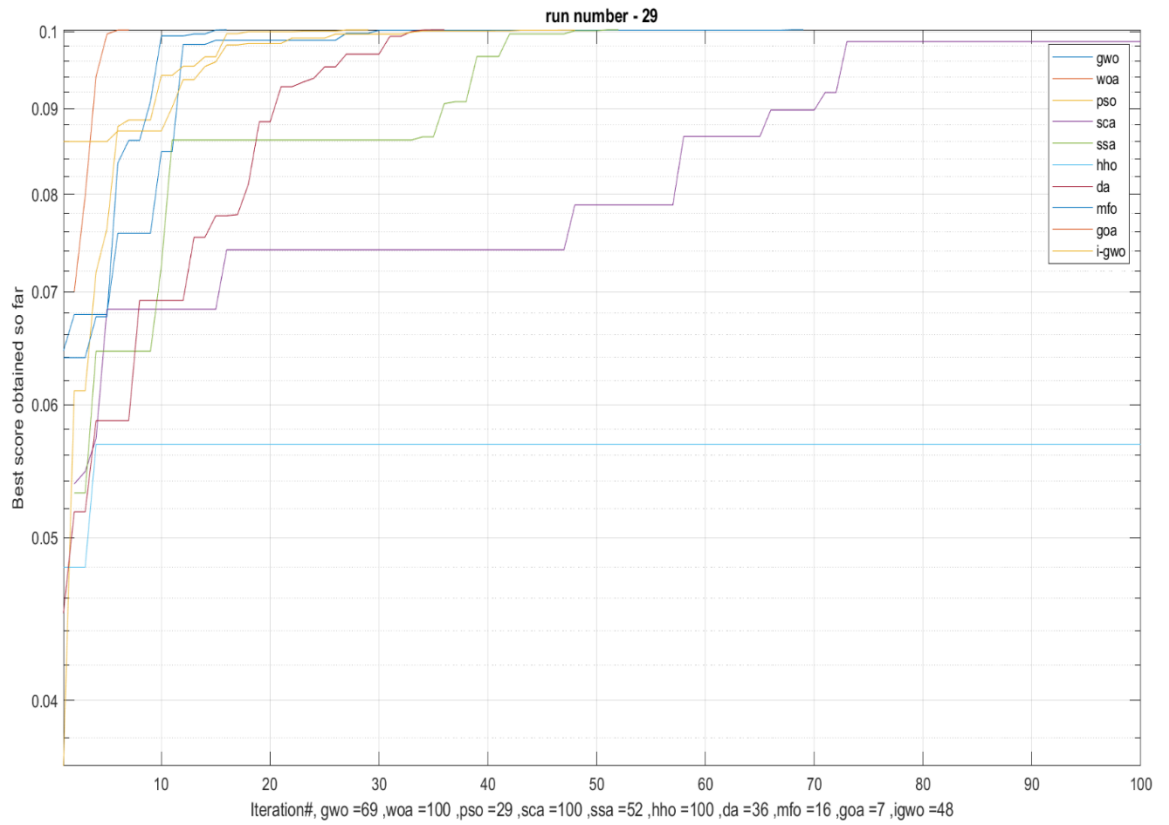


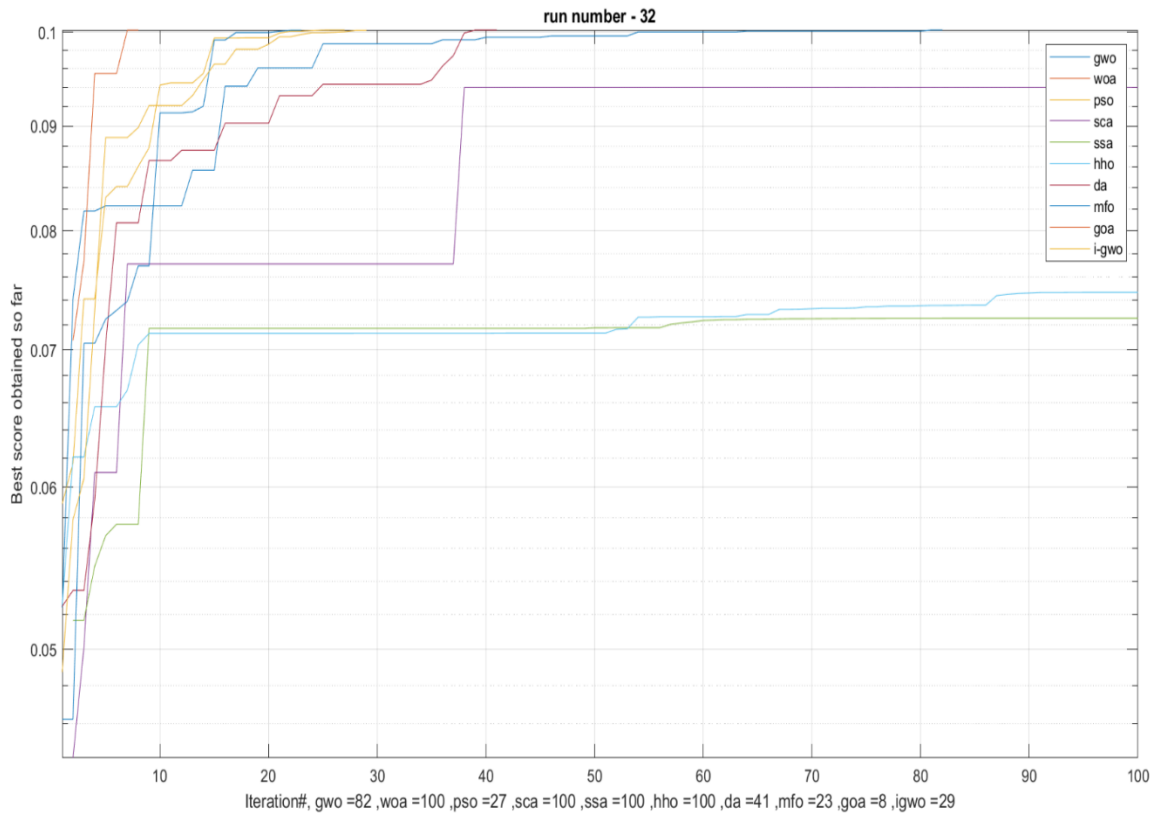
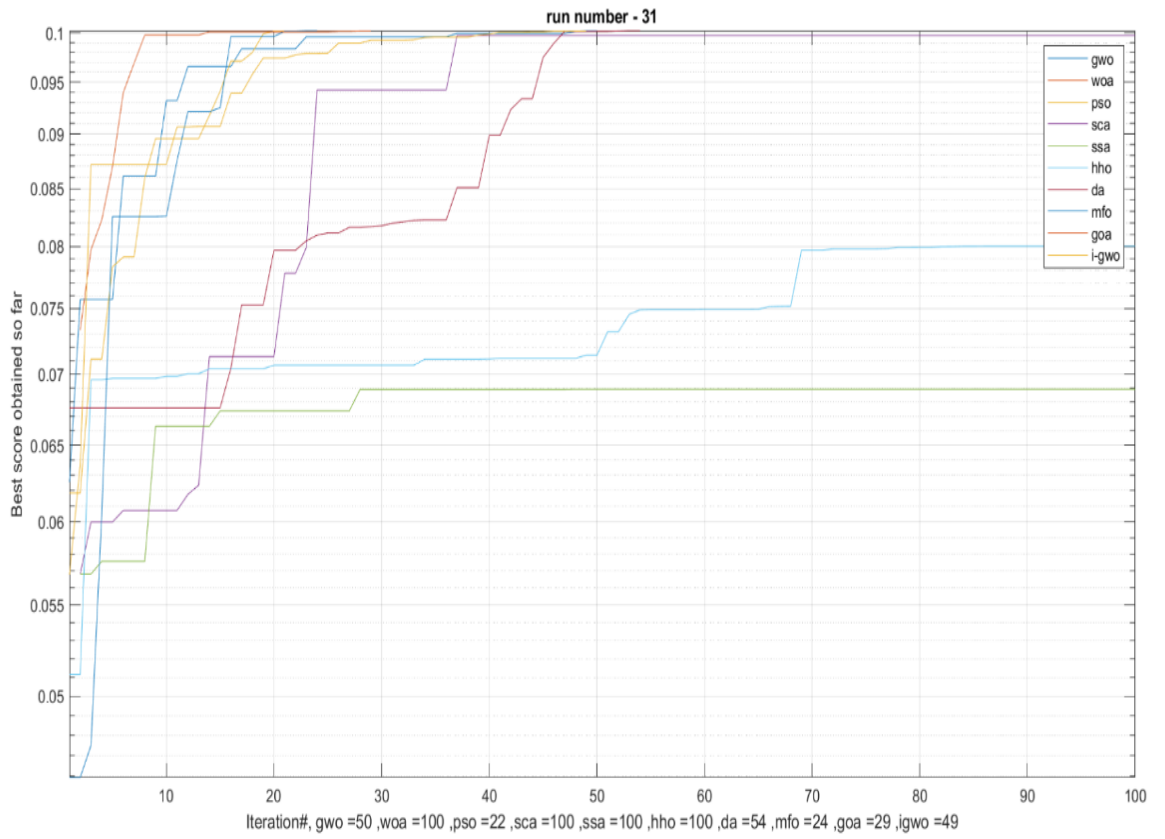


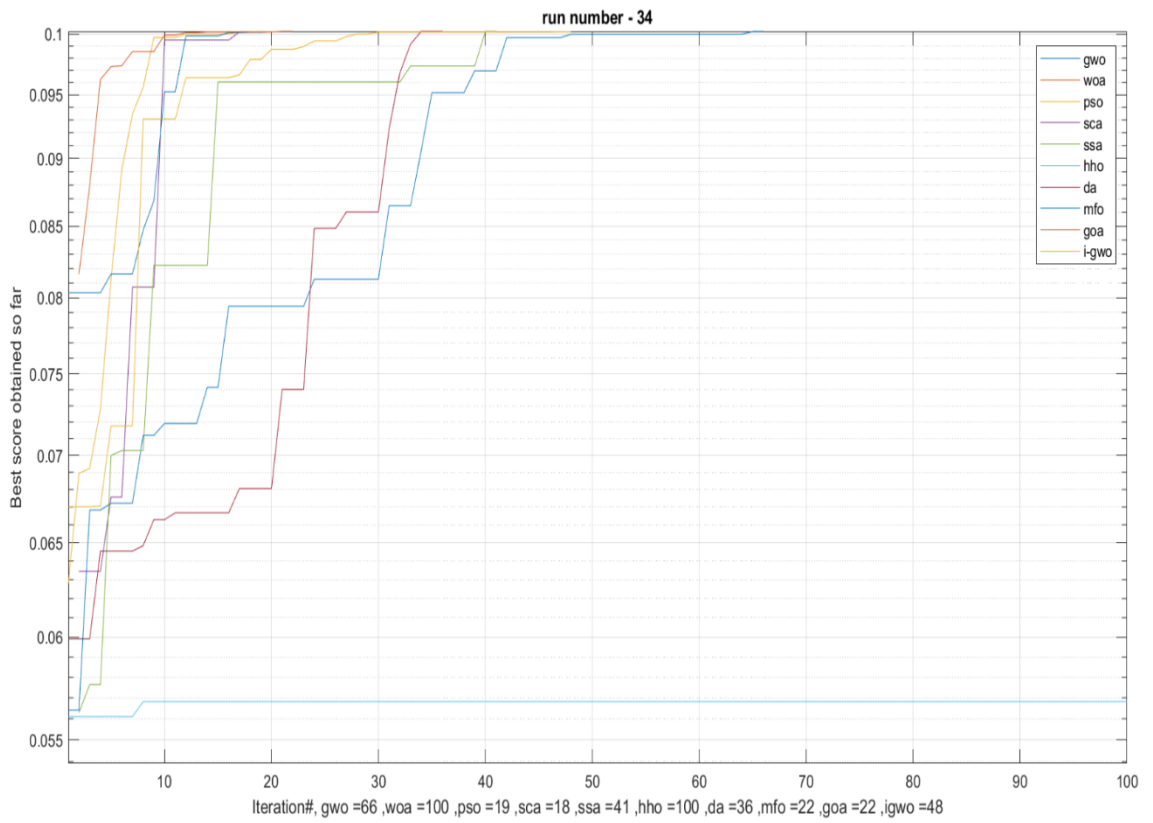
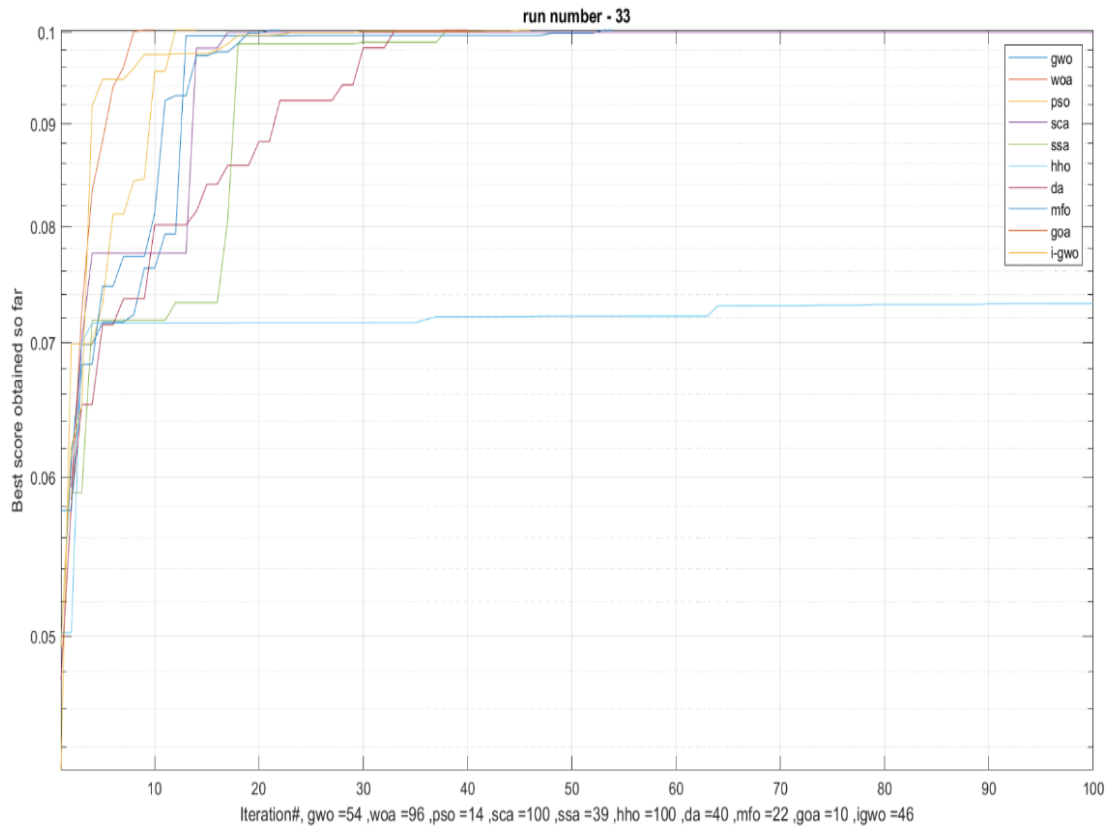


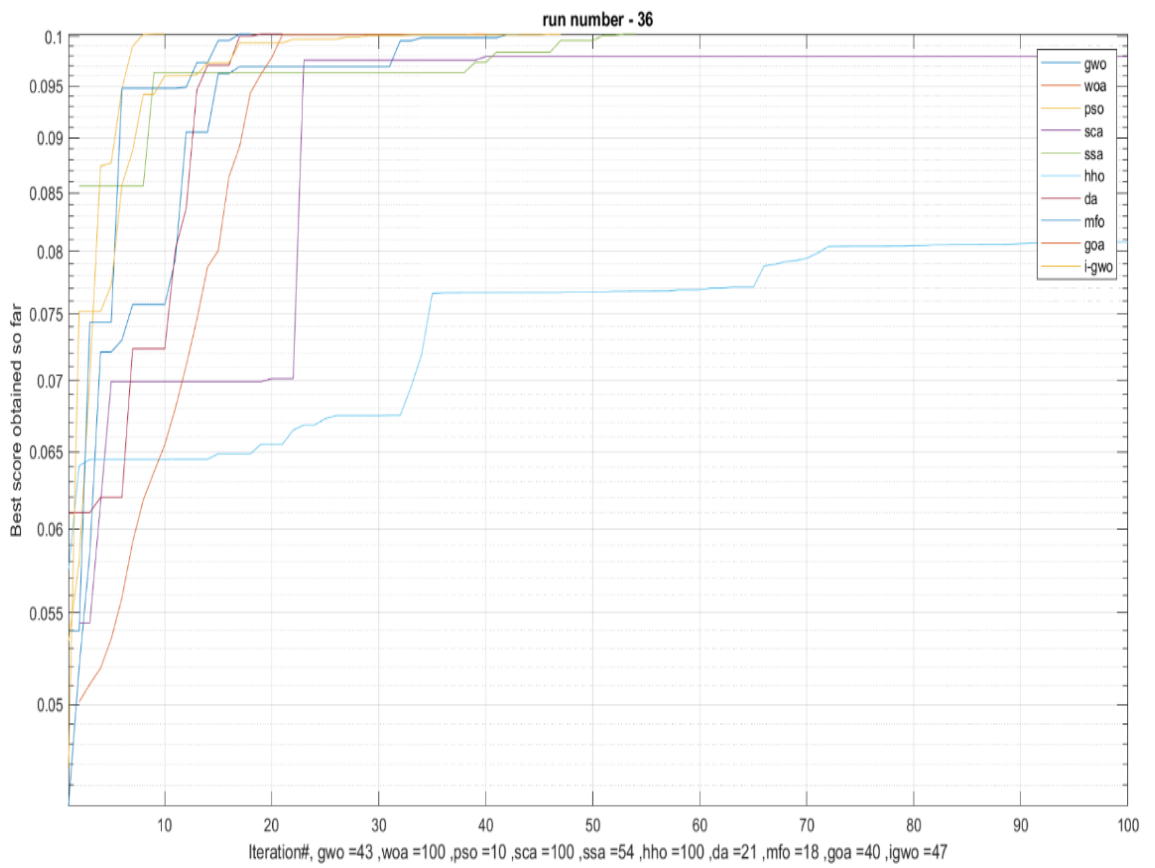
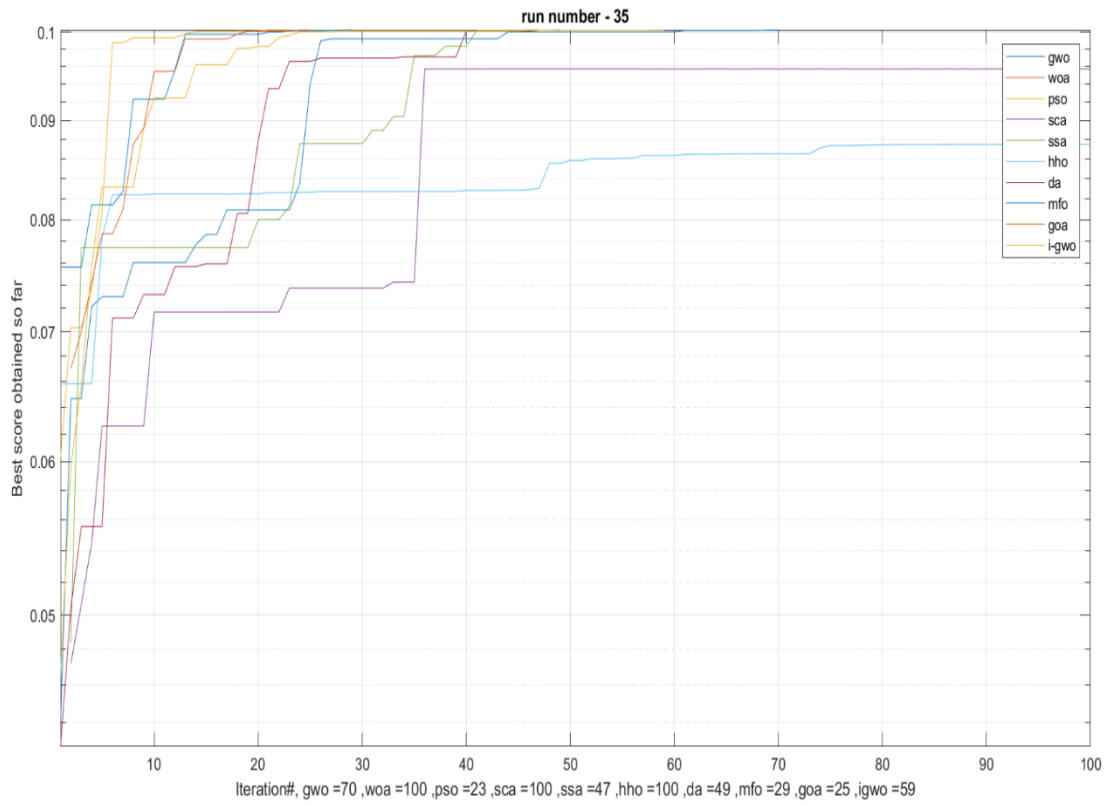


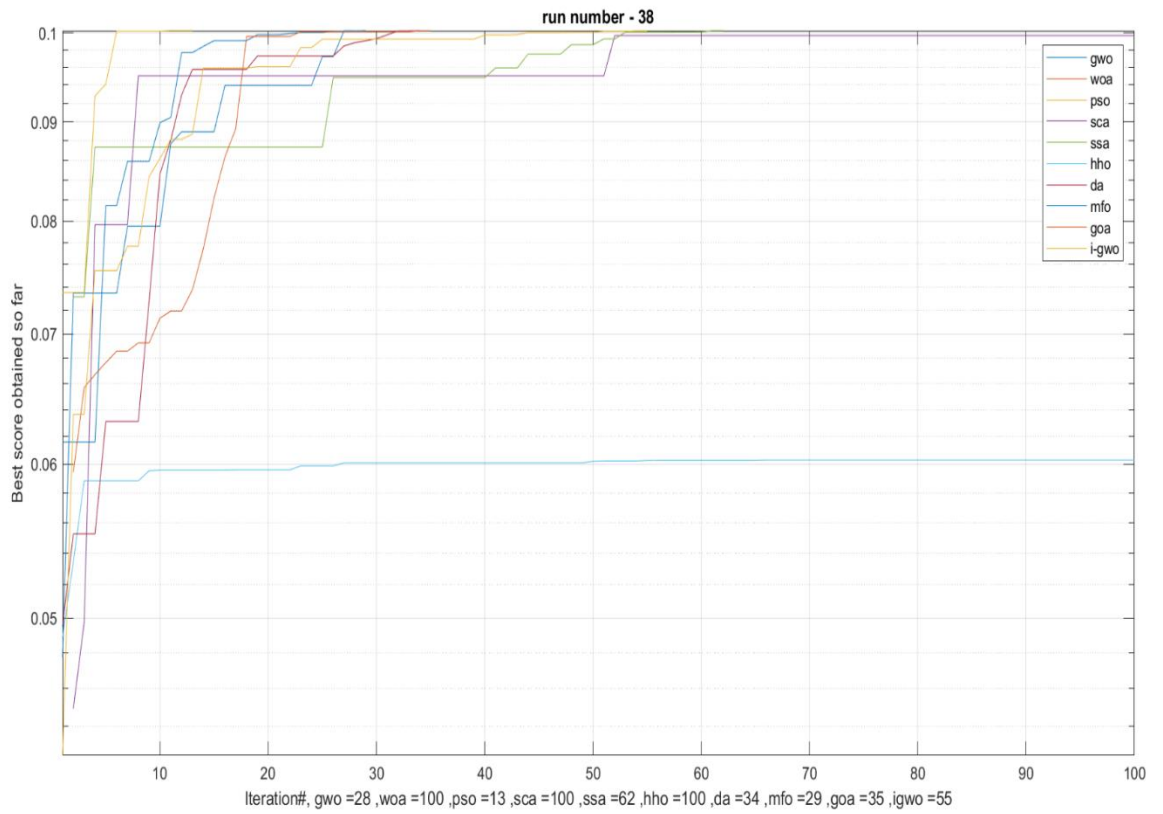
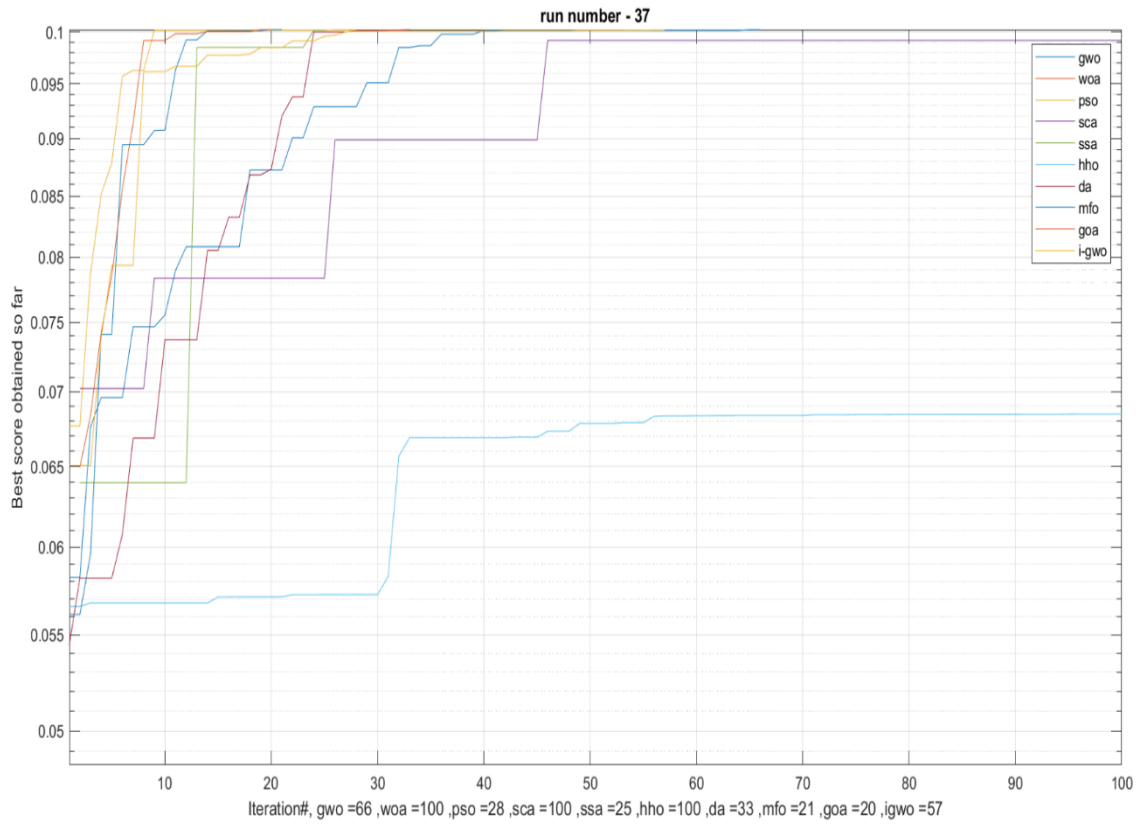




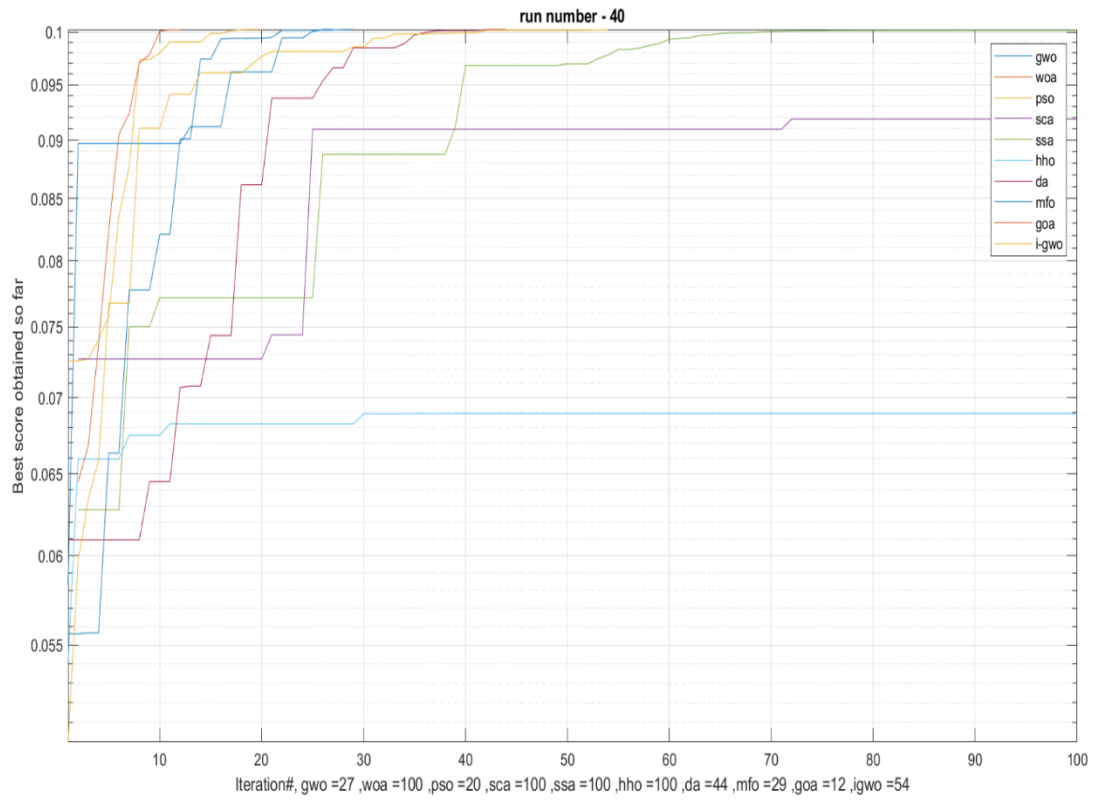
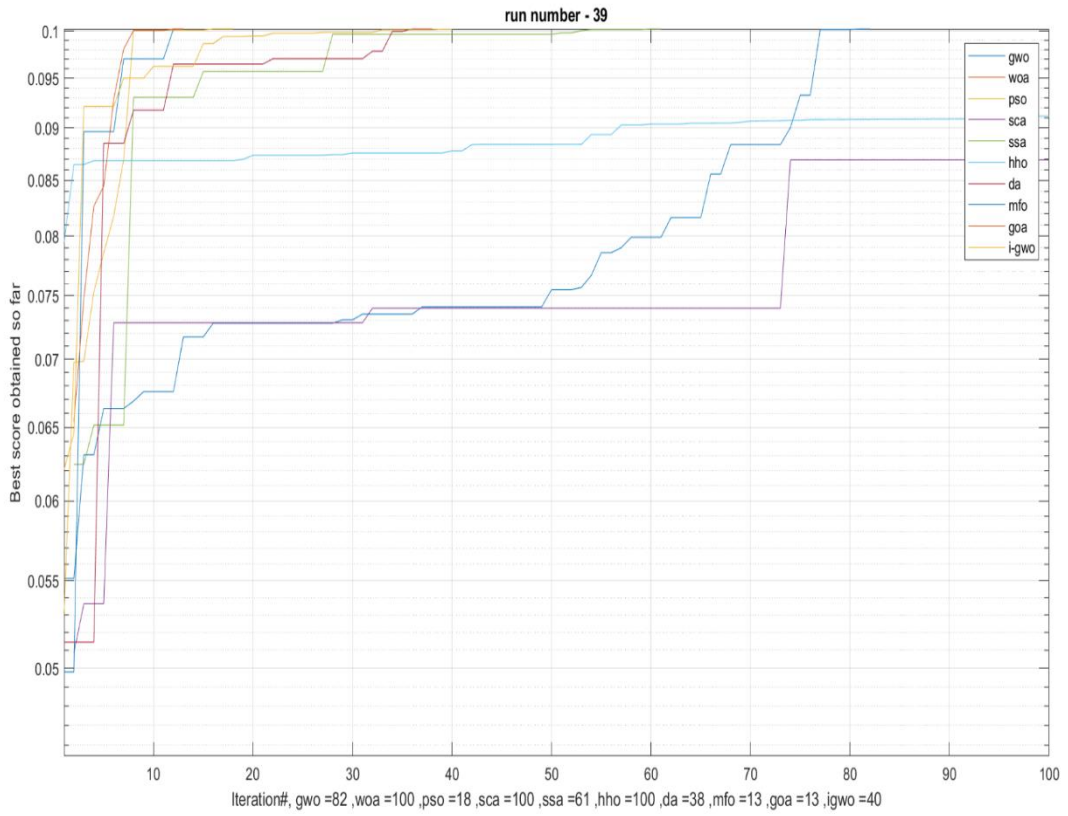


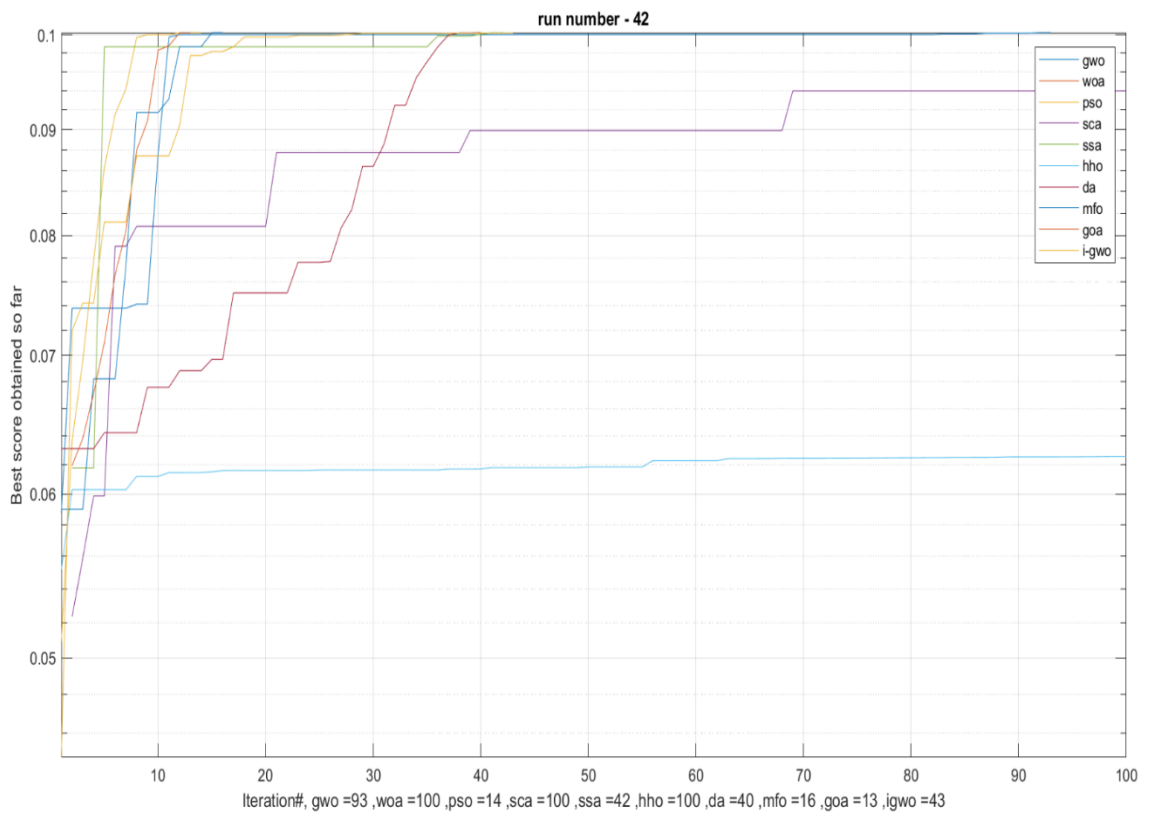
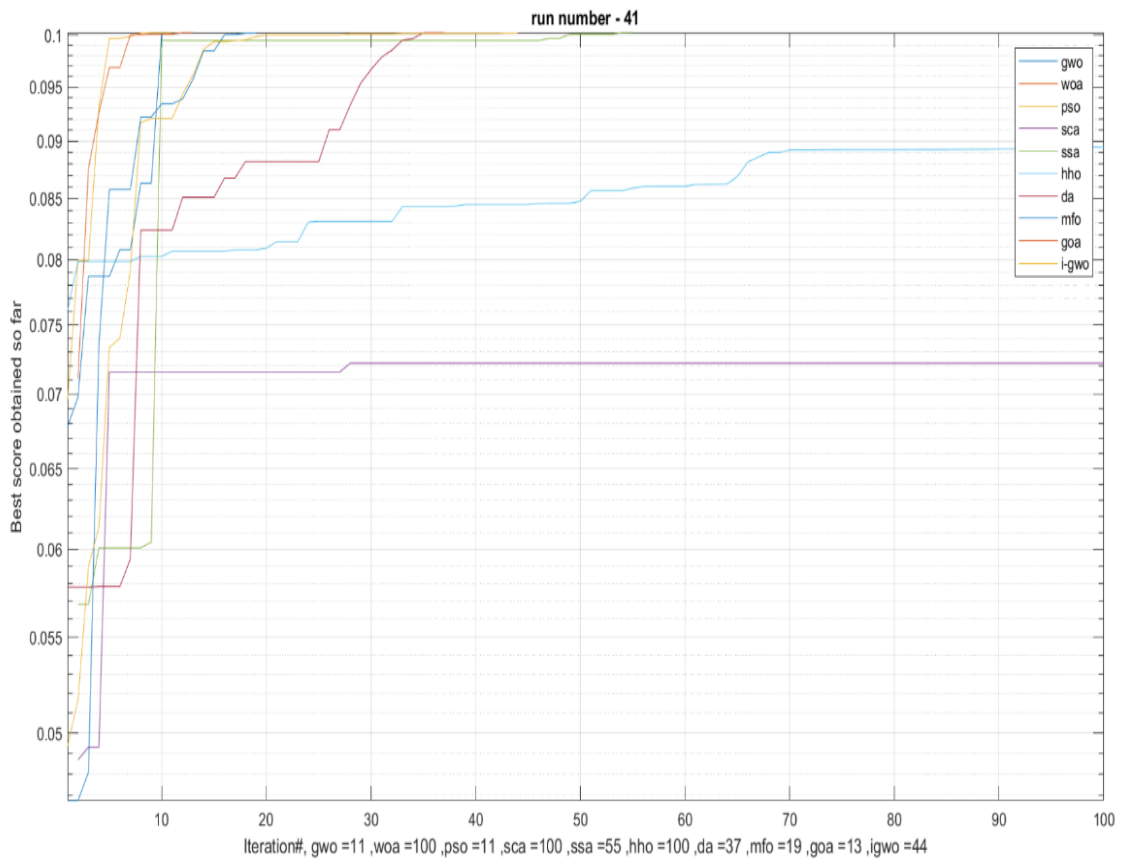


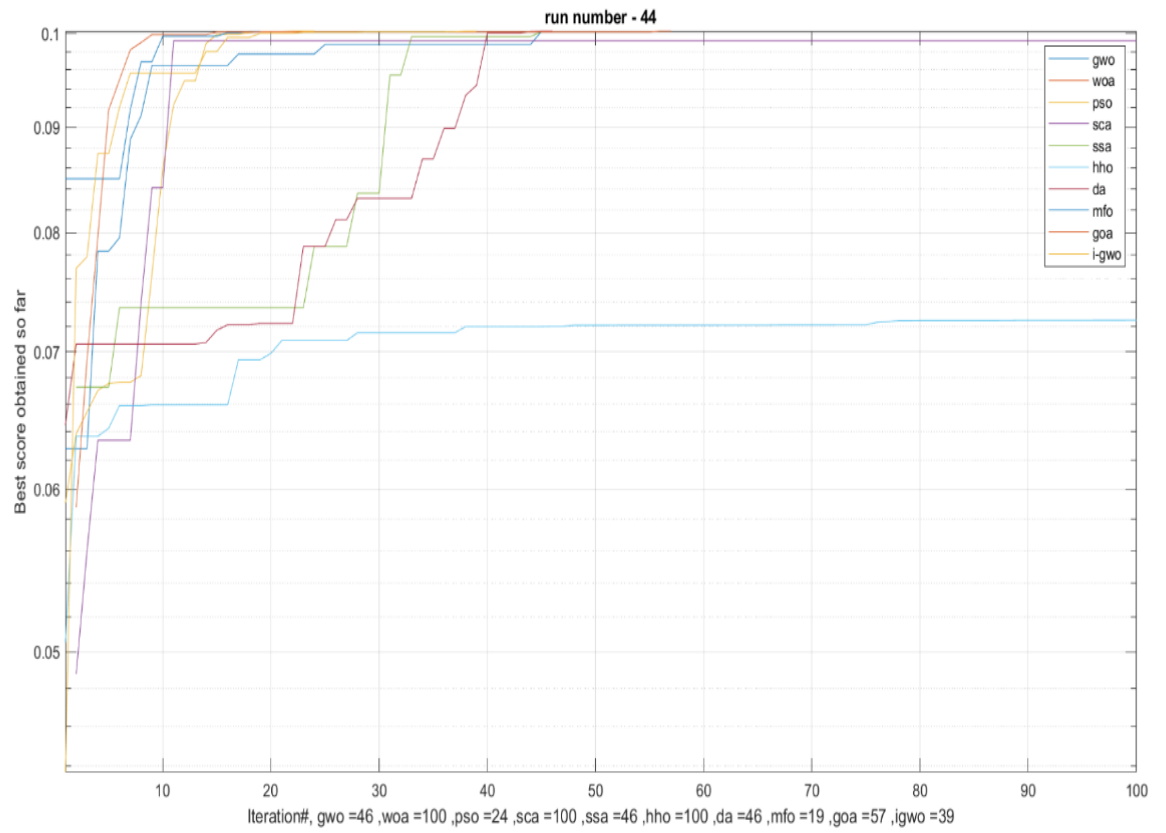
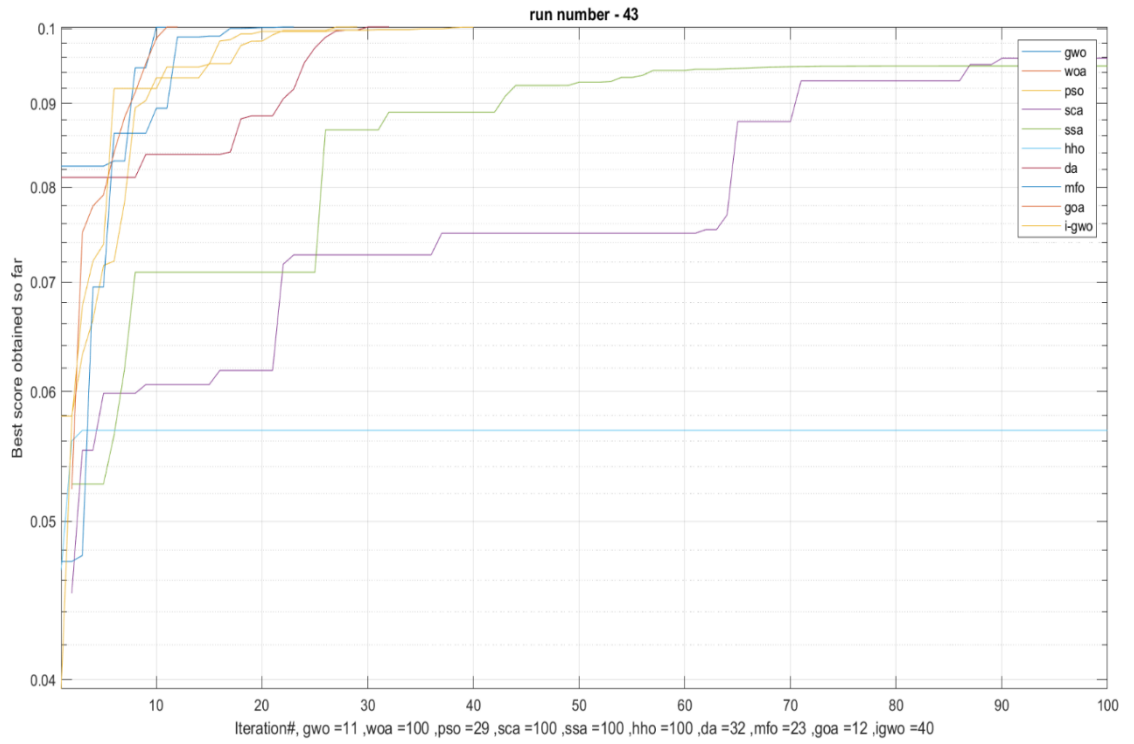


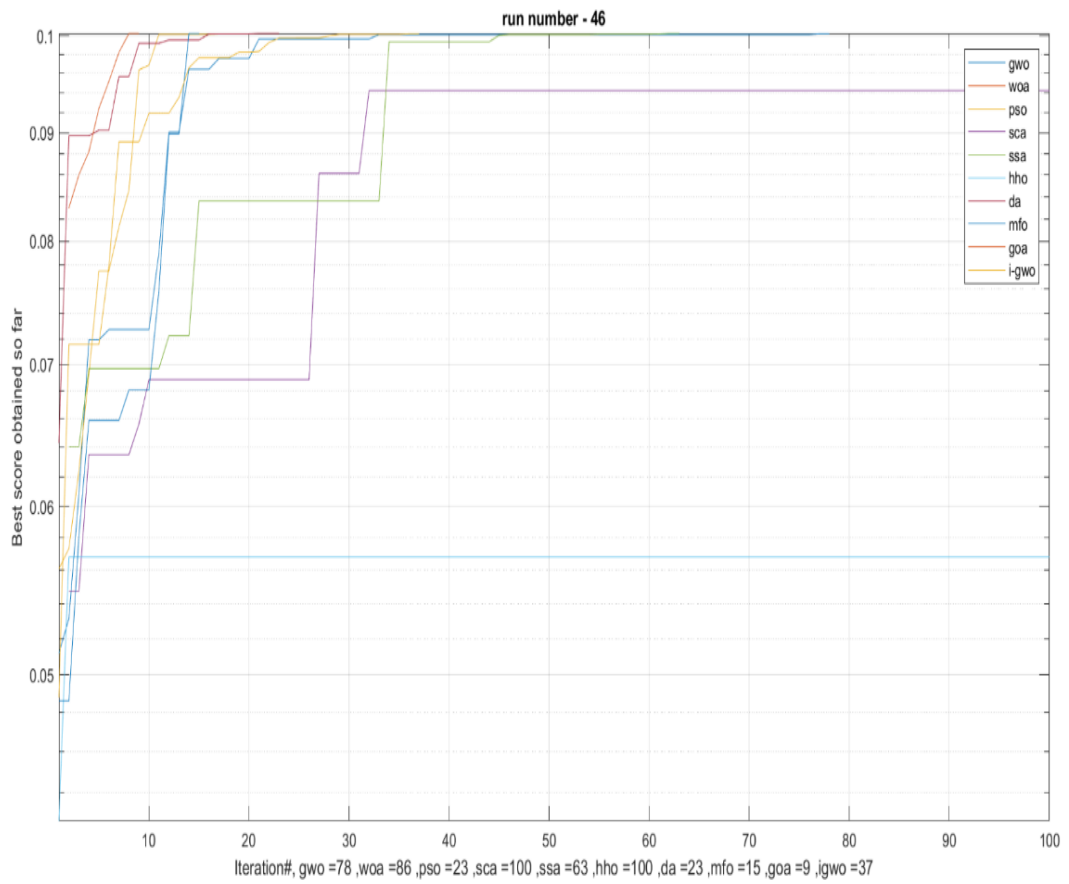
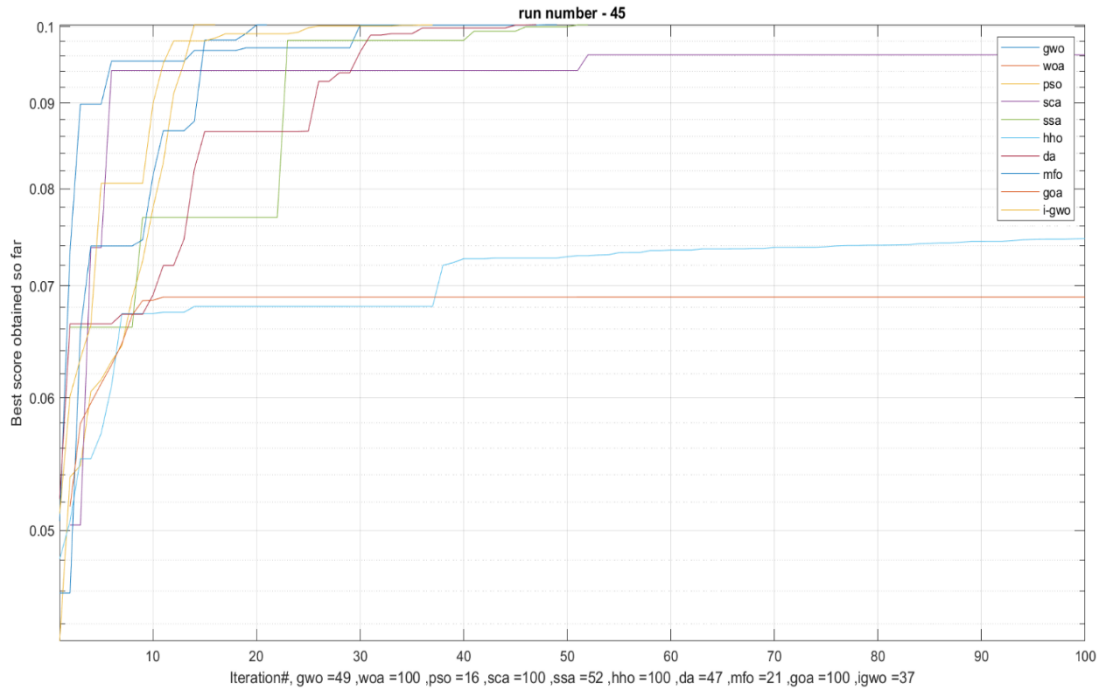


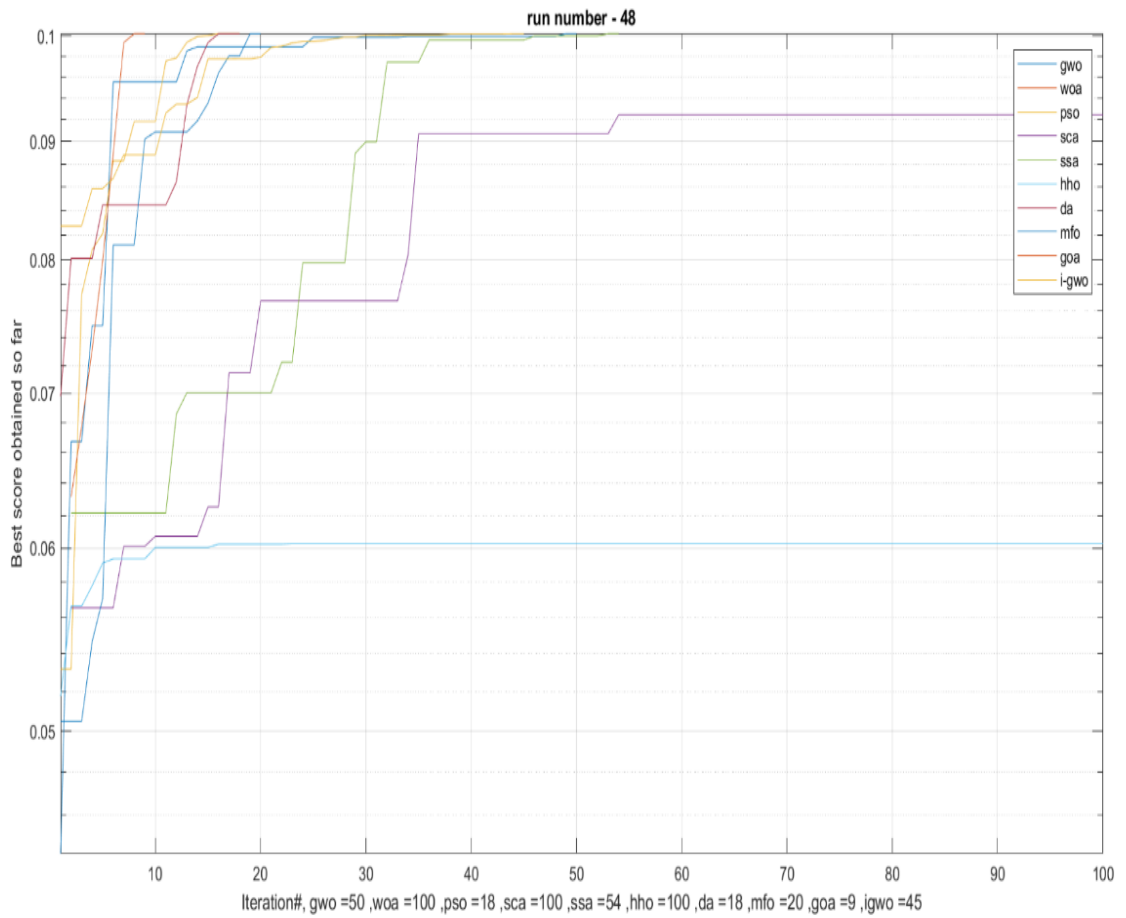
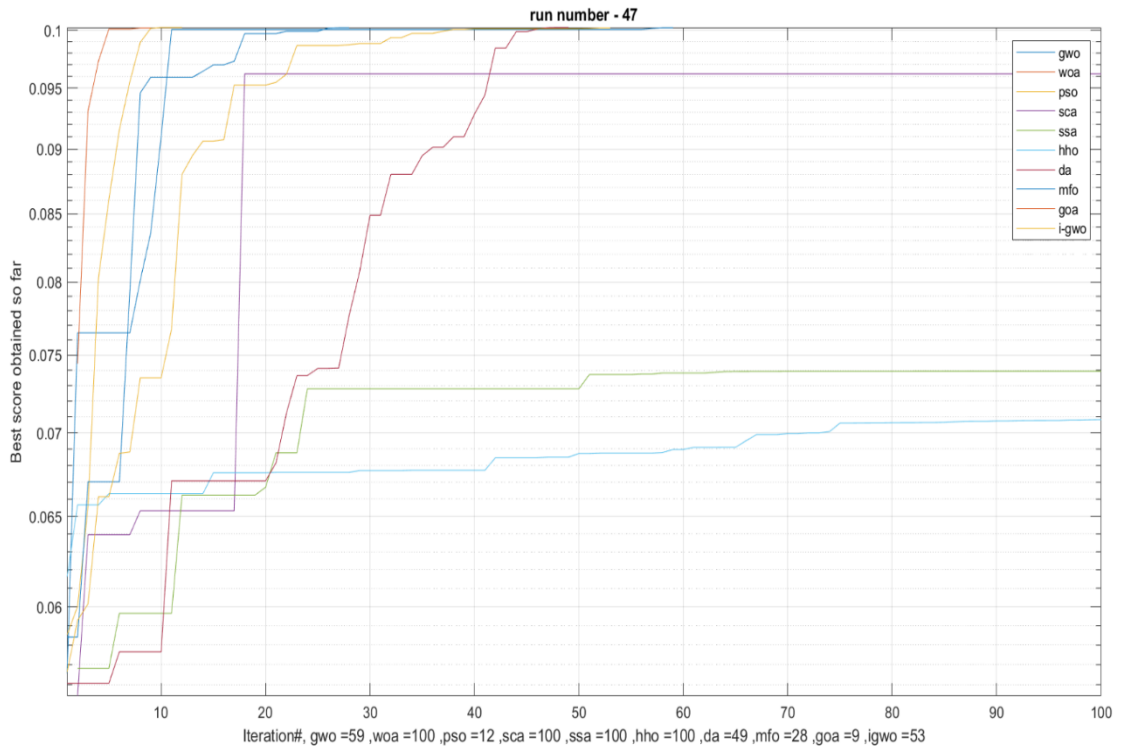


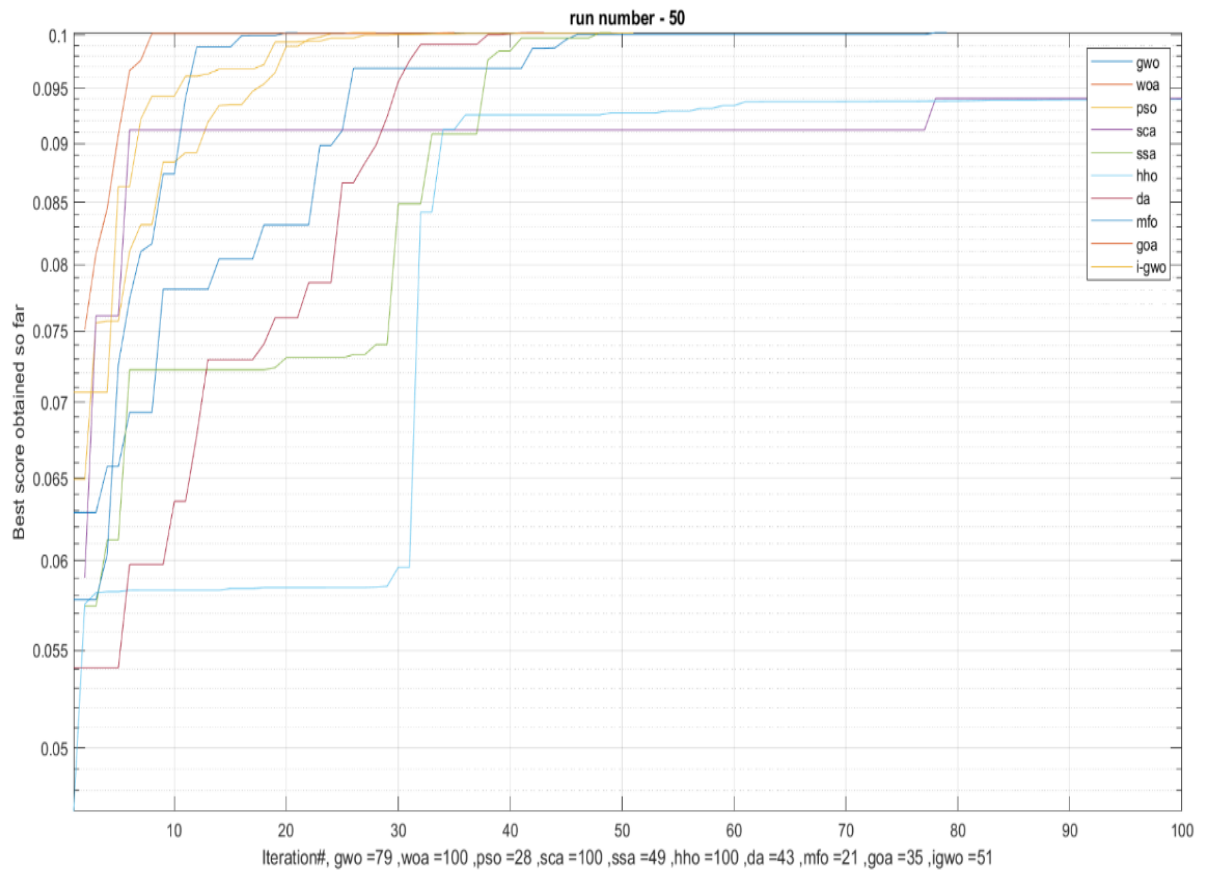
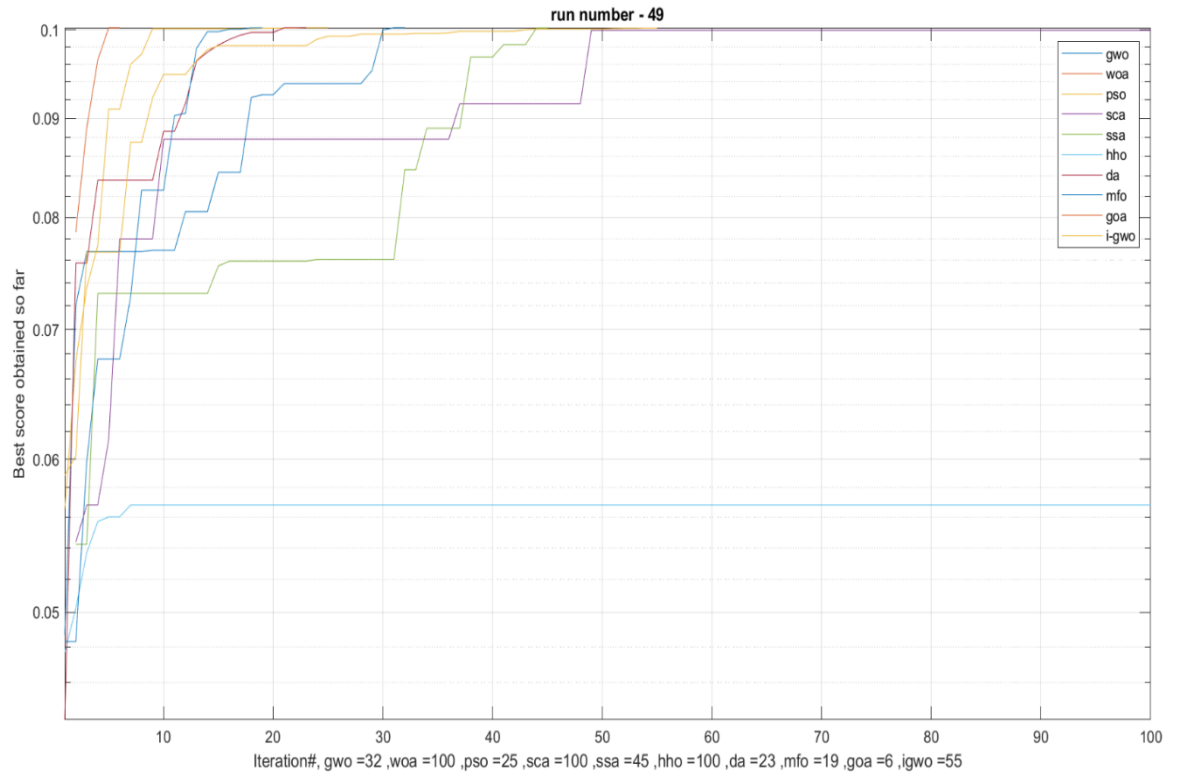


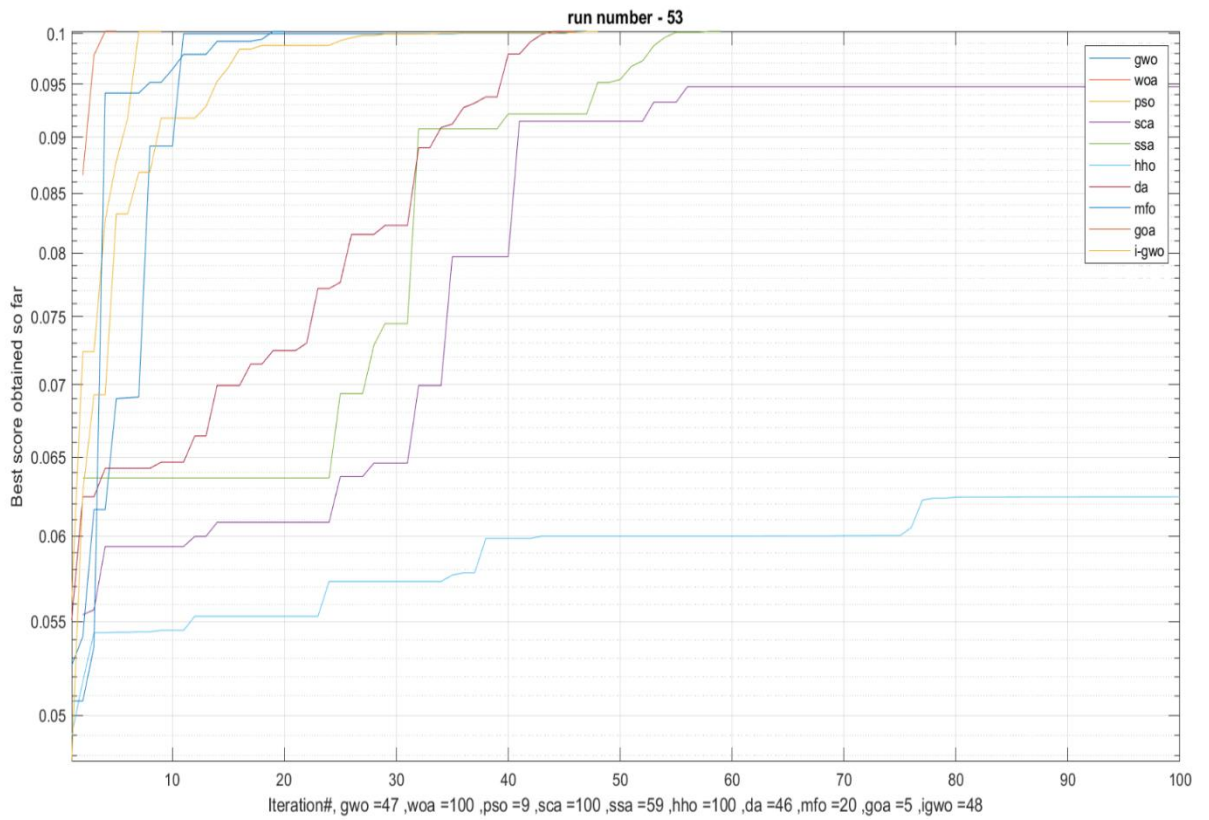
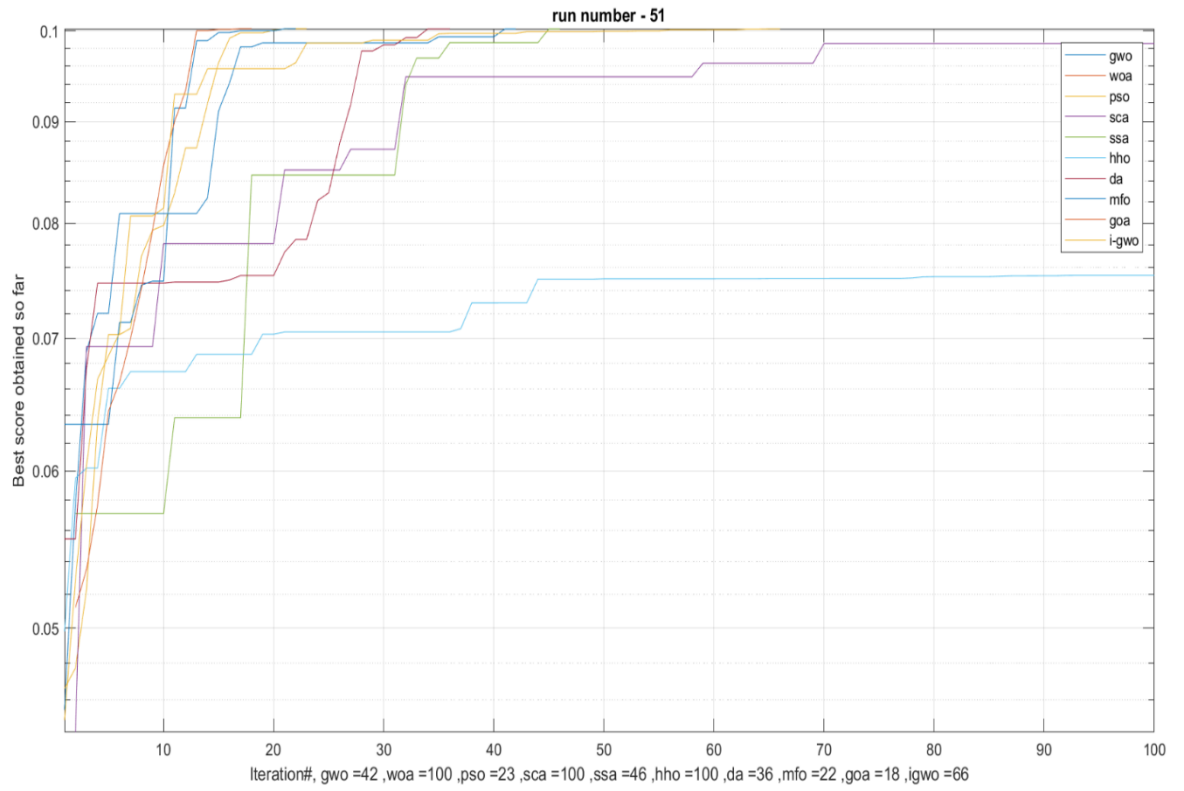


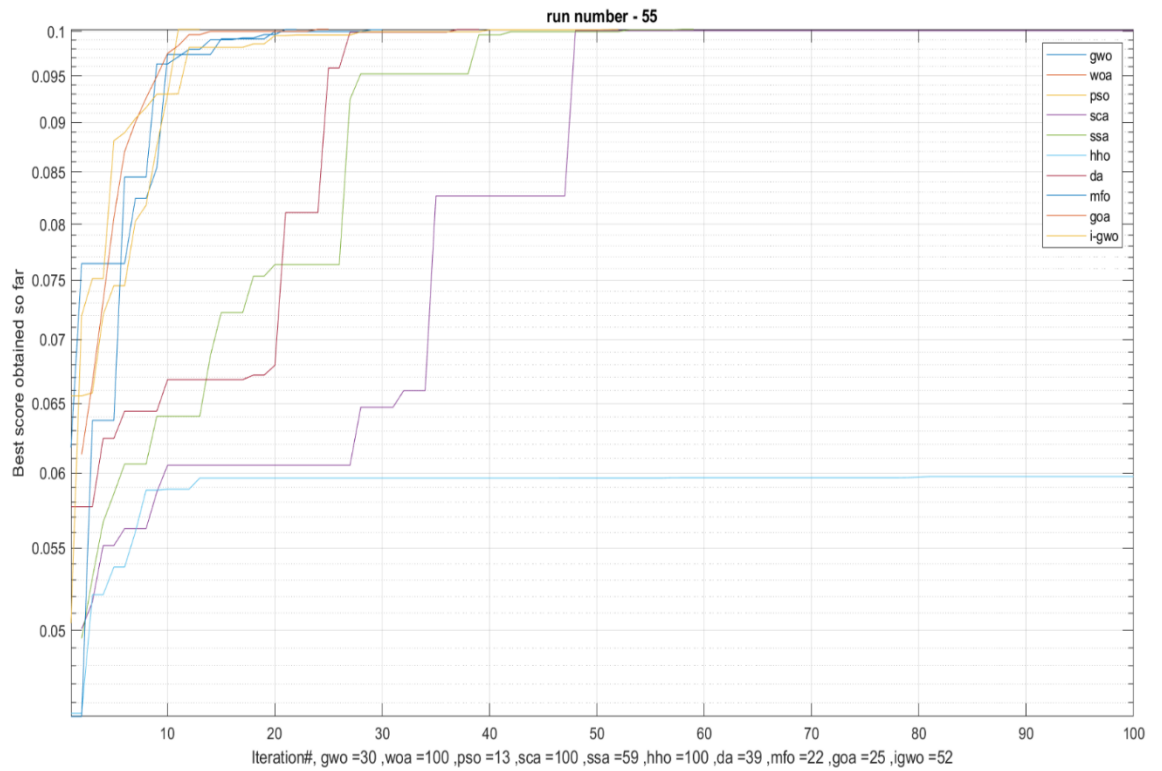
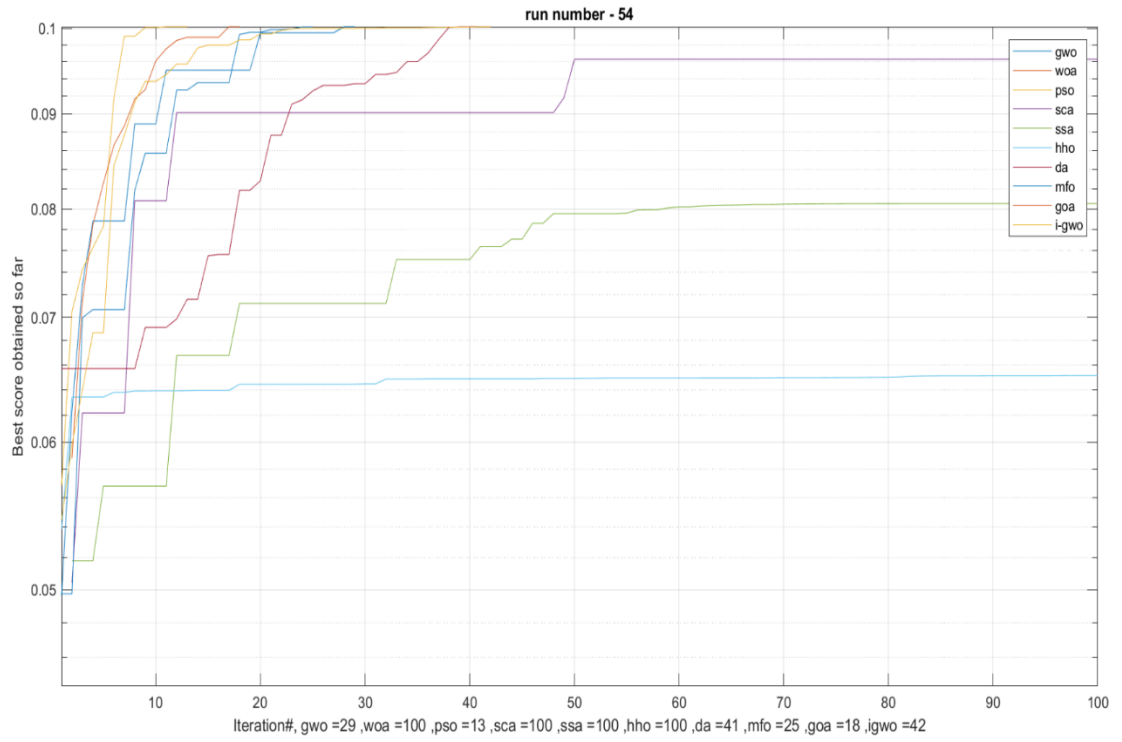




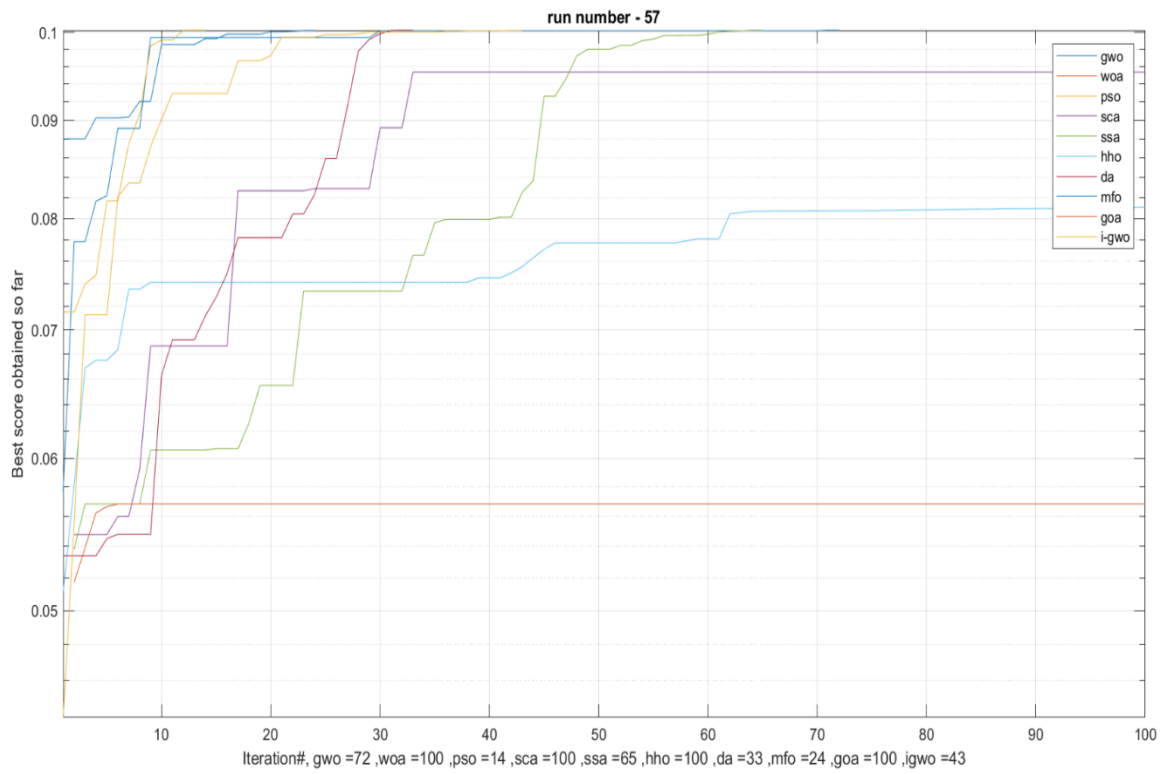
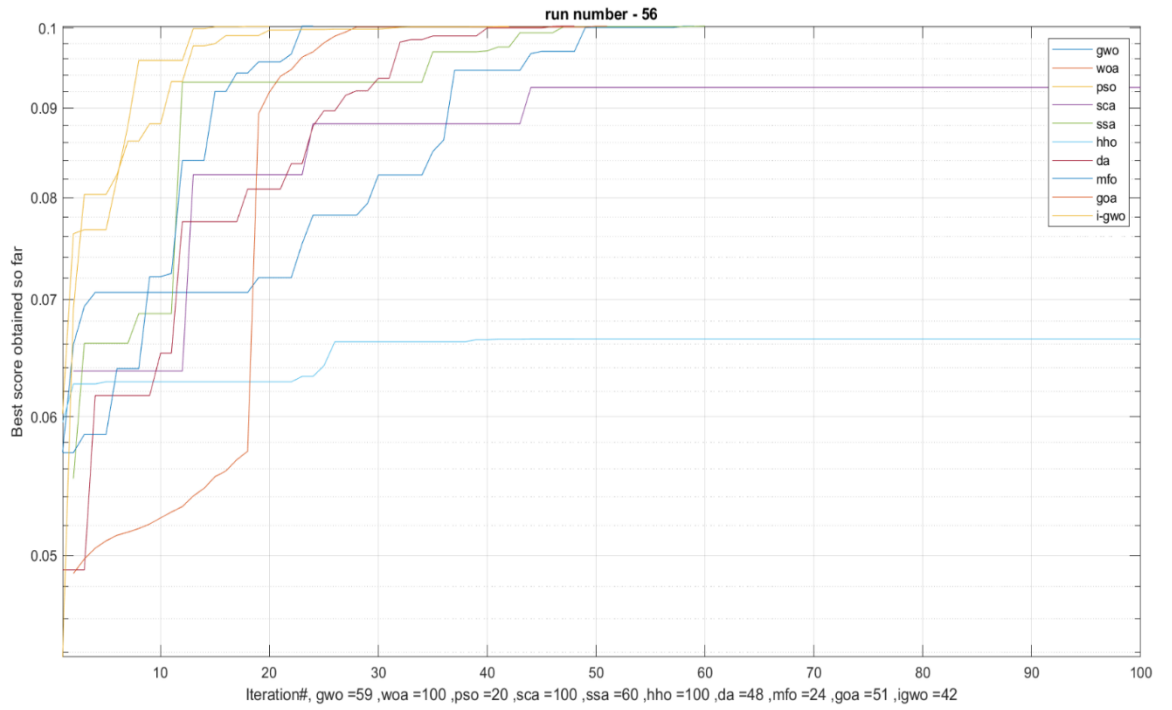


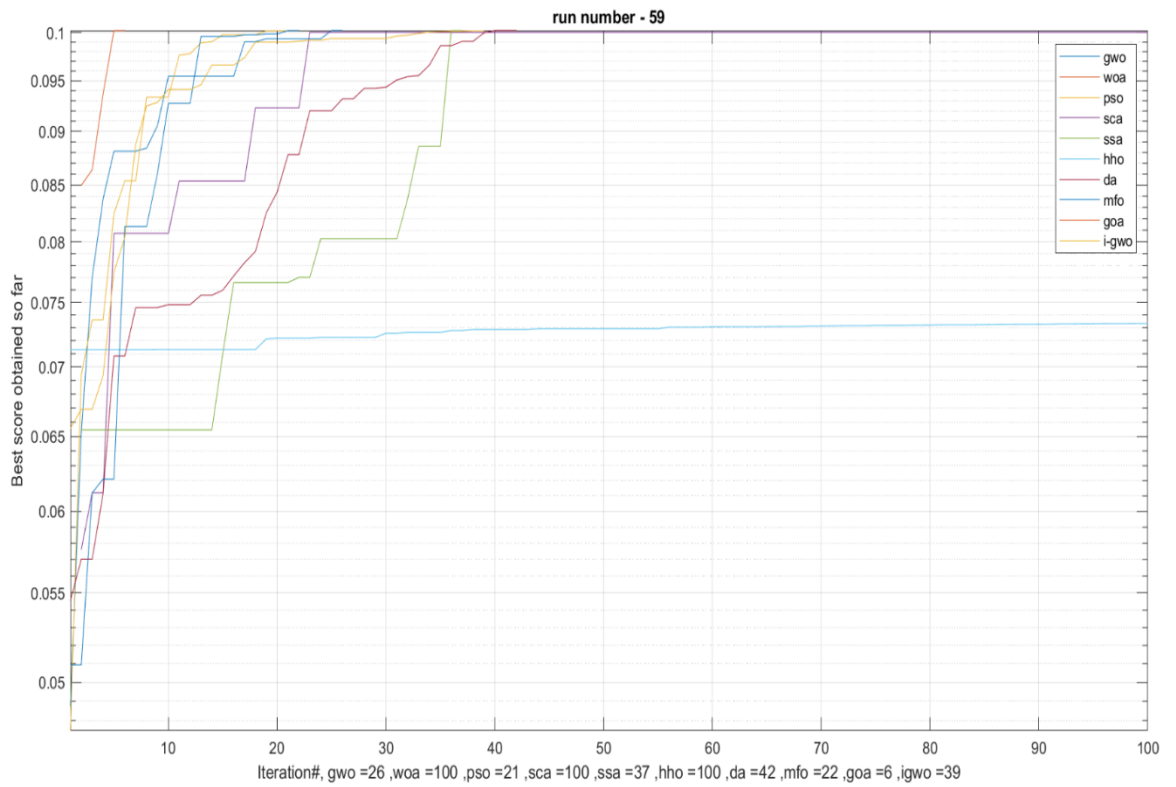
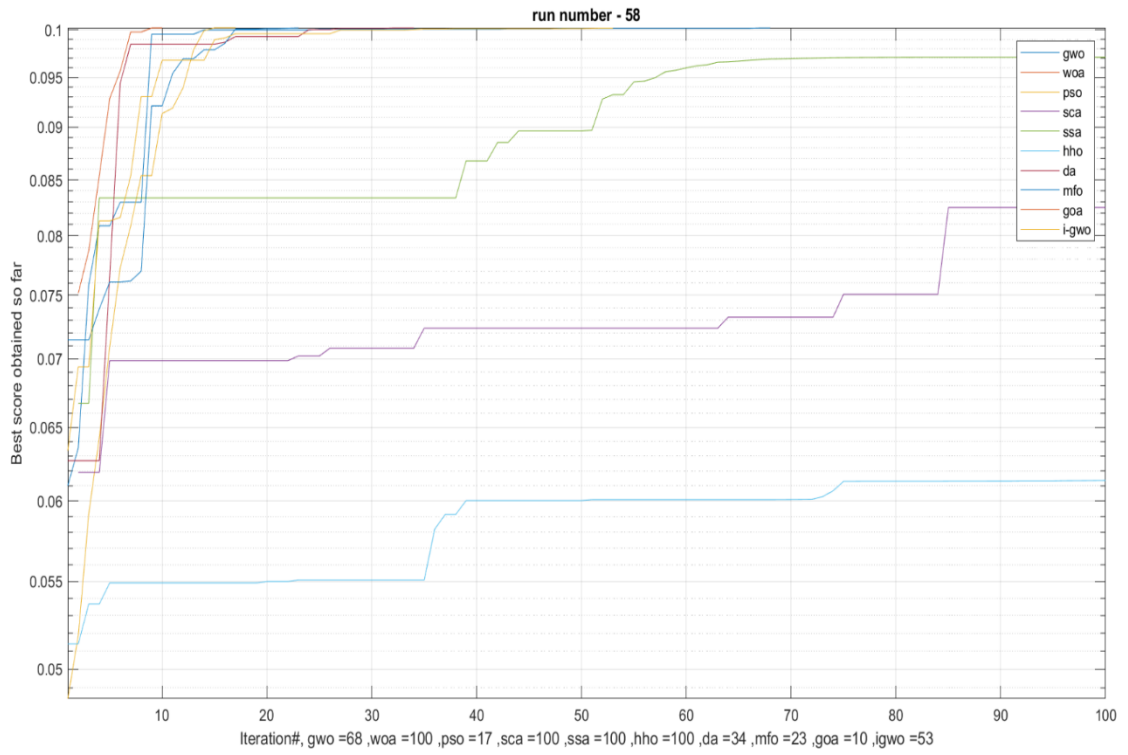


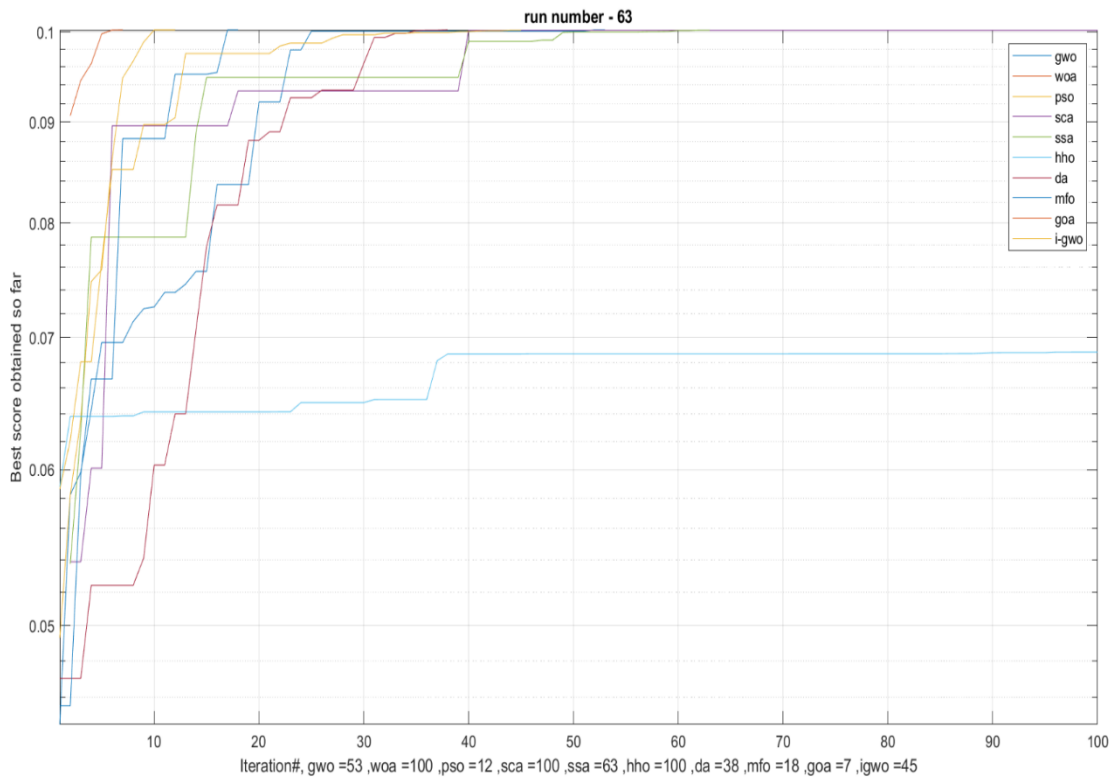
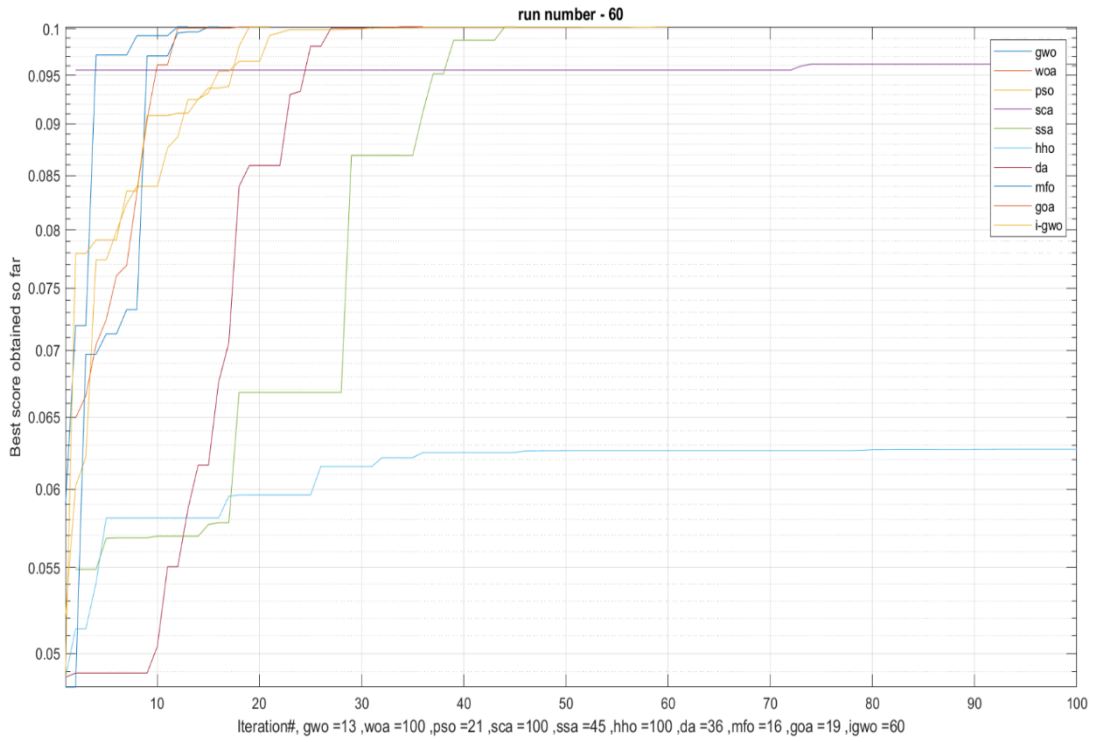


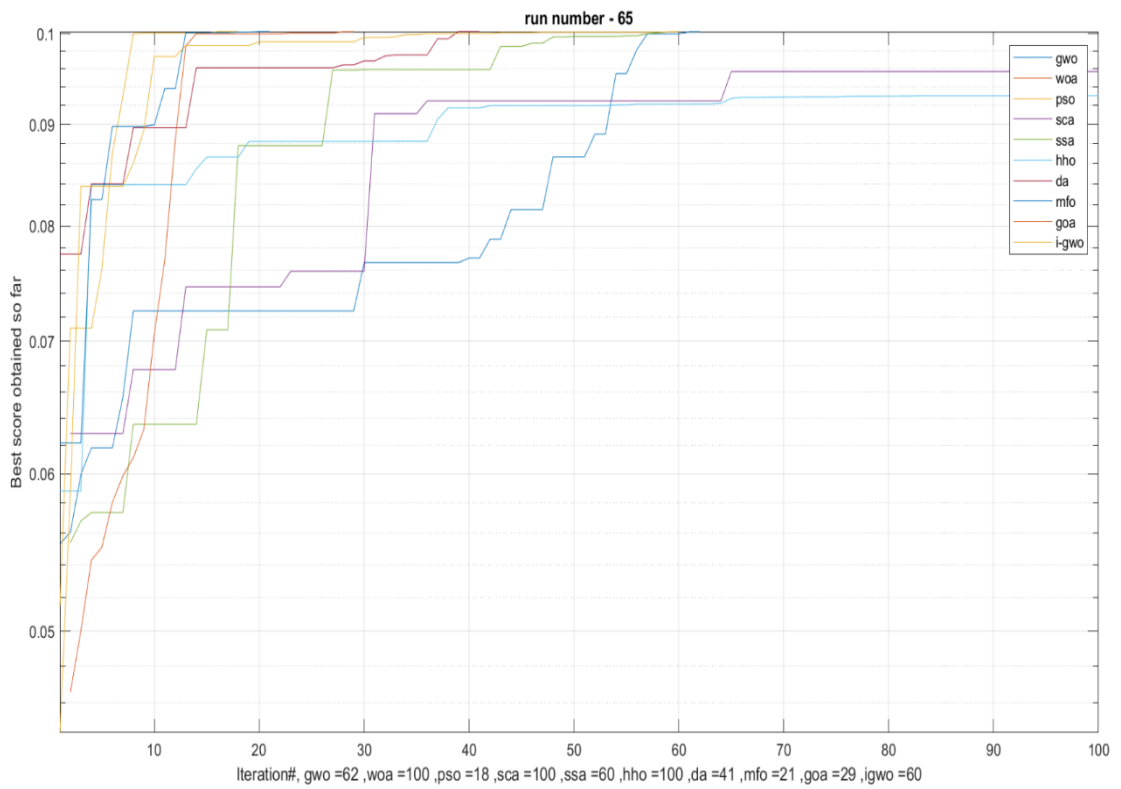
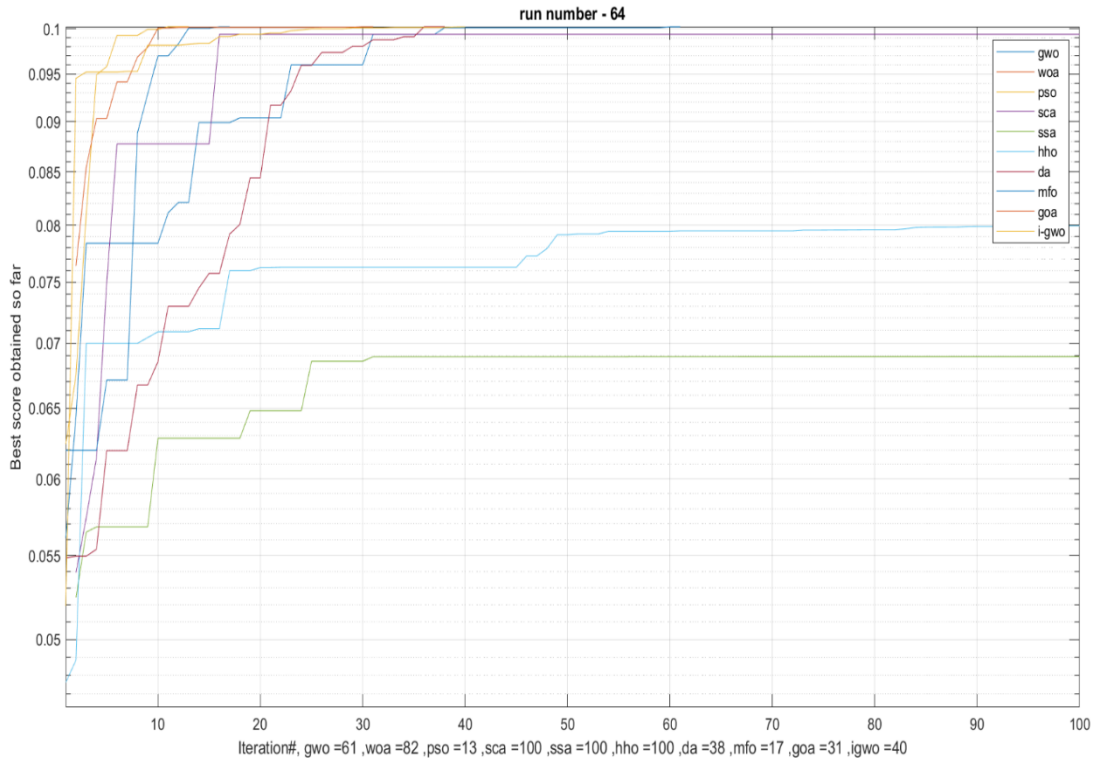


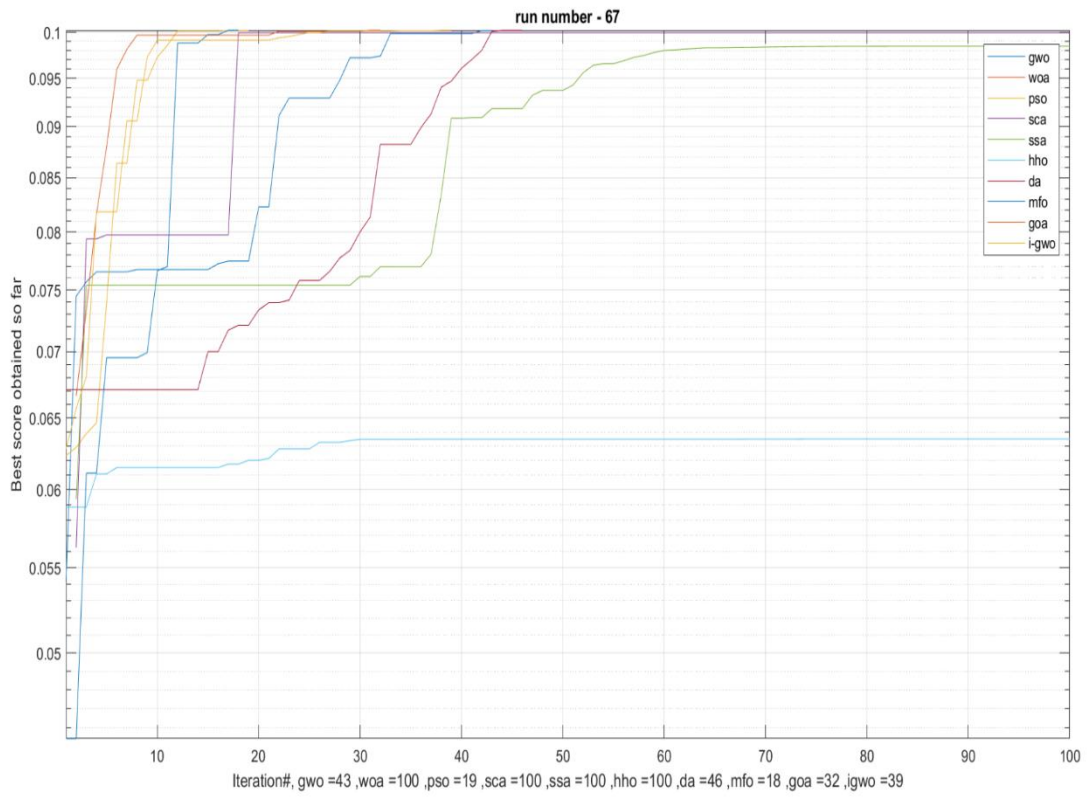
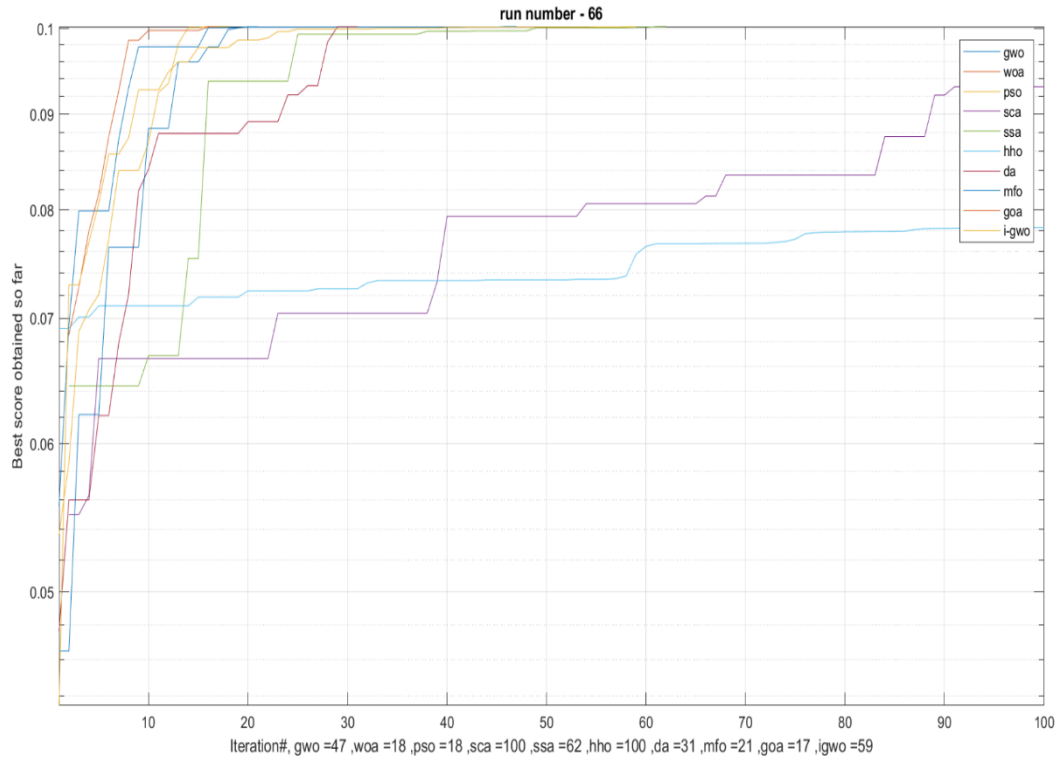


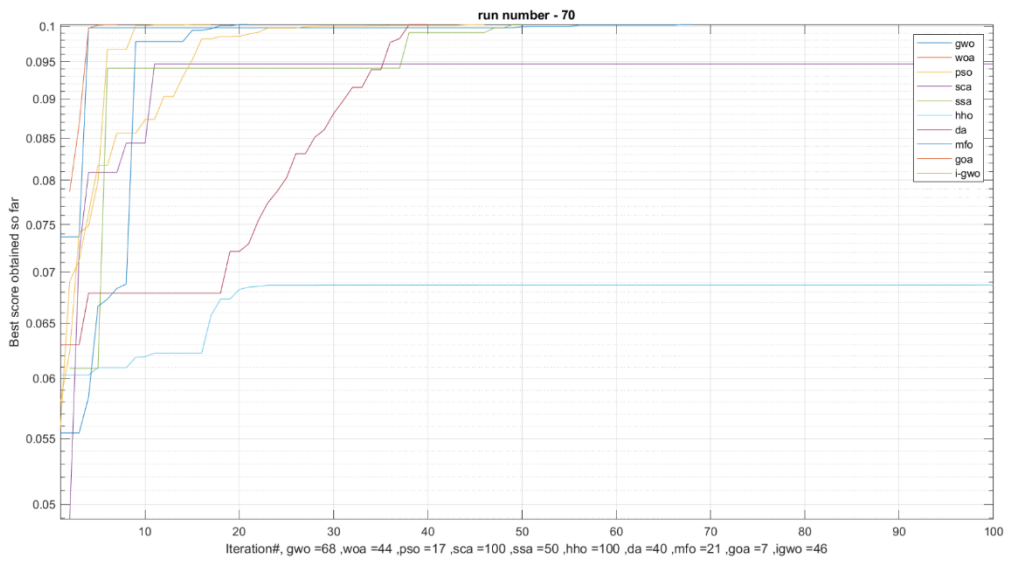
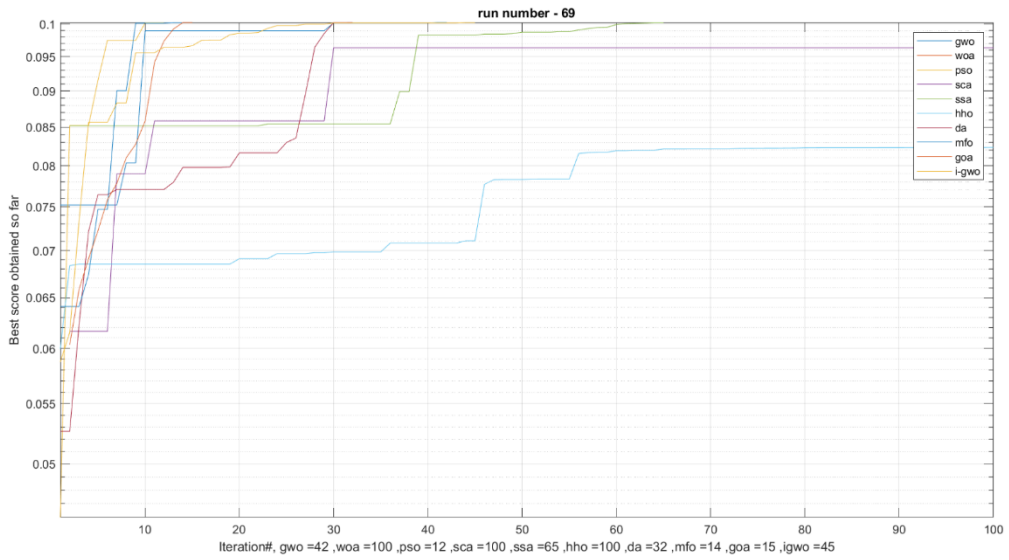
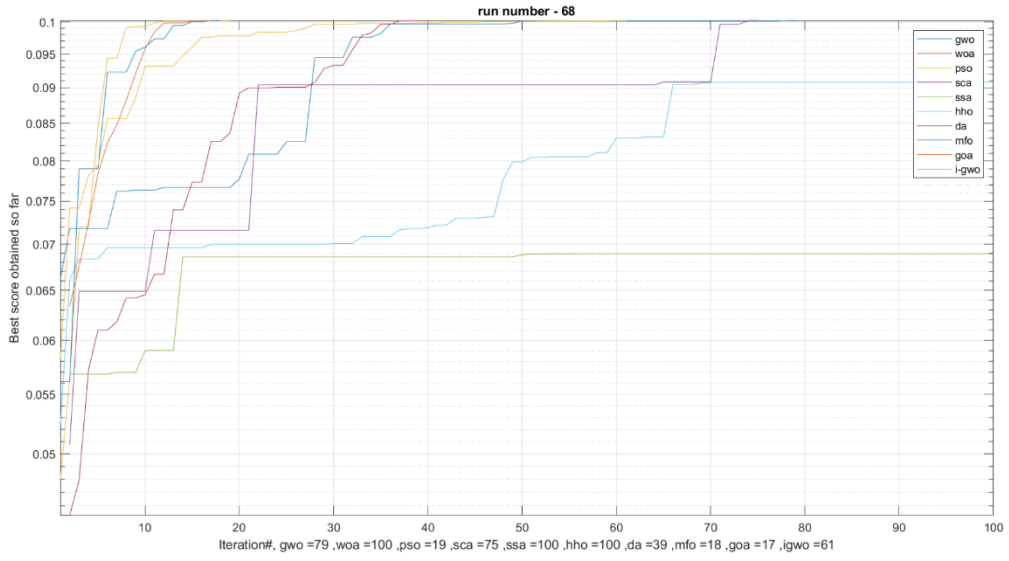


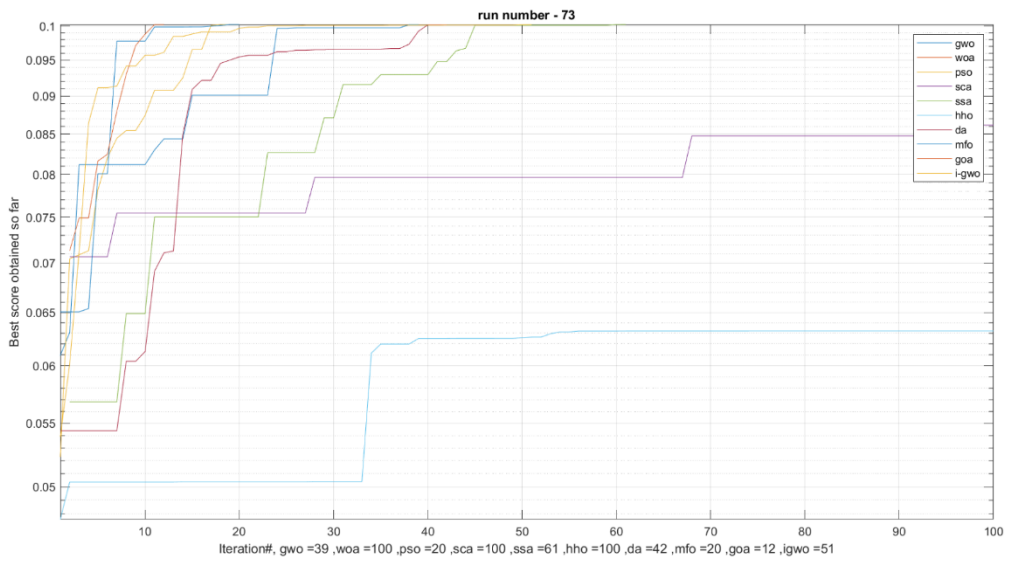
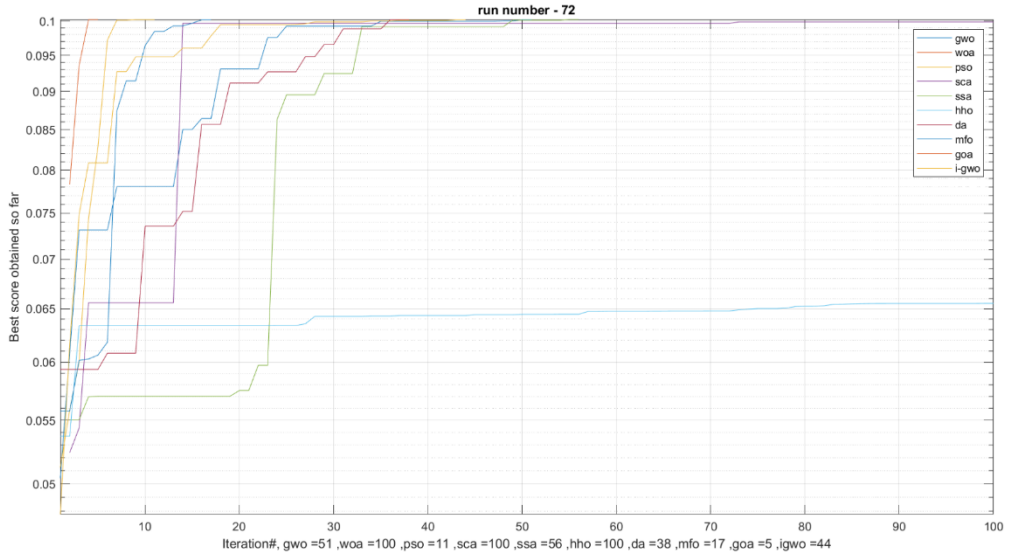
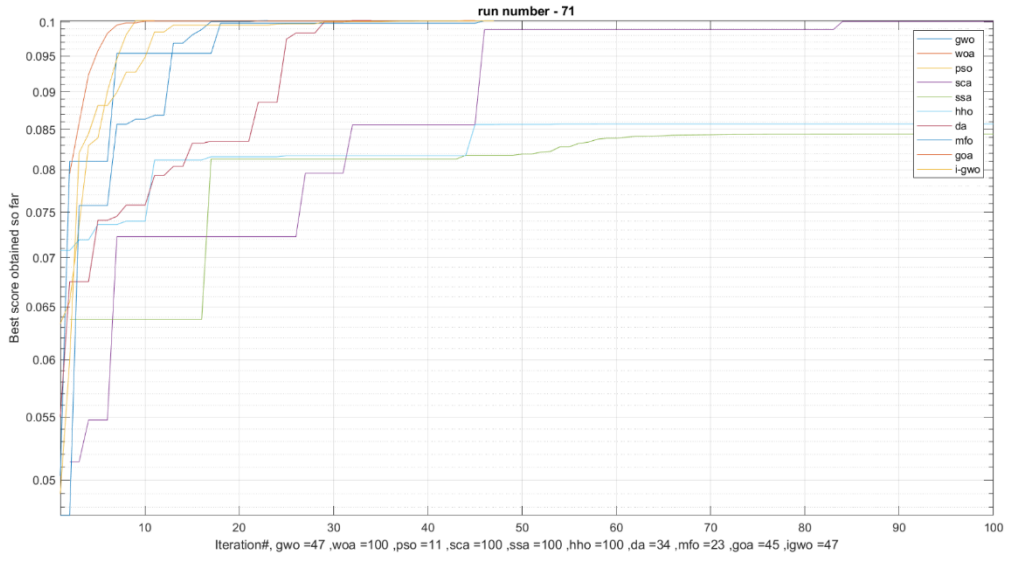


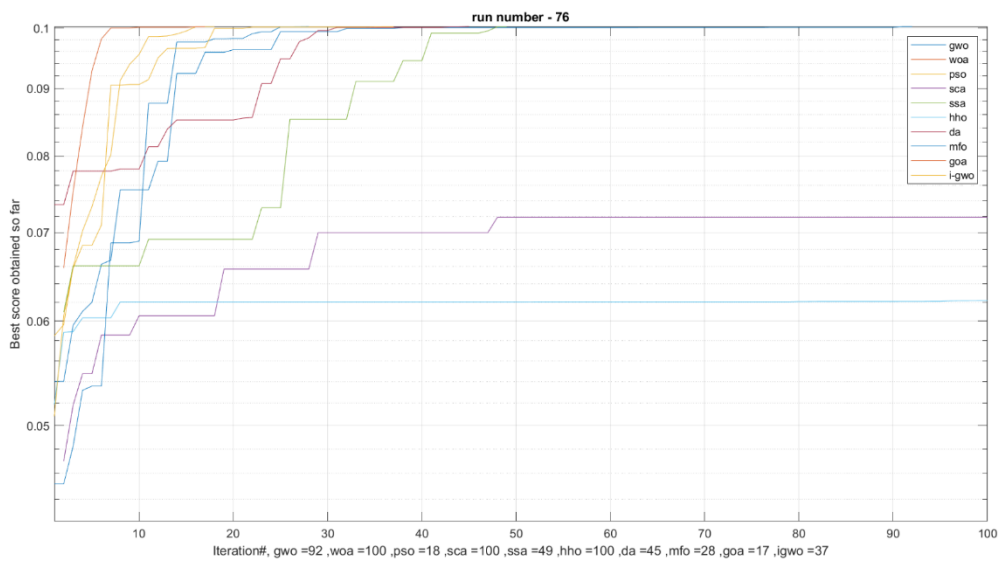
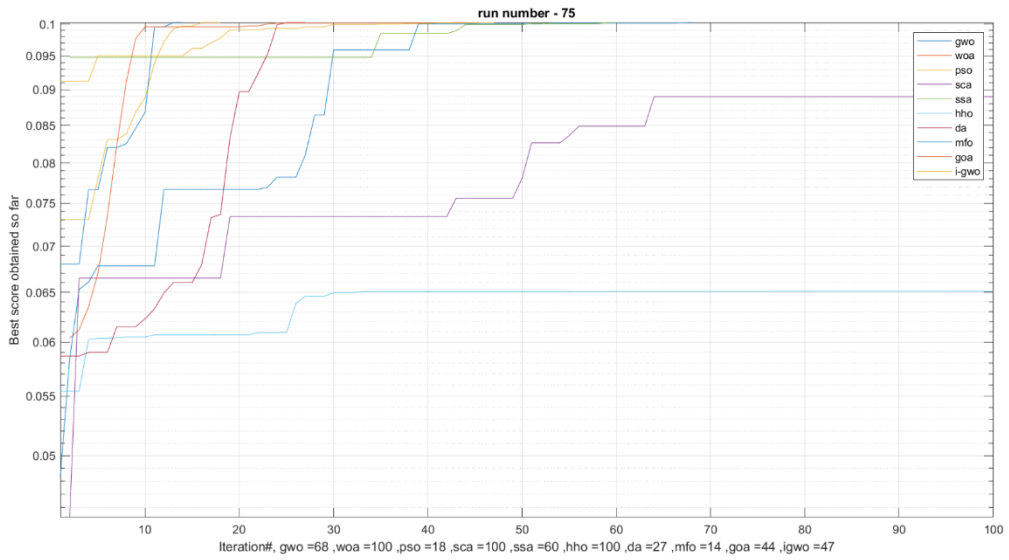
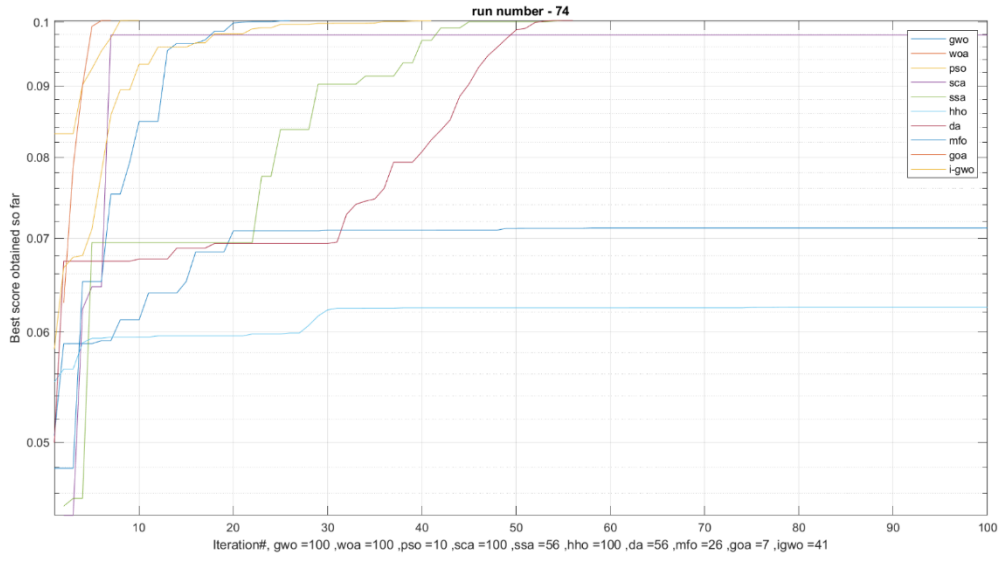




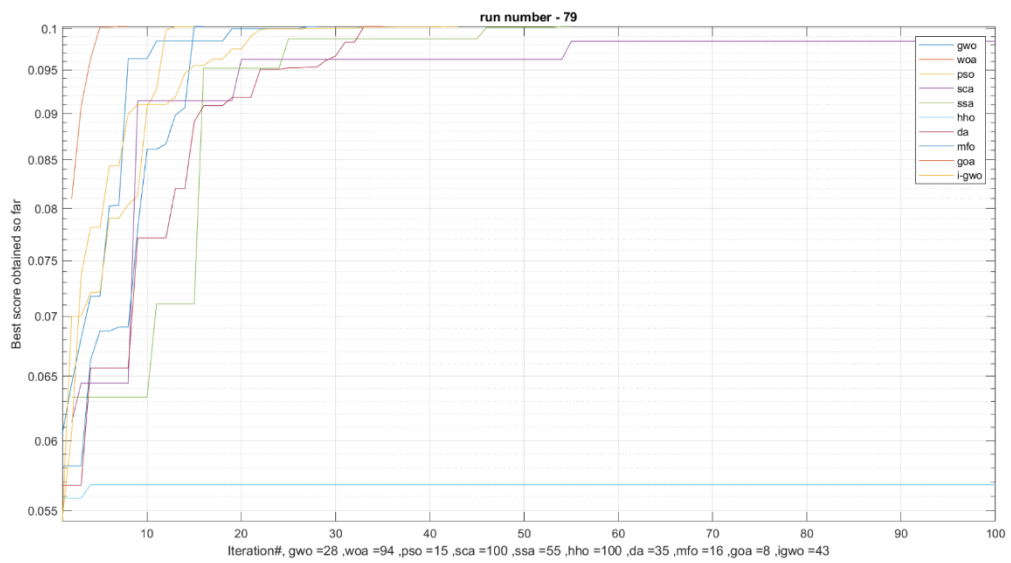
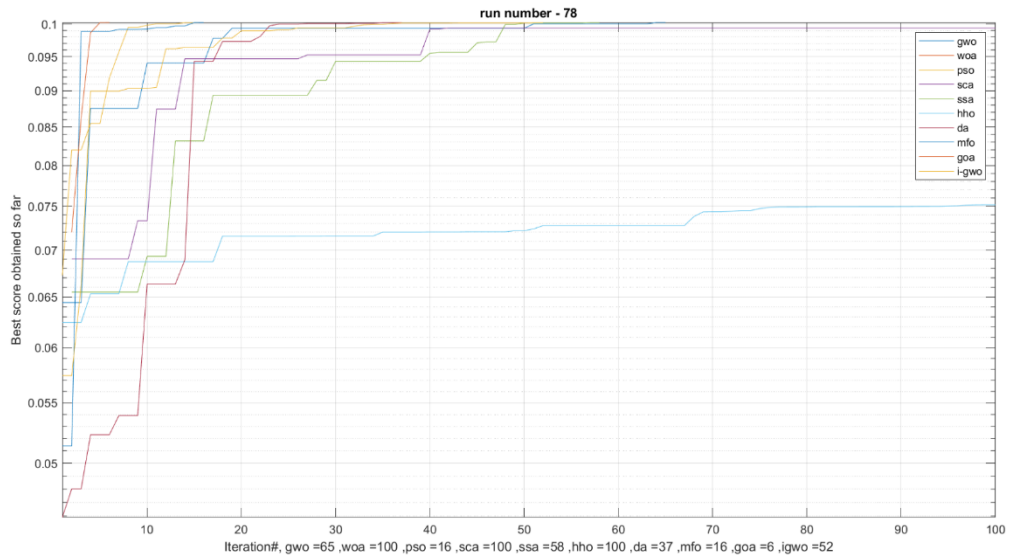
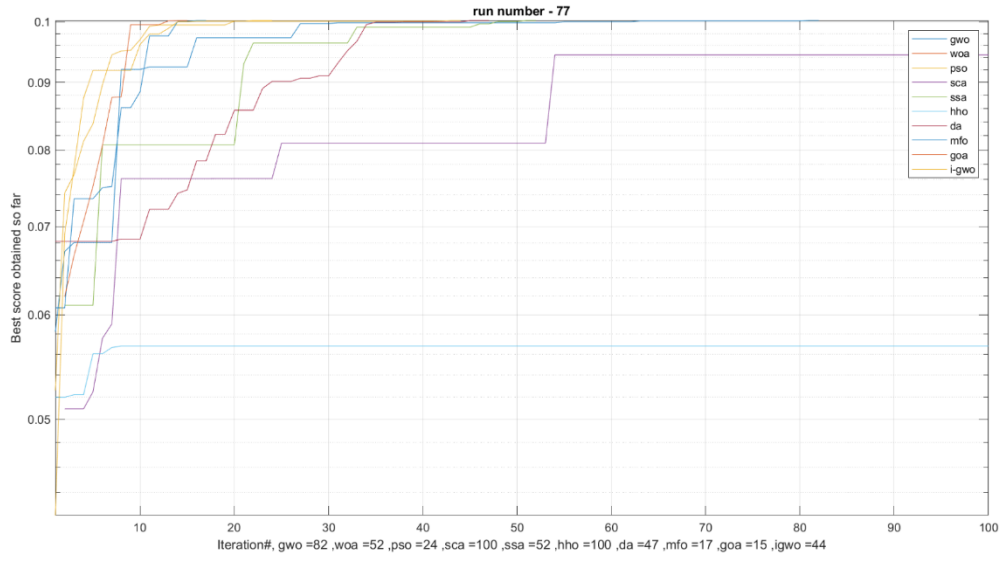


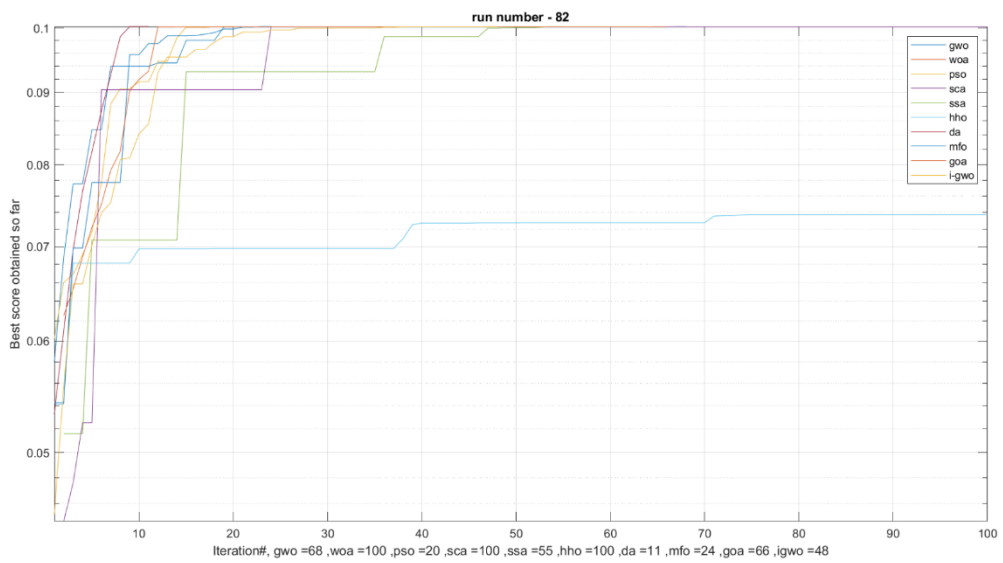
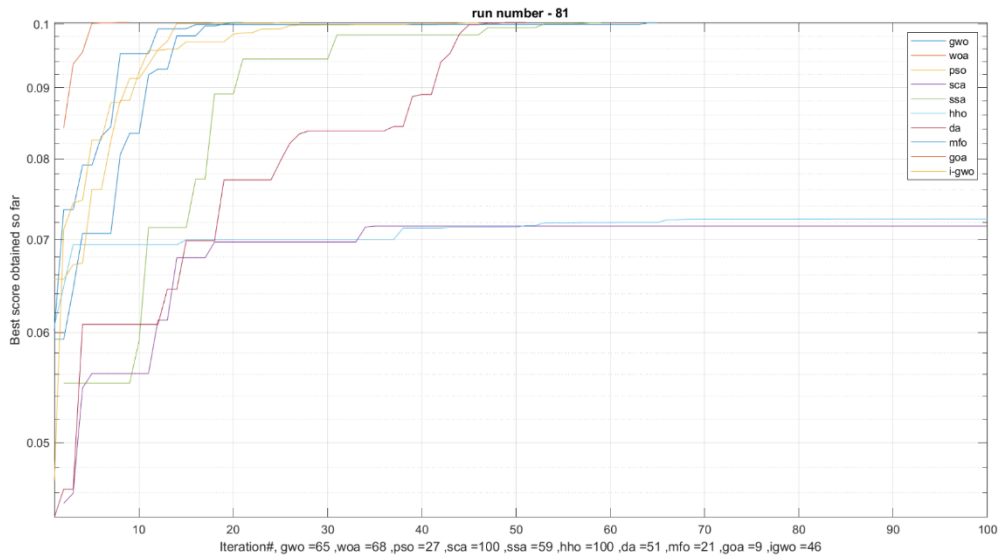
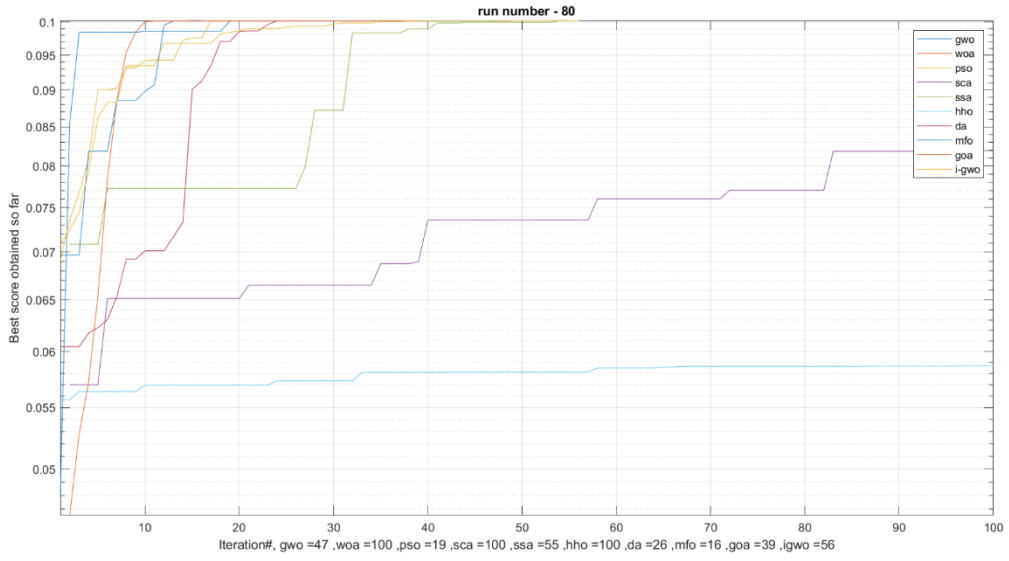


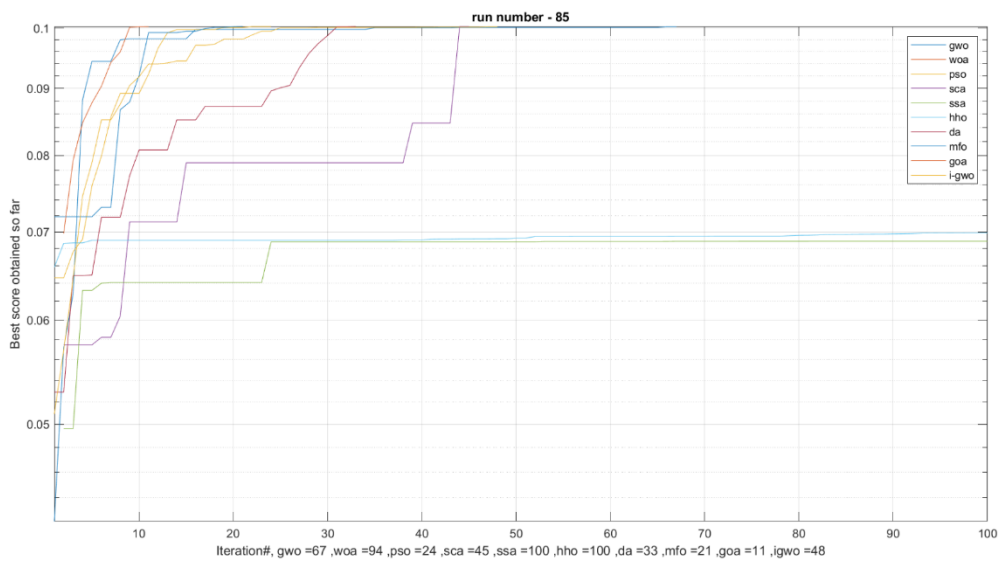
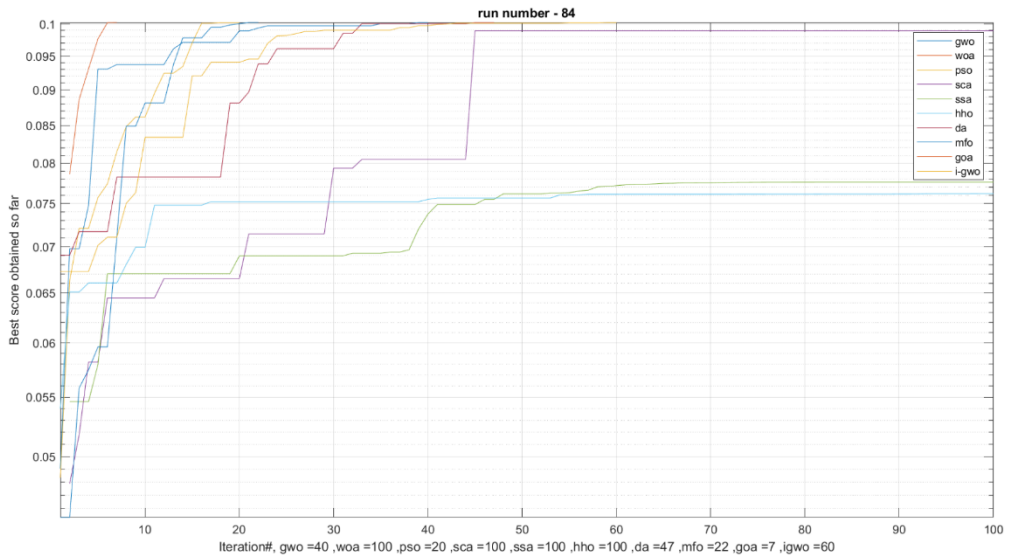
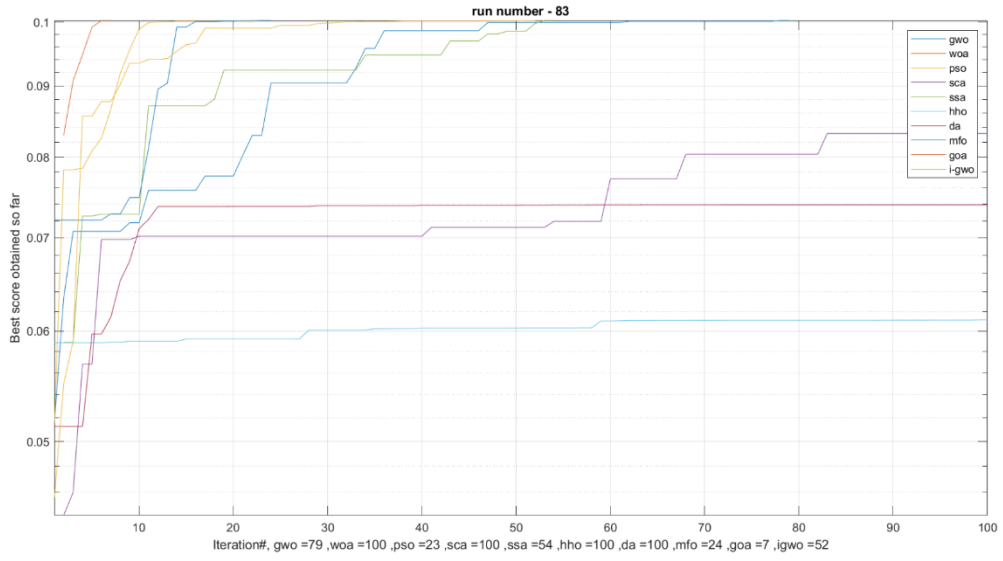


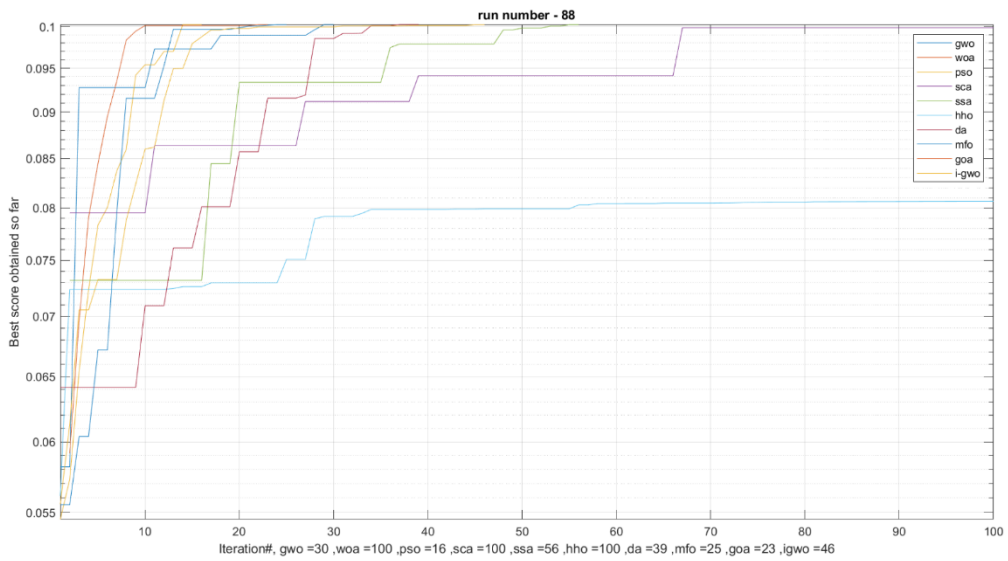
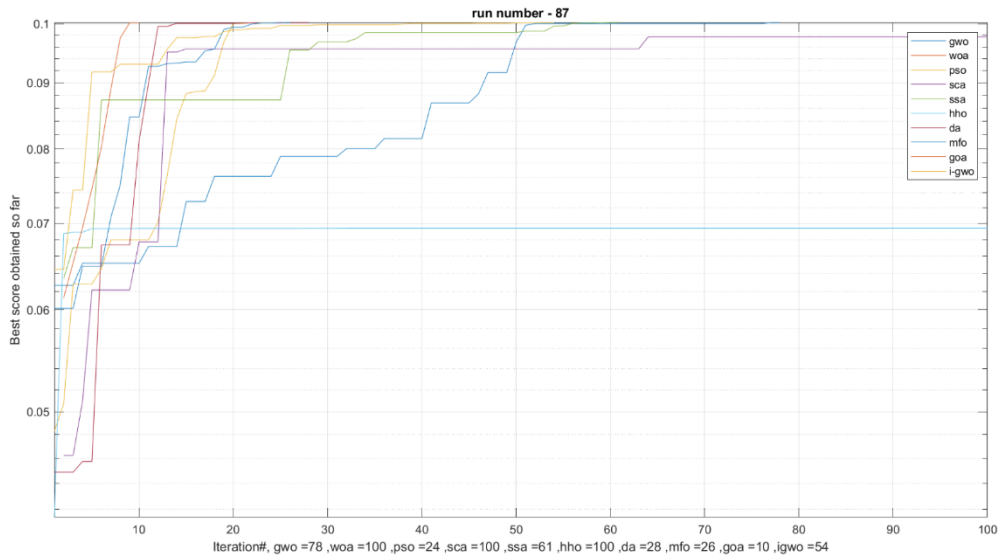
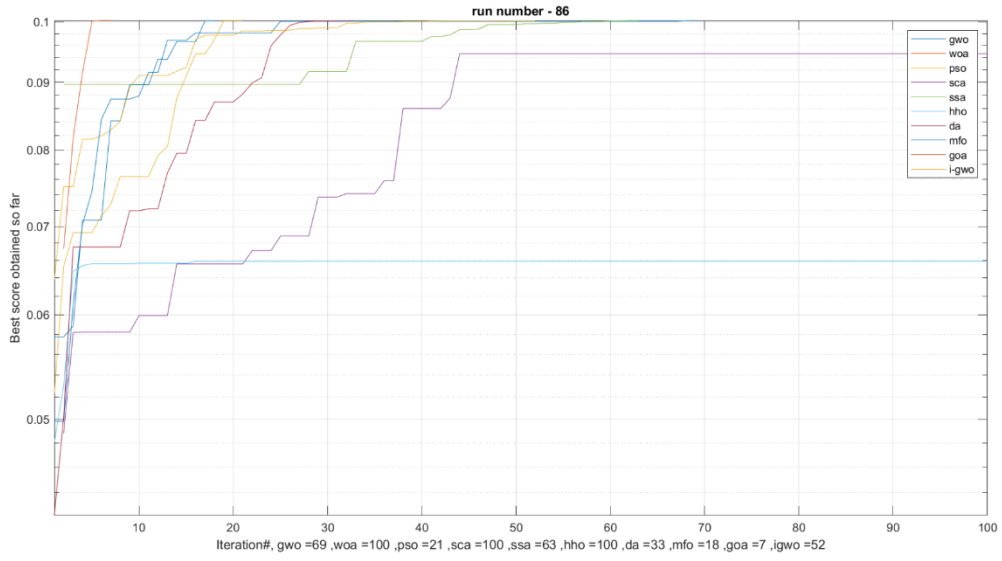


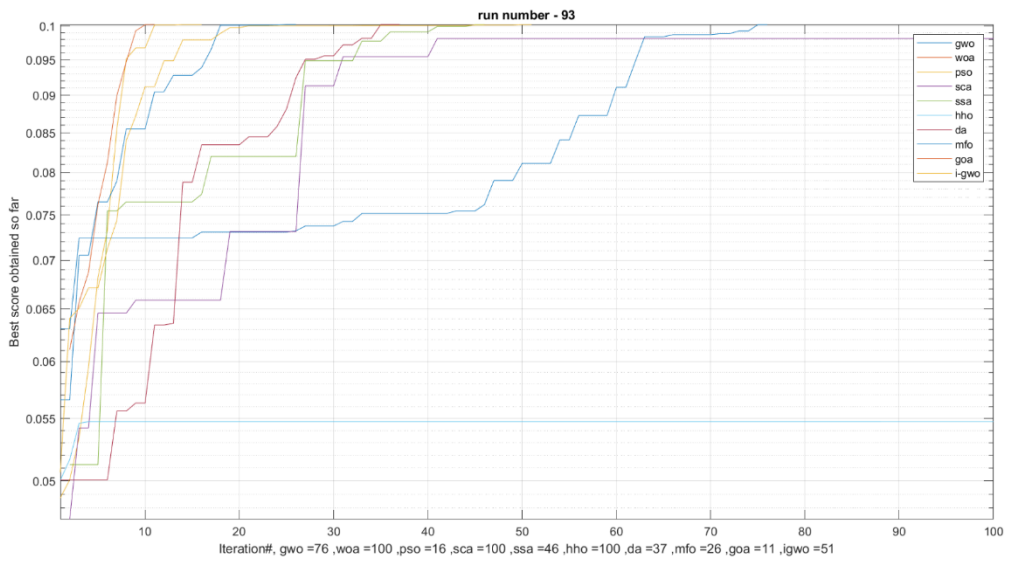
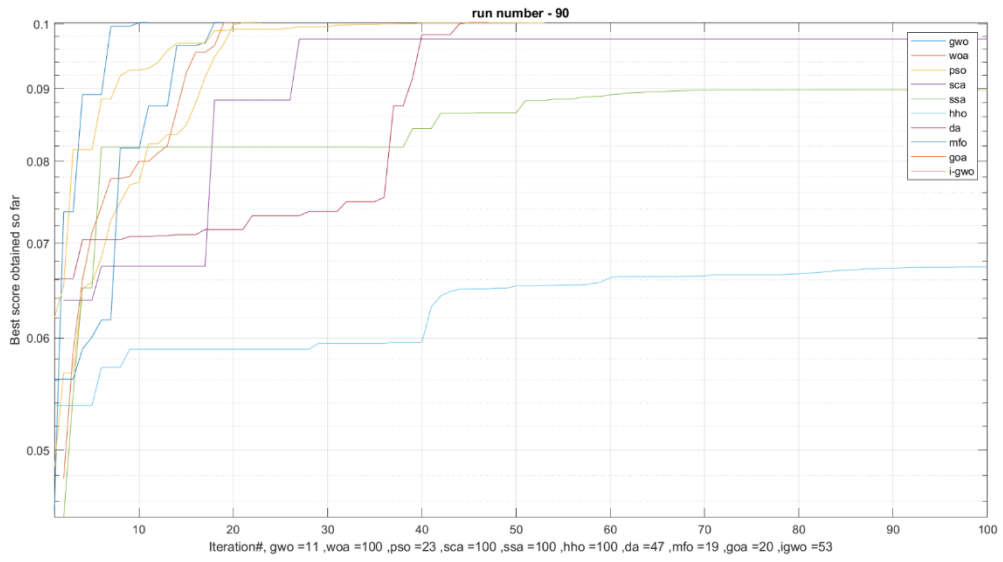
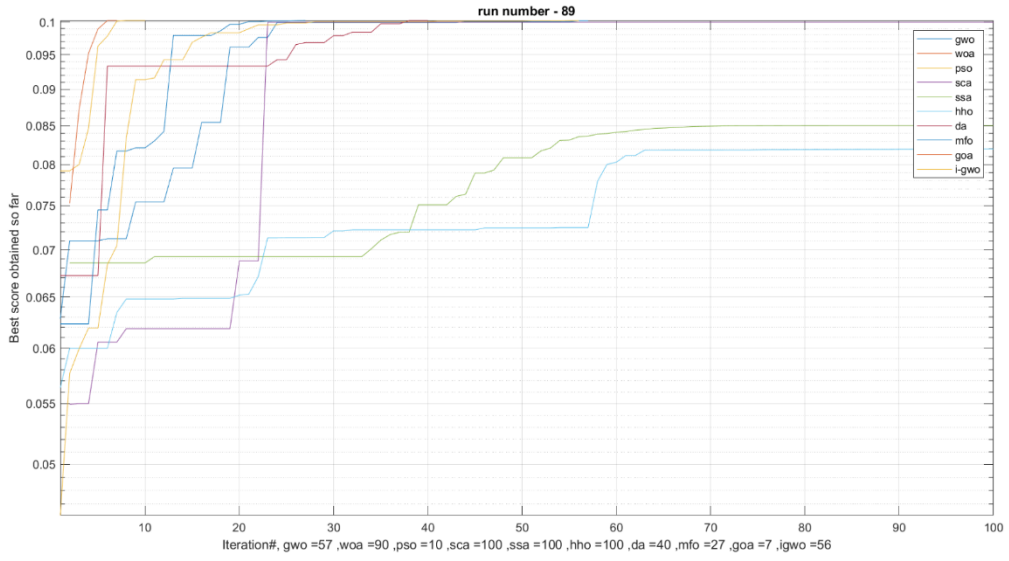


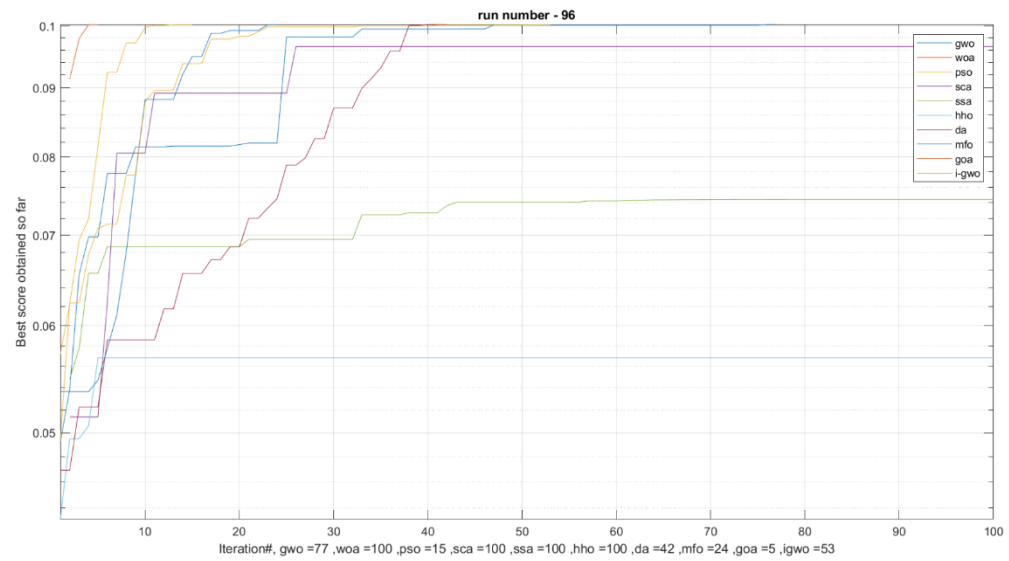
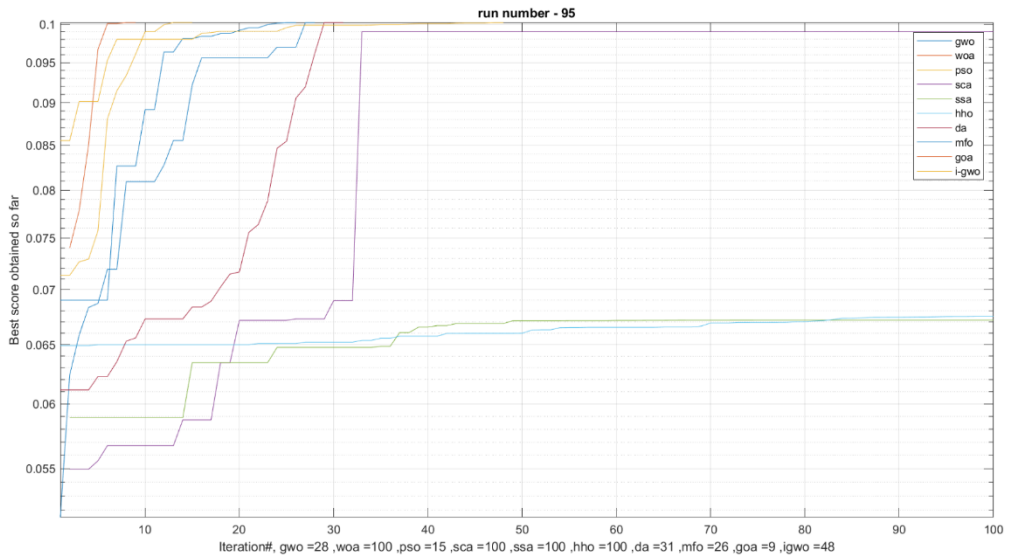
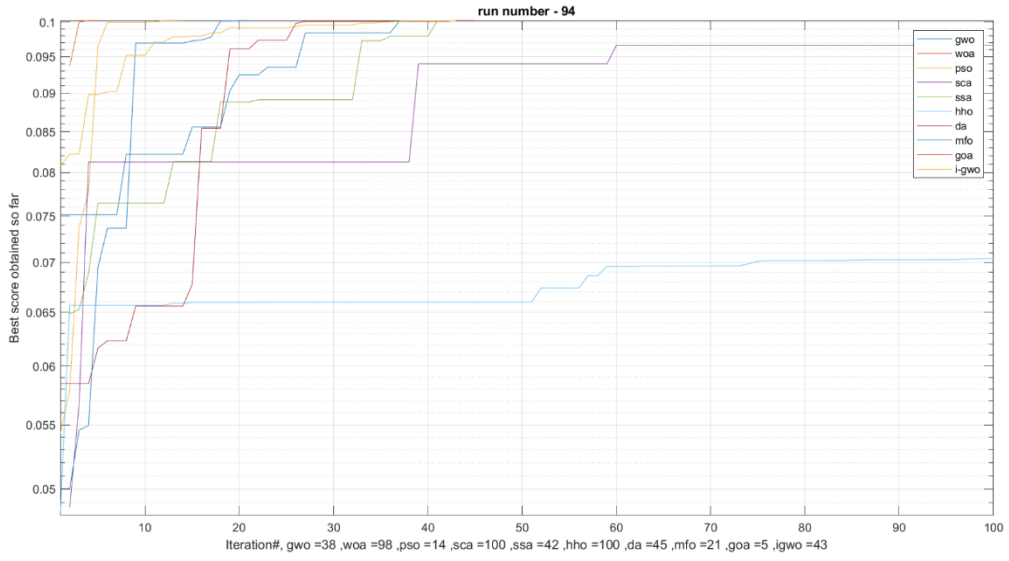


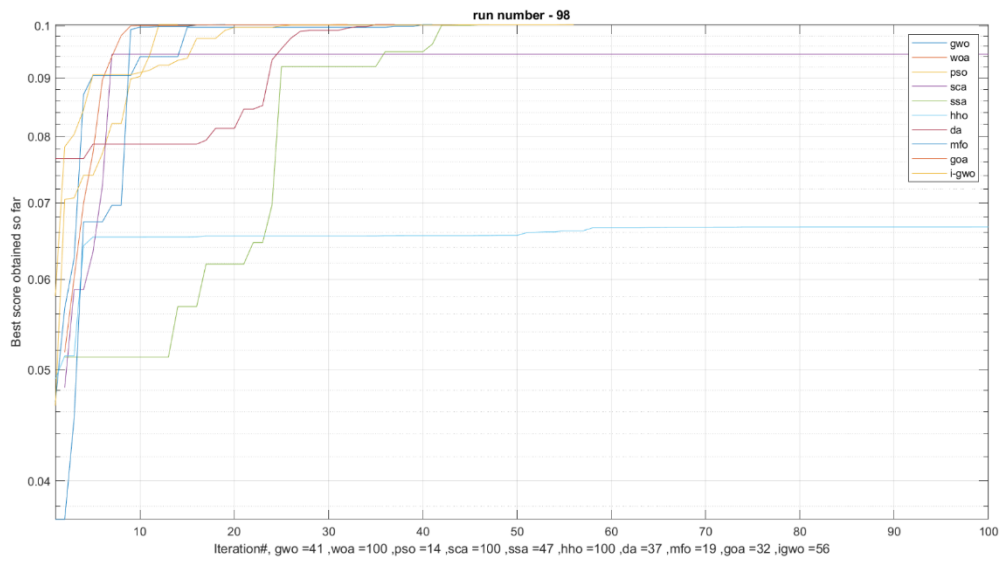
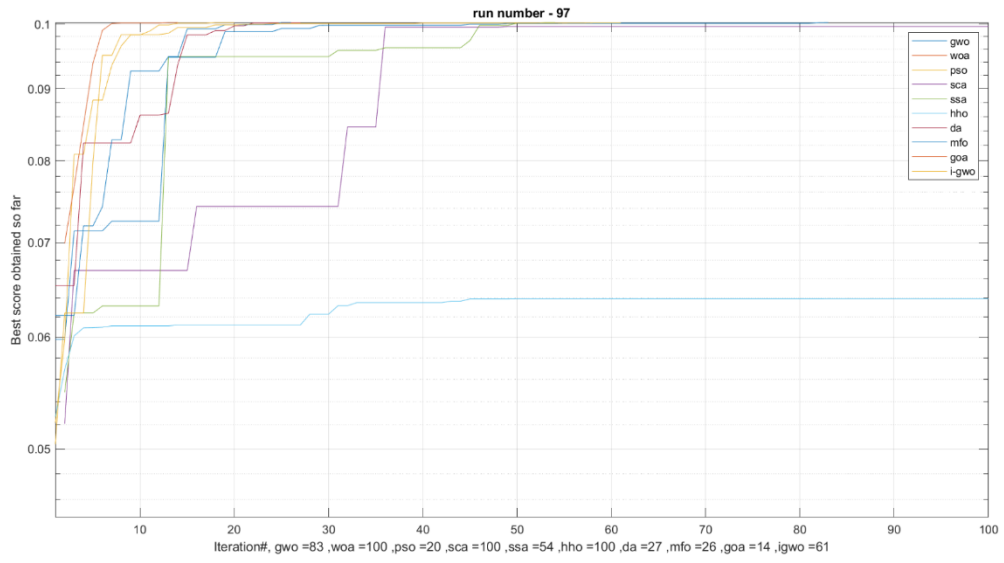


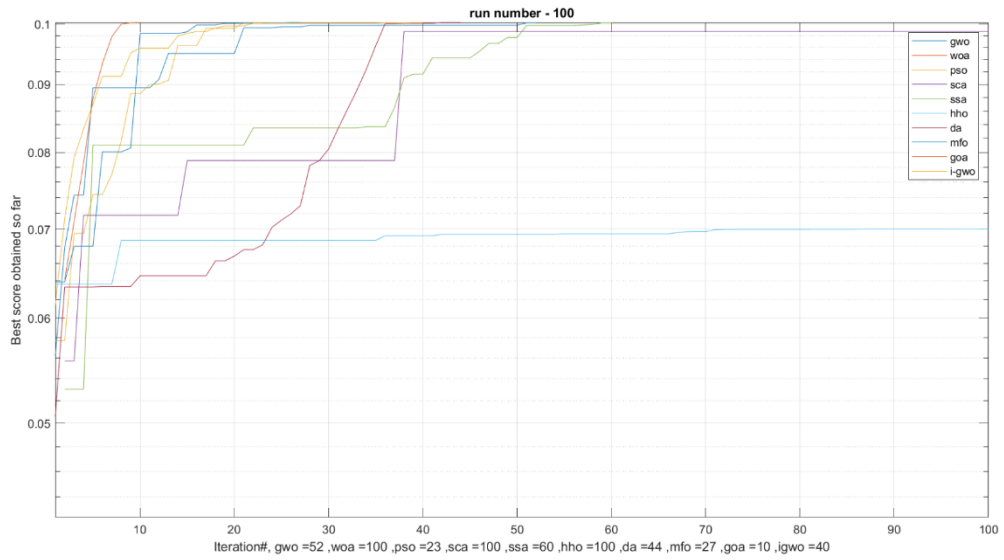
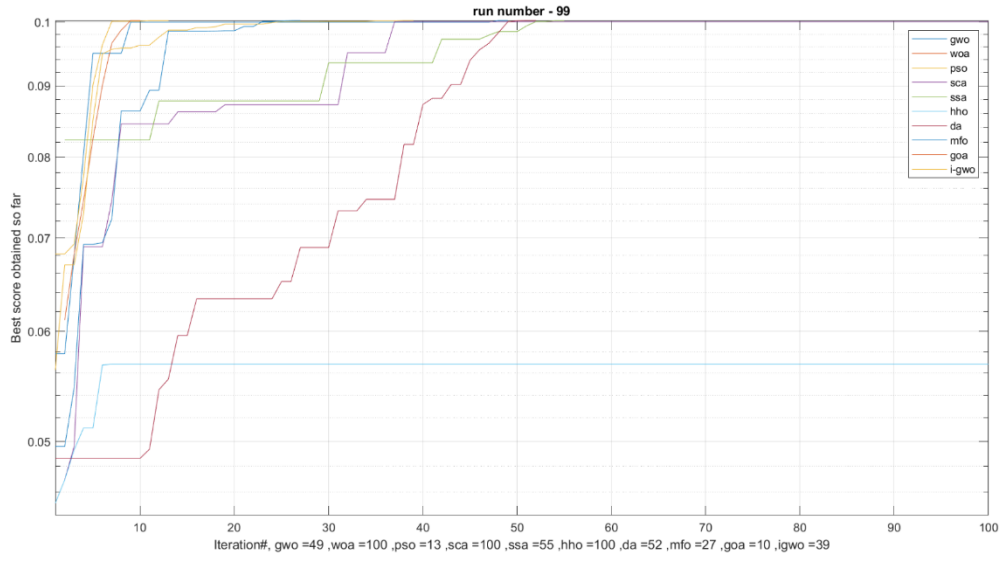














### 2.4.3 Power Loss Optimization

Ten different stochastic optimization algorithms were applied to solve overall path loss in 100 iterations with 30 search agents, and the whole process was repeated 100 times.

$$PL^{CI}(f, d)[dB]$$

$$= FSPL(f, 1m)[dB] + 10n \log_{10}\left(\frac{d}{d_0}\right) + AT[dB] + X_{\sigma}^{CI}, \quad d \geq d_0 \text{ m}$$

$PL^{CI}(f, d)[dB]$  has more parameters unlike attenuation factor. It has in total 7 independent variables and 5 of which are the independent variable of attenuation factor.

| Frequency (GHz) | Pressure(mbar) | Humidity (%) | Temperature (°C) | Rain Rate (mm/hr) | Transmitter and receiver 3D separation(m) | $d_0$ (m) |
|-----------------|----------------|--------------|------------------|-------------------|-------------------------------------------|-----------|
| 1-100           | 300-1013       | 0-100        | (-100) - 50      | 0-150             | 10-500                                    | 1-5       |

$d_0$  is the free space reference distance in meters, which is ranges from 1m to 5m, but  $d_0$  should not exceed 5 m to guarantee free space propagation within  $d_0$ . The problem was specified for Urban Micro cell which ranges from 10-500m with  $n$ , path loss exponent, equals to 2, and  $X_{\sigma}^{CI} = 4$ .

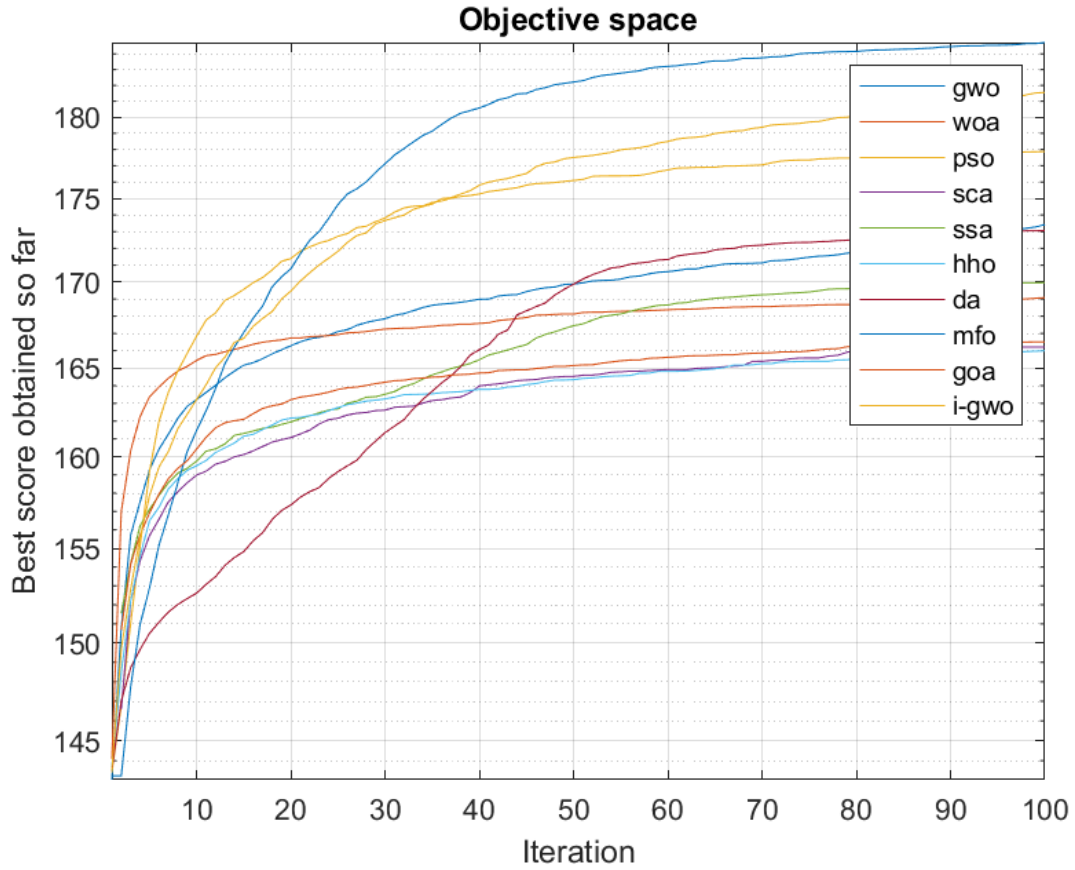


Figure. 2.4.5: Path loss for Urban Micro cell optimization convergence curve

Table 2.4.5: Power Loss Optimization values table

| Algorithm | Frequency                  | Pressure                          | Humidity                   | Temperature                     | Rain Rate                         | Transmitter and receiver 3D separation(m) | $d_0$ (m)                 | Power Loss[dB/m] |
|-----------|----------------------------|-----------------------------------|----------------------------|---------------------------------|-----------------------------------|-------------------------------------------|---------------------------|------------------|
| GWO       | 63.4349<br>6285067<br>8424 | 8.88432<br>5948107<br>823e+0<br>2 | 44.2839<br>1276280<br>8600 | -<br>41.2315<br>4887233<br>3610 | 1.47947<br>9149563<br>125e+0<br>2 | 4.97291<br>0013760<br>902e+0<br>2         | 2.47939<br>9382580<br>016 | 173.425<br>3     |
| WOA       | 93.9595                    | 986.132<br>8                      | 94.4107                    | 34.6589                         | 149.168<br>1                      | 499.097<br>7                              | 4.7532                    | 169.082<br>6     |
| PSO       | 64.6544                    | 842.752<br>4                      | 55.1694                    | -<br>65.5488                    | 149.312<br>9                      | 499.511<br>4                              | 2.7672                    | 177.875<br>1     |
| SCA       | 67.6936                    | 837.902                           | 37.4799                    | -                               | 144.058                           | 497.379                                   | 2.2933                    | 0166.21          |

|      |          |            |         |          |          |          |        |          |
|------|----------|------------|---------|----------|----------|----------|--------|----------|
|      |          | 5          |         | 42.9887  | 4        | 2        |        | 35       |
| SSA  | 74.4292  | 761.4798   | 64.6185 | -17.3115 | 142.7623 | 494.5105 | 3.2895 | 169.9654 |
| HHO  | 94.5039  | 807.6358   | 77.9248 | 29.3738  | 148.2561 | 497.9888 | 3.9748 | 165.9939 |
| DA   | 67.0.131 | 812.958    | 63.4205 | -39.2964 | 147.3633 | 498.7509 | 3.437  | 173.0594 |
| MFO  | 60.5314  | 1.0056e+03 | 51.3077 | -98.1171 | 149.4008 | 499.4687 | 3.1530 | 184.7273 |
| GOA  | 71.6427  | 749.0631   | 55.8721 | -31.1488 | 134.1423 | 493.4342 | 3.2773 | 166.5106 |
| IGWO | 60.1815  | 985.9551   | 47.4701 | -97.5477 | 147.1834 | 494.6919 | 2.8831 | 181.5604 |

The results suggest different performances of algorithms than the performance in optimizing attenuation factor. MFO gave the most optimum result and then IGWO and then PSO. Generally, free space path loss increases with frequency and with distances. However, even at the maximum possible distance, which is 500m in this case, the most loss occurs around 60GHz. However, the result of MFO suggests that the average humidity of 51.3% gives the most loss. However, in certain cases MFO gives 188dB as the maximum point with 60.3232965861214 GHz 1013.25mbar, 98.2533736243023 %, -100°C , 150 mm/hr, 500m, 1m as operating point.

## **2.5 Conclusion**

The overall research has the great potential to contribute in determining the optimum point of cell tower location. Also, this portion of the work is hoped to be of greater importance in terms of contribution as it relates to efficiency of calculation of a complex equation. Since this path loss model is a deterministic model, it can help the cellular operators to grasp the overall operating condition from a theoretical standpoint within a short amount of time by using stochastic algorithms. Also, this research does a comparative analysis between ten different algorithms in this particular problem. This wide comparison can help the operators to choose or to avoid algorithms based on their mode of operation. Solving a deterministic model through brute search is expensive in terms of calculations, so it hoped that introduction of stochastic algorithms to such a genre of problem can improve existing cellular technologies. Also, this work is hoped to pave the way of further research in signal power loss in 60 GHz.

## References

- [1] A. Gupta and R. K. Jha, "A Survey of 5G Network: Architecture and Emerging Technologies," in *IEEE Access*, vol. 3, pp. 1206-1232, 2015, doi: 10.1109/ACCESS.2015.2461602.
- [2] S. Sun, T. S. Rappaport, M. Shafi, P. Tang, J. Zhang and P. J. Smith, "Propagation Models and Performance Evaluation for 5G MillimeterWave Bands," in *IEEE Transactions on Vehicular Technology*, vol. 67, no. 9, pp. 8422-8439, Sept. 2018, doi: 10.1109/TVT.2018.2848208.
- [3] T. S. Rappaport, Y. Xing, G. R. MacCartney, A. F. Molisch, E. Mellios and J. Zhang, "Overview of Millimeter Wave Communications for FifthGeneration (5G) Wireless Networks—With a Focus on Propagation Models," in *IEEE Transactions on Antennas and Propagation*, vol. 65, no. 12, pp. 6213-6230, Dec. 2017, doi: 10.1109/TAP.2017.2734243.
- [4] G. R. Maccartney, T. S. Rappaport, S. Sun and S. Deng, "Indoor Office Wideband Millimeter-Wave Propagation Measurements and Channel Models at 28 and 73 GHz for Ultra-Dense 5G Wireless Networks," in *IEEE Access*, vol. 3, pp. 2388-2424, 2015, doi: 10.1109/ACCESS.2015.2486778. [21] L. N. Huynh, Q.-V. Pham, X.-Q. Pham, T. D. Nguyen, M. D. Hossain, and E.-N. Huh, "Efficient computation offloading in multi-tier multi-access edge computing systems: A particle swarm optimization approach," *Applied Sciences*, vol. 10, no. 1, p. 203, Jan. 2020.
- [5] Mohammed Bahjat Majed, Tharek Abd Rahman, Omar Abdul Aziz, Mohammad Nour Hindia, Effariza Hanafi, "Channel Characterization and Path Loss Modeling in Indoor Environment at 4.5, 28, and 38 GHz for 5G Cellular Networks", *International Journal of Antennas and Propagation*, vol. 2018, Article ID 9142367, 14 pages, 2018. <https://doi.org/10.1155/2018/9142367>
- [6] I. Rodriguez et al., "Analysis of 38 GHz mmWave Propagation Characteristics of Urban Scenarios," *Proceedings of European Wireless 2015; 21th European Wireless Conference*, Budapest, Hungary, 2015, pp. 1-8.

- [7] Zhimeng Zhong, Jianyao Zhao, Chao Li, "Outdoor-to-Indoor Channel Measurement and Coverage Analysis for 5G Typical Spectrums", *International Journal of Antennas and Propagation*, vol. 2019, Article ID 3981678, 10 pages, 2019. <https://doi.org/10.1155/2019/3981678>
- [8] G. Zhang et al., "Experimental Characterization of Millimeter-Wave Indoor Propagation Channels at 28 GHz," in *IEEE Access*, vol. 6, pp. 76516-76526, 2018, doi: 10.1109/ACCESS.2018.2882644.
- [9] T. Imai, K. Kitao, N. Tran, N. Omaki, Y. Okumura and K. Nishimori, "Outdoor-to-Indoor path loss modeling for 0.8 to 37 GHz band," 2016 10th European Conference on Antennas and Propagation (EuCAP), Davos, Switzerland, 2016, pp. 1-4, doi: 10.1109/EuCAP.2016.7481469.
- [10] Y. Mizuno, K. Nishimori and R. Taniguchi, "A study on outdoor to indoor penetration loss characteristics considering vertical and horizontal incident angle at 5 GHz band," 2020 International Symposium on Antennas and Propagation (ISAP), 2021, pp. 535-536, doi: 10.23919/ISAP47053.2021.9391303.
- [11] Mizuno, Yuta & Nishimori, Kentaro & Taniguchi, Ryotaro & Igarashi, Yuki. (2021). A simple model of outdoor to indoor penetration path loss considering incident angles at 0.9, 2.3 and 5.1 GHz. *IEICE Communications Express*. 10. 10.1587/comex.2020XBL0189.
- [12] M. M. Lodro, N. Majeed, A. A. Khuwaja, A. H. Sodhro and S. Greedy, "Statistical channel modelling of 5G mmWave MIMO wireless communication," 2018 International Conference on Computing, Mathematics and Engineering Technologies (iCoMET), Sukkur, Pakistan, 2018, pp. 1-5, doi: 10.1109/ICOMET.2018.8346408.
- [13] T. Anggita and M. Suryanegara, "Outdoor to Indoor Propagation Model of Glass Material Building at 26 GHz for 5G Mobile Technology," 2020 8th International Conference on Information and Communication Technology (ICoICT), Yogyakarta, Indonesia, 2020, pp. 1-5, doi: 10.1109/ICoICT49345.2020.9166323.

- [14] A. B. Zekri, R. Ajgou, A. Chemsas and S. Ghendir, "Analysis of Outdoor to Indoor Penetration Loss for mmWave Channels," 020 1st International Conference on Communications, Control Systems and Signal Processing (CCSSP), El Oued, Algeria, 2020, pp. 74-79, doi: 10.1109/CCSSP49278.2020.9151659.
- [15] S. Ju, Y. Xing, O. Kanhere and T. S. Rappaport, "3-D Statistical Indoor Channel Model for Millimeter-Wave and Sub-Terahertz Bands," GLOBECOM 2020 - 2020 IEEE Global Communications Conference, Taipei, Taiwan, 2020, pp. 1-7, doi: 10.1109/GLOBECOM42002.2020.9322429.
- [16] K. Haneda, J. Zhang, L. Tian et al., "5G 3GPP-Like Channel Models for Outdoor Urban Microcellular and Macrocellular Environments," 2016 IEEE 83rd Vehicular Technology Conference (VTC Spring), Nanjing, 2016, pp. 1-7. doi: 10.1109/VTCSpring.2016.7503971
- [17] H. Zhao, R. Mayzus, S. Sun et al., "28 GHz Millimeter Wave Cellular Communication Measurements for Reflection and Penetration Loss in and Around Buildings in New York City," 2013 IEEE International Conference on Communications (ICC), Budapest, 2013, pp. 5163-5167. doi: 10.1109/ICC.2013.6655403
- [18] 3GPP, "Study on channel model for frequencies from 0.5 to 100 GHz" TR 38.901, Mar. 2017.
- [19] K. Haneda et al., "5G 3GPP-Like Channel Models for Outdoor Urban Microcellular and Macrocellular Environments," 2016 IEEE 83rd Vehicular Technology Conference (VTC Spring), Nanjing, China, 2016, pp. 1-7, doi: 10.1109/VTCSpring.2016.7503971
- [20] H. J. Liebe, G. A. Hufford, and M. G. Cotton, "Propagation modeling of moist air and suspended water/ice particles at frequencies below 1000 GHz," AGARD Conference Proceedings 542, May 1993. [Online]. Available: <http://www.its.bldrdoc.gov/publications/2670.aspx>.

- [21] A. Ali, K. Naguib, and K. Mahmoud, "Optimized resource and power allocation for sum rate maximization in D2D-assisted caching networks," in International Conference on Computer Engineering and Systems (ICCES), Cairo, Egypt, 2019, pp. 438–444
- [22] Q.-V. Pham, S. Mirjalili, N. Kumar, M. Alazab, and W.-J. Hwang, "Whale optimization algorithm with applications to resource allocation in wireless networks," *IEEE Transactions on Vehicular Technology*, vol. 69, no. 4, pp. 4285–4297, Apr. 2020.
- [23] G. Eappen and S. T., "Hybrid PSO-GSA for energy efficient spectrum sensing in cognitive radio network," *Physical Communication*, vol. 40, p. 101091, Jun. 2020.
- [24] Pham, Quoc-Viet, et al. "Whale optimization algorithm with applications to resource allocation in wireless networks." *IEEE Transactions on Vehicular Technology* 69.4 (2020): 4285-4297.
- [25] J. Kennedy and R. Eberhart, "Particle swarm optimization," Proceedings of ICNN'95 - International Conference on Neural Networks, 1995, pp. 1942-1948 vol.4, doi: 10.1109/ICNN.1995.488968.
- [26] Seyedali Mirjalili, Moth-flame optimization algorithm: A novel nature-inspired heuristic paradigm, *Knowledge-Based Systems*, Volume 89, 2015, Pages 228-249, ISSN 0950-7051, <https://doi.org/10.1016/j.knosys.2015.07.006>.
- [27] Seyedali Mirjalili, Andrew Lewis, The Whale Optimization Algorithm, *Advances in Engineering Software*, Volume 95, 2016, Pages 51-67, ISSN 0965-9978,
- [28] Seyedali Mirjalili, Seyed Mohammad Mirjalili, Andrew Lewis, Grey Wolf Optimizer, *Advances in Engineering Software*, Volume 69, 2014, Pages 46-61, ISSN 0965-9978,
- [29] Ali Asghar Heidari, Seyedali Mirjalili, Hossam Faris, Ibrahim Aljarah, Majdi Mafarja, Huiling Chen, Harris hawks optimization: Algorithm and applications, *Future Generation Computer Systems*, Volume 97, 2019, Pages 849-872, ISSN 0167-739X
- [30] Seyedali Mirjalili, Amir H. Gandomi, Seyedeh Zahra Mirjalili, Shahrzad Saremi, Hossam Faris, Seyed Mohammad Mirjalili, Salp Swarm Algorithm: A bio-inspired optimizer for engineering design problems, *Advances in Engineering Software*, Volume 114, 2017, Pages 163-191, ISSN 0965-9978, <https://doi.org/10.1016/j.advengsoft.2017.07.002>.
- [31] Seyedali Mirjalili, SCA: A Sine Cosine Algorithm for solving optimization problems, *Knowledge-Based Systems*, Volume 96, 2016, Pages 120-133, ISSN 0950-7051, <https://doi.org/10.1016/j.knosys.2015.12.022>.



[32] Mirjalili, S. Dragonfly algorithm: a new meta-heuristic optimization technique for solving single-objective, discrete, and multi-objective problems. *Neural Comput & Applic* 27, 1053–1073 (2016). <https://doi.org/10.1007/s00521-015-1920-1>

[33] S. Saremi, S. Mirjalili and A. Lewis, "Grasshopper optimisation algorithm: Theory and application", *Adv. Eng. Softw.*, vol. 105, pp. 30-47, Mar. 2017.

[34] T. S. Rappaport, G. R. MacCartney, M. K. Samimi and S. Sun, "Wideband Millimeter-Wave Propagation Measurements and Channel Models for Future Wireless Communication System Design," in *IEEE Transactions on Communications*, vol. 63, no. 9, pp. 3029-3056, Sept. 2015, doi: 10.1109/TCOMM.2015.2434384.

[35] S. Sun *et al.*, "Investigation of Prediction Accuracy, Sensitivity, and Parameter Stability of Large-Scale Propagation Path Loss Models for 5G Wireless Communications," in *IEEE Transactions on Vehicular Technology*, vol. 65, no. 5, pp. 2843-2860, May 2016, doi: 10.1109/TVT.2016.2543139.

[36] T. S. Rappaport, R. W. Heath, Jr., R. C. Daniels, and J. N. Murdock, *MillimeterWaveWireless Communications*. Pearson/Prentice Hall 2015.